



polymers

Performance and Application of Novel Biocomposites

Edited by
Oisik Das

Printed Edition of the Special Issue Published in *Polymers*

Performance and Application of Novel Biocomposites

Performance and Application of Novel Biocomposites

Editor

Oisik Das

MDPI • Basel • Beijing • Wuhan • Barcelona • Belgrade • Manchester • Tokyo • Cluj • Tianjin



Editor

Oisik Das

Luleå University of Technology

Sweden

Editorial Office

MDPI

St. Alban-Anlage 66

4052 Basel, Switzerland

This is a reprint of articles from the Special Issue published online in the open access journal *Polymers* (ISSN 2073-4360) (available at: https://www.mdpi.com/journal/polymers/special_issues/Per_App_Nov_Bio).

For citation purposes, cite each article independently as indicated on the article page online and as indicated below:

LastName, A.A.; LastName, B.B.; LastName, C.C. Article Title. *Journal Name* **Year**, Volume Number, Page Range.

ISBN 978-3-0365-0312-7 (Hbk)

ISBN 978-3-0365-0313-4 (PDF)

© 2021 by the authors. Articles in this book are Open Access and distributed under the Creative Commons Attribution (CC BY) license, which allows users to download, copy and build upon published articles, as long as the author and publisher are properly credited, which ensures maximum dissemination and a wider impact of our publications.

The book as a whole is distributed by MDPI under the terms and conditions of the Creative Commons license CC BY-NC-ND.

Contents

About the Editor	vii
Oisik Das and Seeram Ramakrishna Education and Research during Pandemics: Illustrated by the Example of Experimental Biocomposites Research Reprinted from: <i>Polymers</i> 2020 , <i>12</i> , 1848, doi:10.3390/polym12081848	1
Estefanía Lidón Sánchez-Safont, Abdulaziz Aldureid, José María Lagarón, Luis Cabedo and José Gámez-Pérez Study of the Compatibilization Effect of Different Reactive Agents in PHB/Natural Fiber-Based Composites Reprinted from: <i>Polymers</i> 2020 , <i>12</i> , 1967, doi:10.3390/polym12091967	5
Miguel A. Hidalgo-Salazar, Juan P. Correa-Aguirre, Serafín García-Navarro and Luis Roca-Blay Injection Molding of Coir Coconut Fiber Reinforced Polyolefin Blends: Mechanical, Viscoelastic, Thermal Behavior and Three-Dimensional Microscopy Study Reprinted from: <i>Polymers</i> 2020 , <i>12</i> , 1507, doi:10.3390/polym12071507	25
Juan P. Correa-Aguirre, Fernando Luna-Vera, Carolina Caicedo, Bairo Vera-Mondragón and Miguel A. Hidalgo-Salazar The Effects of Reprocessing and Fiber Treatments on the Properties of Polypropylene-Sugarcane Bagasse Biocomposites Reprinted from: <i>Polymers</i> 2020 , <i>12</i> , 1440, doi:10.3390/polym12071440	45
Hua-Wei Chen and Min-Feng Lin Characterization, Biocompatibility, and Optimization of Electrospun SF/PCL/CS Composite Nanofibers Reprinted from: <i>Polymers</i> 2020 , <i>12</i> , 1439, doi:10.3390/polym12071439	69
Radwa M. Ashour, Ahmed F. Abdel-Magied, Qiong Wu, Richard T. Olsson and Kerstin Forsberg Green Synthesis of Metal-Organic Framework Bacterial Cellulose Nanocomposites for Separation Applications Reprinted from: <i>Polymers</i> 2020 , <i>12</i> , 1104, doi:10.3390/polym12051104	85
Fatemeh Khosravi, Saied Nouri Khorasani, Shahla Khalili, Rasoul Esmaeely Neisiany, Erfan Rezvani Ghomi, Fatemeh Ejeian, Oisik Das and Mohammad Hossein Nasr-Esfahani Development of a Highly Proliferated Bilayer Coating on 316L Stainless Steel Implants Reprinted from: <i>Polymers</i> 2020 , <i>12</i> , 1022, doi:10.3390/polym12051022	95
Lei Zhang, Huicheng Xu and Weihong Wang Performance of Straw/Linear Low Density Polyethylene Composite Prepared with Film-Roll Hot Pressing Reprinted from: <i>Polymers</i> 2020 , <i>12</i> , 860, doi:10.3390/polym12040860	109
Jiajie Wang, Yingzhuo Lu, Qindan Chu, Chaoliang Ma, Lianrun Cai, Zhehong Shen and Hao Chen Facile Construction of Superhydrophobic Surfaces by Coating Fluoroalkylsilane/Silica Composite on a Modified Hierarchical Structure of Wood Reprinted from: <i>Polymers</i> 2020 , <i>12</i> , 813, doi:10.3390/polym12040813	127

Lin Jiang, Xin-Rui Yang, Xu Gao, Qiang Xu, Oisik Das, Jin-Hua Sun and Manja Kitek Kuzman Pyrolytic Kinetics of Polystyrene Particle in Nitrogen Atmosphere: Particle Size Effects and Application of Distributed Activation Energy Method Reprinted from: <i>Polymers</i> 2020 , <i>12</i> , 421, doi:10.3390/polym12020421	139
Mohanad Mousa and Yu Dong The Role of Nanoparticle Shapes and Structures in Material Characterisation of Polyvinyl Alcohol (PVA) Bionanocomposite Films Reprinted from: <i>Polymers</i> 2020 , <i>12</i> , 264, doi:10.3390/polym12020264	157
Rhoda Afriyie Mensah, Jie Xiao, Oisik Das, Lin Jiang, Qiang Xu and Mohammed Okoe Alhassan Application of Adaptive Neuro-Fuzzy Inference System in Flammability Parameter Prediction Reprinted from: <i>Polymers</i> 2020 , <i>12</i> , 122, doi:10.3390/polym12010122	181
Mauro Giorcelli and Mattia Bartoli Development of Coffee Biochar Filler for the Production of Electrical Conductive Reinforced Plastic Reprinted from: <i>Polymers</i> 2019 , <i>11</i> , 1916, doi:10.3390/polym11121916	197
Francesca Ferrari, Raffaella Striani, Paolo Visconti, Carola Esposito Corcione and Antonio Greco Durability Analysis of Formaldehyde/Solid Urban Waste Blends Reprinted from: <i>Polymers</i> 2019 , <i>11</i> , 1838, doi:10.3390/polym11111838	215
Karthik Babu, Gabriella Rendén, Rhoda Afriyie Mensah, Nam Kyeun Kim, Lin Jiang, Qiang Xu, Ágoston Restás, Rasoul Esmaeely Neisiany, Mikael S. Hedenqvist, Michael Försth, Alexandra Byström and Oisik Das A Review on the Flammability Properties of Carbon-Based Polymeric Composites: State-of-the-Art and Future Trends Reprinted from: <i>Polymers</i> 2020 , <i>12</i> , 1518, doi:10.3390/polym12071518	227
Shuvra Singha and Mikael S. Hedenqvist A Review on Barrier Properties of Poly(Lactic Acid)/Clay Nanocomposites Reprinted from: <i>Polymers</i> 2020 , <i>12</i> , 1095, doi:10.3390/polym12051095	247

About the Editor

Oisik Das research activities pertain to carbon-based materials and polymeric composites, specifically improvement of their performance properties (e.g., mechanical, flammability, dimensional) through physical and chemical means. Of particular interest is the production and characterisation of biochar (i.e., bio-based carbon materials) for composite applications. Oisik has extensive experience in determining the material properties of numerous types of biochars through nanoindentation. Additionally, Oisik is interested in enhancing the fire-resistant properties of polymeric composites by using both conventional and natural fire retardants. Oisik teaches courses related to material science and fire engineering and supervises students. Oisik worked at the KTH Royal Institute of Technology, Stockholm, Sweden for two years as a post-doctoral fellow conducting research on bio-based polymers and their composites. Oisik completed his PhD at the Centre for Advanced Composite Materials (CACM) at the University of Auckland, New Zealand. His research was focused on the utilisation of biochar (obtained from the pyrolysis/thermochemical conversion of lignocellulosic wastes) in areas of biocomposite development. Oisik's master's degree is from Washington State University, Pullman, USA where he worked on the thermochemical conversion of lignocellulosic biomass to produce value-added products (e.g., biocarbon and bio-oil). In the past, Oisik served Maharishi Markandeshwar (M.M.) University in India as an Assistant Professor where he worked with students regarding various applications of biocarbon/biochar.

Editorial

Education and Research during Pandemics: Illustrated by the Example of Experimental Biocomposites Research

Oisik Das ^{1,*} and Seeram Ramakrishna ^{2,*}

¹ Department of Engineering Sciences and Mathematics, Luleå University of Technology, 97187 Luleå, Sweden

² Department of Mechanical Engineering, National University of Singapore, Singapore 117575, Singapore

* Correspondence: oisik.das@ltu.se (O.D.); seeram@nus.edu.sg (S.R.)

Received: 5 August 2020; Accepted: 17 August 2020; Published: 18 August 2020

In late 2019, a novel Coronavirus was detected in Wuhan city of China, giving rise to the catastrophic pandemic that is still rampant today. Initially, the worst-hit districts were put under lockdown, which then extended to cities and eventually whole countries. Travel of people, along with logistics of goods and services, were (and still are) severely affected. Most nations of the world urged their citizens to stay indoors so as to avoid exposure to the virus, and thus remain infection-free. One of the demographics that are negatively affected by the lockdown measures is the students and researchers. Numerous universities around the world had to shut their premises at short notice, thus prompting a rapid shift from in-classroom education to online education, a transition that normally would take decades to happen. In particular, students received their classes through digital platforms, which included Zoom, Microsoft Teams, Skype, etc., whereas the researchers adopted tele-working. Although this strategy employed by universities is effective in curbing the further spread of the virus, it has some unintended consequences. Firstly, owing to the uncertainty regarding the end date for the current coronavirus pandemic, millennials and freshmen are unsure about their immediate enrolment in their chosen courses and programmes. For example, the University of Ohio in USA and the University of Cambridge in the United Kingdom will hold online classes for the upcoming fall and until the summer of 2021, respectively. This is particularly disheartening for international students, who are anticipating an active academic experience that includes campus life, engagement in classrooms, obtaining in-person feedback from lecturers, bonding and networking in cafes, etc. Secondly, and more importantly, students whose programmes warrant undertaking a significant amount of laboratory work are stressed about the stagnant nature of their research. While a few fields of study can be conducted on a digital platform, experimental research requires the presence of the person in laboratories for a substantial amount of time. Biocomposite education is at its core an experimental one, which includes the design of the biocomposite, preparation of raw materials, fabrication and manufacturing, prototyping, and finally testing and characterisation. Therefore, it is critical to identify some effective means to propagate biocomposites education during pandemics, wherein students and researchers are confined to quarantines. In other words, educators should create paths for effective learning in the biocomposite field in a distanced education system via alternative routes and remote controlled laboratories and equipment.

In light of the aforementioned, five strategies could be adopted by the students and researchers to sustain biocomposites education and learning during viral outbreaks and disruptions. The first strategy, which is one of the most obvious ones, is to bolster the theoretical knowledge regarding composite science and technology. Often, a student or a researcher learns on the job, i.e., learning by doing. While this is imperative to activate the psychomotor taxonomic domain, the cognitive domain can be made robust by indulging in the comprehension of background knowledge regarding various scientific phenomena and engineering concepts [1]. Although a student can progress through his/her

academic career and reach higher positions of lecturer or assistant professor by relying solely on the 'working knowledge' of biocomposites, an in-depth understanding of concepts like micromechanics, macromechanics, laminate theory, structural mechanics, analytical modelling and finite element modelling will make them reflective practitioners [2]. Additionally, these academics will be intrinsically motivated [3] to conduct effective teaching and ground-breaking research. Therefore, the imparting of theoretical knowledge on biocomposites will garner self-regulation [4], confidence and self-efficacy [5] in the students and researchers.

In the second strategy, the students and researchers can devote their time to preparing comprehensive and critical review articles meant for beginners and experienced researchers, respectively. Not only does the preparation of review articles inadvertently facilitate the absorbance of overall knowledge, but also their eventual publication in peer-reviewed journals attracts more citations (compared to the narrowly focused research articles), which will boost the person's academic career and visibility. The writing of review articles enables the author to develop a holistic overview regarding specific aspects of the biocomposite field. Additionally, the author becomes aware of the latest developments in the state-of-the-art research, and is able to critically analyse and well position his/her own research so as to address specific scientific and technological challenges and needs. Thus, the above-mentioned facets of writing a review article are conducive for the development of biocomposites education because students/researchers will learn by immersing themselves in loops of experience, theories and practice, as specified by Boyatzis and Kolb, 1995 [6].

In the third strategy, the students and researchers can perform life cycle analyses (LCA) of various biocomposite products. LCA does not require access to laboratories, and thus can be performed from the safety of one's home. Through LCA analysis, the student/researcher will be able to grasp the importance of manufacturing and environmental sustainability, and attaining a circular economy mind-set. It is critical to reduce greenhouse gas (GHG) emissions and wastage at every stage of the biocomposites' life cycle, and LCA will shine light into the environmental impact of sourcing raw materials and feedstock, processing, manufacture, distribution, use, repair, maintenance and disposal or recycling, i.e., the cradle-to-grave life of the product. The performing of LCA studies will not only create opportunities for journal publications, but also encourage the student/researcher to undertake industry-facing and market-oriented sustainable design and re-design of biocomposites in the future. This will lead to the academic being environmentally conscious and striving towards waste minimisation and pollution reduction during the biocomposite's development and life cycle.

The fourth strategy is related to simulation studies of various aspects of biocomposites. Simulation studies can be related to the determination of process feasibility parameters, its lifetime prediction, failure mechanisms, etc. Although simulation without experimental validation could be futile, students/researchers can delve into the modelling world, which can enable process optimisation and effective product life cycle engineering. Furthermore, the students/researchers can visualise the performance of the biocomposite without having to actually manufacture the product. Therefore, simulation studies will not only enhance one's theoretical understanding of composite science, but also prepare one to tailor the design in order to have desirable performance properties and functionalities. Simulation studies will be the closest thing for the students/researchers to experimentally designing and developing biocomposites, and characterising their various properties in a manner akin to a real-life laboratory session.

If performing real-world experiments is unavoidable, maybe the students/researchers can do so in a simulated laboratory environment of virtual reality (VR), which is the fifth strategy. Nevertheless, VR technology would not be accessible to all the students, especially in developing nations where such technologies could be non-existent. VR technology can potentially allow students/researchers to collaborate and interact with the artificially created biocomposite laboratory by moving through its spaces and experiencing visual and auditory feedback from common instruments, such as injection moulding machines, Instron Universal testing machines, cone calorimetry equipment, etc. Since VR has been used in medicine in a way that has allowed the trainee doctors to rectify errors [7], the same can

be emulated in biocomposite education. VR in biocomposite education will be beneficial in enabling the student/researcher to develop his/her experimental skills, and will reduce the total cost of the programme, since raw materials will not be expended.

In summary, there are several ways by which a student or a researcher can be immersed in continuing biocomposites education during pandemics and massive disruptions. Adherence to the aforementioned strategies will ensure that students/researchers can come back with a strong foundation once the pandemic ends and the laboratories reopen. The following Figure 1 depicts the ideas put forward in this article. An ideal solution for maintaining the flow of biocomposites research and education is the combination of all the five strategies in some form or another.

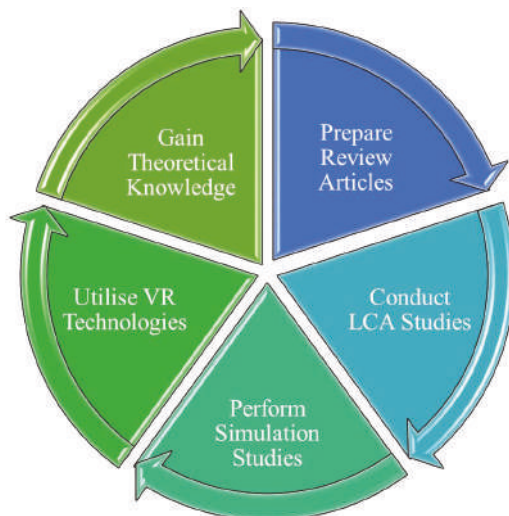


Figure 1. The five strategies for students and researchers to adopt in order to maintain the continuity of biocomposites education during a pandemic.

References

1. Adesoji, F.A. Bloom taxonomy of educational objectives and the modification of cognitive levels. *Adv. Soc. Sci.* **2018**, *5*, 5. [CrossRef]
2. Schön, D.A. *Educating the Reflective Practitioner*; Jossey-Bass: San Francisco, CA, USA, 1987.
3. Rust, C. The impact of assessment on student learning: How can the research literature practically help to inform the development of departmental assessment strategies and learner-centred assessment practices? *Act. Learn. High. Educ.* **2002**, *3*, 145–158. [CrossRef]
4. Ng, E.M. Integrating self-regulation principles with flipped classroom pedagogy for first year university students. *Comput. Educ.* **2018**, *126*, 65–74. [CrossRef]
5. Baker, D. What works: Using curriculum and pedagogy to increase girls' interest and participation in science. *Theory Pract.* **2013**, *52*, 14–20. [CrossRef]
6. Boyatzis, R.E.; Kolb, D.A. From learning styles to learning skills: The executive skills profile. *J. Manag Psychol.* **1995**, *10*, 3–17. [CrossRef]
7. Li, L.; Yu, F.; Shi, D.; Shi, J.; Tian, Z.; Yang, J.; Wang, X.; Jiang, Q. Application of virtual reality technology in clinical medicine. *Am. J. Transl.* **2017**, *9*, 3867.



© 2020 by the authors. Licensee MDPI, Basel, Switzerland. This article is an open access article distributed under the terms and conditions of the Creative Commons Attribution (CC BY) license (<http://creativecommons.org/licenses/by/4.0/>).

Article

Study of the Compatibilization Effect of Different Reactive Agents in PHB/Natural Fiber-Based Composites

Estefanía Lidón Sánchez-Safont ¹, Abdulaziz Aldureid ¹, José María Lagarón ², Luis Cabedo ¹ and José Gámez-Pérez ^{1,*}

¹ Polymers and Advanced Materials Group (PIMA), Universitat Jaume I (UJI), Av. Vicent Sos Baynat s/n, 12071 Castelló de la Plana, Spain; esafont@uji.es (E.L.S.-S.); aldureid@uji.es (A.A.); lcabedo@uji.es (L.C.)

² Novel Materials and Nanotechnology Group, Institute of Agrochemistry and Food Technology (IATA), Spanish National Research Council (CSIC), Calle Catedrático Agustín Escardino Benlloch 7, 46980 Paterna, Spain; lagaron@iata.csic.es

* Correspondence: gamez@uji.es

Received: 5 August 2020; Accepted: 26 August 2020; Published: 30 August 2020

Abstract: Fiber–matrix interfacial adhesion is one of the key factors governing the final properties of natural fiber-based polymer composites. In this work, four extrusion reactive agents were tested as potential compatibilizers in polyhydroxybutyrate (PHB)/cellulose composites: dicumyl peroxide (DCP), hexamethylene diisocyanate (HMDI), resorcinol diglycidyl ether (RDGE), and triglycidyl isocyanurate (TGIC). The influence of the fibers and the different reactive agents on the mechanical properties, physical aging, and crystallization behavior were assessed. To evaluate the compatibilization effectiveness of each reactive agent, highly purified commercial cellulose fibers (TC90) were used as reference filler. Then, the influence of fiber purity on the compatibilization effect of the reactive agent HMDI was evaluated using untreated (U_RH) and chemically purified (T_RH) rice husk fibers, comparing the results with the ones using TC90 fibers. The results show that reactive agents interact with the polymer matrix at different levels, but all compositions showed a drastic embrittlement due to the aging of PHB. No clear compatibilization effect was found using DCP, RDGE, or TGIC reactive agents. On the other hand, the fiber–polymer interfacial adhesion was enhanced with HMDI. The purity of the fiber played an important role in the effectiveness of HMDI as a compatibilizer, since composites with highly purified fibers showed the greatest improvements in tensile strength and the most favorable morphology. None of the reactive agents negatively affected the compostability of PHB. Finally, thermoformed trays with good mold reproducibility were successfully obtained for PHB/T_RH/HMDI composition.

Keywords: PHB; natural fiber; compatibilizer; cellulose; biocomposite

1. Introduction

The development of biobased biodegradable thermoplastic materials is a topic research of special interest because it can represent a cost-effective and environmental-friendly alternative to commodities [1]. Among the different biopolymers, polyhydroxybutyrate (PHB), a bacterial origin biopolyester from the polyhydroxyalcanoates family (PHAs), has attracted a lot of attention. The applicability fields where the PHB-based material results are more interesting are those in which biodegradability is desired either because composting could be a viable option for their waste management or because they can potentially end up in the environment. Among those applications, we can highlight food packaging or disposable products such as single-use tableware, hygiene-related single-use products, straws, etc. [1–4]. The main strengths of the PHB that make it suitable for this type

of application are its natural origin, its biodegradability, the absence of toxicity, and the high service temperature [5]. Indeed, PHB presents mechanical properties in terms of a stiffness and strength that is similar to PP, good barrier properties, which are comparable or even superior to PET [6–10], and it is biodegradable in different environments, such as soil and marine [7,11,12], and compostable at lab-scale, industrial, and home composting conditions [13].

However, PHB presents some shortcomings that limit its industrial applicability. PHB is a semicrystalline polymer that is capable of a high degree of crystallinity but has a relatively low crystallization rate. Hence, PHB suffers an appreciable embrittlement with time due to secondary crystallization and physical aging [14–17], and its long-term mechanical properties are characterized by low ductility and toughness. Indeed, the processing temperature window of PHB is very narrow: the lower limit is relatively high due to its high crystallinity, and the upper limit is relatively low because of its poor thermal stability in molten state (the degradation temperature is close to the melting temperature [7]). Altogether, these factors make PHB quite difficult to process, especially in the case of thermoforming [18]. In addition, one of the main limiting factors is its current high price. In this sense, the development of PHB-based composites using lignocellulosic fibers as fillers could contribute to a large extent to overcome the cost drawback maintaining the biodegradability and even improving the mechanical performance of PHB, allowing the valorization of vegetal wastes contributing to the circular economy.

Lignocellulosic fibers are hydrophilic materials composed by bundles of cellulose fibers embedded in a matrix of other non-cellulosic materials such as lignin, hemicelluloses, pectin, waxes, and other minor components [19]. The advantages of use lignocellulosic fibers as fillers are their availability, low cost, biodegradability, low density, high stiffness, and acceptable specific strength [20]. However, they also present shortcomings related to their thermal sensitivity and hydrophilic nature. In addition, depending on the vegetal source and/or the plant location and time of harvest, the composition, properties, morphology, and surface characteristics of different lignocellulosic fibers may differ significantly [21].

It is well known that the resultant properties of fiber-based composites depend not only on the properties of the constituents but are also determined by the fiber–matrix adhesion. The hydrophilic nature of the lignocellulosic fibers lowers the compatibility with the hydrophobic polymer. Nevertheless, according to Bhardwaj et al. [22], the relatively polar nature and presence of carbonyl groups ($-C=O$) in PHB as compared with other nonpolar matrices such as PP might cause a hydrogen-bonding-type interaction with the cellulosic fibers and relative better compatibility, as it has been also noticed by others in PHA/lignocellulosic composites [23,24]. However, these interactions are not enough to provide strong adhesion of PHB with lignocellulosic fibers, as it has been shown previously in PHA-based composites, which are filled with untreated lignocellulosic fibers [25–27]. Thus, the enhancement of fiber–matrix adhesion may be a key factor to exploit the full capabilities of these composites.

Some attempts to improve interfacial adhesion are physical treatments (plasma or corona discharge), chemical purification treatments (dewaxing and delignifying treatments) of the fibers, grafting, or the use of additives such as compatibilizers or coupling agents [19,28,29]. Reactive compatibilization is an interesting cost-effective one-step strategy consisting of the use of small amounts of reactive agents that possess functional groups with a tendency to react with the $-OH$ groups of the fibers and with the carboxylic end groups from polyesters by covalent bond interactions. Thus, the most popular reactive agents used include maleic anhydride groups, epoxy groups, or isocyanate groups [30,31]. Several examples of the use of reactive agents in polyester/fiber-based composites can be found in the literature. Diisocyanates have been used in PHBV/bamboo fibers [32] or poly(3-hydroxybutyrate-co-3-hydroxyvalerate) (PHBV)/poly(butylene adipate-co-terephthalate) (PBAT)/Switchgrass systems [33]. Epoxy-based reactive agents have been used in PLA/sisal fiber composites [34,35].

Another strategy could be by using radical generators that could arouse random linkages between the matrix and the reinforcement via radical intermediate species, such as peroxides. Dycumil

peroxide (DCP) has been used to compatibilize PHBV/Miscanthus fiber composites [31] or PHB and PHBV/ α -cellulose composites [36].

In this work, the efficiency as compatibilizers of four different reactive agents in fiber-based PHB composites was tested. The reactive agents used were dicumyl peroxide (DCP), hexamethylene diisocyanate (HMDI), resorcinol diglycidyl ether (RDGE), and triglycidyl isocyanurate (TGIC). The chemical structures of them are shown in Figure 1. In order to reduce variables and better understand the role of each reactive agent in this study, a high purified commercial cellulose fiber (TC90) with an α -cellulose content >99.5 % was selected, being the filler load set at 10 phr (i.e., per hundred mass of resin) for all compositions.

The effect of the different reactive agents on the PHB/cellulose interfacial interactions was studied by scanning electron microscopy (SEM), tensile tests, and dynamic mechanical analysis (DMA). Indeed, the effect of aging was assessed for all compositions. As maintained biodegradability is an important requirement for the applicability of these systems, the effect of the different reactive agents on the biodegradation under standard composting conditions (ISO 20200) was also evaluated.

With the aim of analyzing the influence of fiber purity on the compatibilization efficiency, untreated rice fibers (U_RH) and chemically purified rice husk fibers (T_RH) according to a previous work [37] were used using HMDI as a compatibilizer. The mechanical performance and the morphology were analyzed, and the results were compared with the use of the commercial cellulose.

Finally, since packaging is one of the potential application fields for these composites, the suitability of PHB/T_RH/HMDI composites to be processed by thermoforming was tested. This process has been chosen for both its difficulty and for being one of the most popular forming techniques used in the packaging industry.

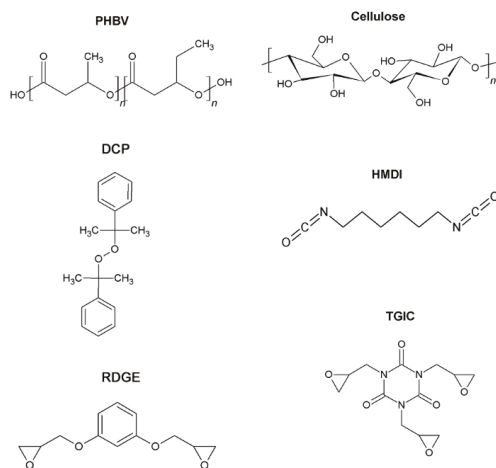


Figure 1. Chemical structures of polyhydroxybutyrate (PHB), cellulose, and the reactive agents.

2. Materials and Methods

2.1. Materials

Poly(3-hydroxybutyrate) was supplied by Biomer[®] (Schwalbach, Germany) in pellet form (P309). Purified α -cellulose fiber grade with an α -cellulose content >99.5% (TC90) was purchased from CreaFill Fibers Corp. (Chestertown, MD, USA). Rice husk (RH) by-product from the rice production process was kindly provided by Herba Ingredients (Valencia, Spain). The four reactive agents used (dicumyl peroxide (DCP), hexamethylene diisocyanate (HMDI), resorcinol diglycidyl ether (RDGE), and triglycidyl isocyanurate (TGIC)) were purchased from Sigma Aldrich (Madrid, Spain). Sodium

hydroxide (NaOH, 98%), hydrogen peroxide (H₂O₂, 30%), glacial acetic acid (CH₃COOH, 99%), and sulfuric acid (H₂SO₄, 98%) were purchased from Sigma Aldrich (Madrid, Spain).

2.2. Rice Husk Fibers Preparation

RH fibers were ground in a mechanical knife mill and then sieved in 140 µm mesh. These untreated RH fibers were named U_RH. A fraction of the ground and sieved RH fibers were subjected to a two-stage purification treatment in order to remove the major parts of impurities and non-cellulosic components such as waxes, lignin, and hemicelluloses. The first stage consisted of an alkaline attack with NaOH (5% *w/v*, fiber/liquid ratio of 1:20, 80 °C, 2 h). This treatment was applied twice. The second stage consisted of an oxidative attack with peracetic acid (PAA) (fiber/liquid ratio of 1:20, 80 °C, 4 h). The peracetic acid was prepared by the mixing of 30% (*v/v*) hydrogen peroxide and acetic acid in the reaction medium with a volume ratio of 3:1 at room temperature and 1% (*w/w*) of sulfuric acid as catalyzer. This procedure was adapted from the literature [38,39]. After each stage, the fibers were filtered and washed repeatedly in distilled water until neutral pH was reached. The purified powder was dried at 60 °C for at least 24 hours and ground again to break the aggregates formed during the filtration process and then sieved in a 140 µm mesh. The as-treated RH fibers were named as T_RH.

2.3. Composites Preparation

In order to assess the role of reactive agents as compatibilizers, compounds of purified commercial cellulose (TC90) were prepared with all reactive agents. The effect of the cellulose purity was studied on rice husk fibers, with and without chemical treatment, using HMDI as the reactive agent. For the sake of comparison and to evaluate the effects of the compatibilizers on the matrix, blank compounds (without cellulose) were prepared as controls. All the compositions studied are summarized in Table 1.

The compounds were prepared by melt extrusion in a twin-screw co-rotating extruder (DUPRA SL, Castalla, Spain) with an L/D ratio of 24 and a diameter of 2.5 cm. All the components were dried before extrusion; PHB pellets were dried in a dehumidifier Piovan DPA50 (Piovan, Maria di Sala VE, Italy) at 60 °C following the producer's drying recommendations and the fibers (TC90, U_RH and T_RH) were dried in an oven at 100 °C for at least 2 h. The formulations were manually premixed in zip-bags. The temperature profile of the extruder was set as follows: 165/170/175/180 °C (from the hopper to the extruder die), and the screw speed was kept constant at 40 rpm. The extrudate material was pelletized and dried following the same considerations as pure PHB.

Table 1. Summary of studied formulations. DCP: dicumyl peroxide, HMDI: hexamethylene diisocyanate, RDGE: resorcinol diglycidyl ether, TGIC: triglycidyl isocyanurate.

Sample	Component (phr)							
	PHB	TC90	U_RH	T_RH	DCP	HMDI	RDGE	TGIC
PHB	100			-	-	-	-	-
PHB/DCP	100			-	1	-	-	-
PHB/HMDI	100			-	-	1	-	-
PHB/RDGE	100			-	-	-	1	-
PHB/TGIC	100			-	-	-	-	1
PHB/TC90	100	10		-	-	-	-	-
PHB/TC90/DCP	100	10		-	1	-	-	-
PHB/TC90/HMDI	100	10		-	-	1	-	-
PHB/TC90/RDGE	100	10		-	-	-	1	-
PHB/TC90/TGIC	100	10		-	-	-	-	1
PHB/U_RH	100		10	-	-	-	-	-
PHB/U_RH/HMDI	100		10	-	-	-	-	-
PHB/T_RH	100			10	-	-	-	-
PHB/T_RH/HMDI	100			10	-	1	-	-

From the extruded pellets, different samples were obtained by compression molding in a parallel plate hot-press (180 °C, 2 min for premelting followed by 2 min at 3 bar): bars of 50 × 12.5 × 3.5 mm for dynamic mechanical analysis tests, films of 0.4 mm nominal thickness for uniaxial mechanical tests, films of 0.2 mm nominal thickness for composting tests, and films of 0.8 mm nominal thickness for thermoforming essays. Samples with neat PHB were processed and tested at the same conditions as the compounds.

2.4. Methods

The morphology of PHB/TC90, PHB/U_RH, and PHB/T_RH composites with and without reactive agents was examined by scanning electron microscopy (SEM), using a high-resolution field-emission microscope (JEOL 7001F, Tokyo, Japan). The samples were prepared by cryofracturing after immersion in liquid nitrogen and then coated by sputtering with a thin layer of Pt.

Differential scanning calorimetry (DSC) experiments were conducted on a DSC2 (Mettler Toledo, Columbus, OH, USA) with an intracooler Julabo FT900 (Julabo, Seelbach, Germany) calibrated with Indium standard before use. Samples were analyzed at 0 days (after hot-pressed films obtention) and after 100 days, to account for physical aging at room temperature. The samples weighing typically 6 mg were first heated from −20 °C to 200 °C at 10 °C/min, kept for 5 min to erase thermal history, and cooled down to −20 °C at 10 °C/min. Then, a second heating scan to 200 °C at 10 °C/min was performed. Crystallization temperatures (T_c), melting temperatures (T_m), and melting enthalpies (ΔH_m) were calculated from all respective heating/cooling scans. The crystallinity (X_c) of the PHB-reactive agent compositions was determined by applying the expression (1) [40]:

$$X_c(\%) = \frac{\Delta H_m}{w \cdot \Delta H_m^0} \times 100 \quad (1)$$

where ΔH_m (J/g) is the melting enthalpy of the polymer matrix, ΔH_m^0 is the melting enthalpy of 100% crystalline PHB (perfect crystal) (146 J/g) [16], and w is the PHB weight fraction in the blend.

Tensile tests were conducted in a universal testing machine Shimadzu AGS-X 500N (Shimadzu, Kyoto, Japan) at room temperature with a crosshead speed of 10 mm/min. Dumbbell 400 μm -thick samples were die-cut from the hot-pressed films and tested according to ASTM D638 (Type IV) standard. The samples were tested immediately after processing (0 days) and after 15 days of aging at room temperature. All the samples were stored in a vacuum desiccator at ambient temperature until tested.

Dynamic mechanical analysis (DMA) experiments were conducted on hot-pressed sample bars (55 × 12.5 × 3.5 mm) in an AR G2 oscillatory rheometer (TA Instruments, New Castle, DE, USA) equipped with a clamp system for solid samples (torsion mode). Samples were heated from −20 °C to melting temperature with a heating rate of 2 °C/min at a constant frequency of 1 Hz. The maximum deformation (γ) was set to 0.1%.

Disintegration tests under standard composting conditions (ISO 20200 [41]) were carried out with samples of (15 × 15 × 0.2 mm³) obtained from hot-pressed plates. Solid synthetic waste was prepared by mixing 10% of activated mature compost (VIGORHUMUS H-00, purchased from Burás Profesional, S.A., Girona, Spain), 40% sawdust, 30% rabbit feed, 10% corn starch, 5% sugar, 4% corn seed oil, and 1% urea. The water content of the mixture was adjusted to 55%. The samples were placed inside mesh bags to simplify their extraction and allow the contact of the compost with the specimens; then, they were buried in compost bioreactors at 4–6 cm depth. Bioreactors were incubated at 58 °C. The aerobic conditions were guaranteed by mixing the synthetic waste periodically and adding water according to the standard requirements. Two replicates of each sample were removed from the boxes at different composting times for analysis. Samples were washed with water and dried under vacuum at 40 °C until reaching a constant mass. The disintegration degree was calculated by normalizing the sample weight to the initial weight with Equation (2):

$$D = \frac{m_i - m_f}{m_i} \times 100 \quad (2)$$

where m_i is the initial dry mass of the test material and m_f is the dry mass of the test material recovered at different incubation stages. The disintegration study was completed taking photographs for visual evaluation.

The thermoformability of PHB/T_{RH}/HMDI was tested by a vacuum-assisted thermoforming technique in a pilot plant (SB 53c, Illig, Helmut Roegele, Heilbronn, Germany) equipped with an infrared emitter heating device. The mold used was a female circular tray that was 55 mm in diameter and 15 mm in depth with an edge radius of 5 mm. Rectangular hot-pressed sheets of a typical thickness of 800 μm were used for this study. The sheets were stamped with a square grid pattern (0.5 \times 0.5 cm) in order to track the deformation that occurred during their mold conformation. The infrared heater was set to 600 $^{\circ}\text{C}$, whereas the heating and vacuum times (ranging between 20–45 s and 3–20 s, respectively) were optimized in each case to obtain the best results.

3. Results

3.1. Influence of Reactive Agents in PHB/Cellulose Composites

3.1.1. Morphological Analysis

In order to assess the role of the reactive agents, blends with TC90 were prepared as detailed in the experimental section. The morphology of the PHB/TC90 composites with and without the reactive agents has been analyzed by SEM. Low magnification images were used to study the distribution of the fibers within the polymer matrix, and high magnification ones were used to examine the fiber/matrix interface. The micrographs of the different composites are shown in Figure 2.

As it can be observed in Figure 2a,c,e,g,i, in general, the fibers are well distributed within the polymer matrix, and we do not detect the presence of fiber aggregates, indicating an effective compounding. Despite this well dispersed and distributed morphology points to some type of fiber/matrix interaction (probably hydrogen bonding), the presence of some voids and prints caused by detached fibers (Figure 2a) as well as the gap observed between the fiber and the matrix (Figure 2b) are indicative of a certain lack of adhesion. Then, it can be said that there are some interactions in the melt that favor homogeneous dispersion, but those are not strong enough to provide an effective interface between both components.

Regarding the reactive agents, no remarkable differences in morphology are detected in PHB/TC90 composites with reactive agents compared with the composite without them. Although the major part of the fibers seems to be well embedded into the polymer matrix, some pull-out and detached fibers are detected, as well as a small gap between the fibers and the matrix. With regard to the use of DCP, contrary to other works reported in literature [31,36,42], in our case, no clear enhancement of compatibilization between fibers and matrix can be appreciated by SEM. In the same way, any compatibilization effect was found for the RDGE. Similarly, the TGIC did not show any additional compatibilization effect, as this was unexpected [34]. However, in PHB/TC90/HMDI composites, there is an improvement of fiber–matrix adhesion, finding no fiber pull-outs or detachment in the micrographs (Figure 2e). In this case, the fibers seem to be well covered by the polymer, and fibers broken on their longitudinal direction can be observed (Figure 2f), thus indicating a cohesive failure. Thus, SEM observations would be in agreement with a strong adhesion between the fibers and the PHB matrix. This is probably due to the formation of urethane linkages between the isocyanate groups of HMDI and hydroxyl (–OH) groups from the fibers and/or hydroxyl or carboxylic chain ends of PHB, as it has been proposed in the literature for biopolyester/fiber systems compatibilized with isocyanates [33].

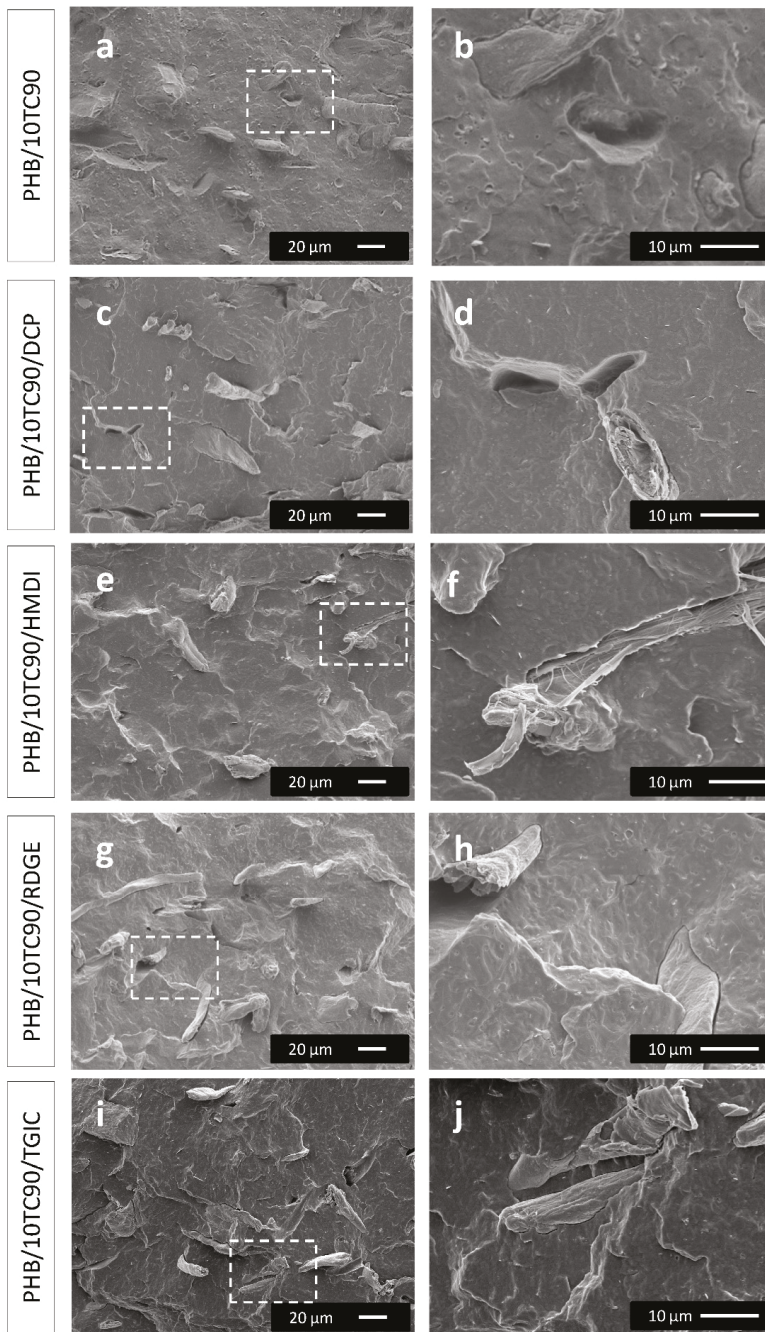


Figure 2. SEM micrographs of PHB/TC90 composites with and without reactive agents. The images in the right column (**b,d,f,h,j**) show higher magnifications of the areas indicated with a square in their corresponding images in the left column (**a,c,e,g,i**).

3.1.2. Thermal Properties

DSC experiments were run in all samples. The thermograms were obtained from the films recently processed (0 days) and after 100 days of storage at room temperature, when it is supposed that all secondary crystallization and physical aging phenomena has taken place [15,43]. It can be seen in the thermograms that aging only affected the first heating scans. The second heating scans, after erasing the thermal history and controlled cooling at 10 °C/min, were the same for 0 and 100 days, thus confirming that there were no significant structural changes during storage. Therefore, no signs of degradation were evidenced for this period. All the results are summarized in Table 2.

Table 2. Differential scanning calorimetry (DSC) parameters for neat PHB with and without reactive agents and PHB/TC90 composites with and without reactive agents.

	1st Heating Scan						Cooling Scan		2nd Heating Scan		
	0 days			100 days			T _c (°C)	ΔH _c (J/g)	T _m (°C)	ΔH _m (J/g)	X _c (%)
	T _m (°C)	ΔH _m (J/g)	X _c (%)	T _m (°C)	ΔH _m (J/g)	X _c (%)					
PHB	175	72	49	170	86	59	117	91	170	94	64
PHB/DCP	167	71	49	167	73	50	115	81	160	84	58
PHB/HMDI	173	69	48	173	79	55	106	86	167	90	62
PHB/RDGE	172	75	52	173	81	56	115	88	168	91	63
PHB/TGIC	173	77	53	172	80	56	116	89	168	92	64
PHB/TC90	173	74	56	173	73	55	117	82	169	84	63
PHB/TC90/DCP	166	67	51	165	66	50	118	75	161	78	59
PHB/TC90/HMDI	173	71	49	173	72	55	111	78	169	81	62
PHB/TC90/RDGE	172	76	52	173	73	56	115	79	169	85	65
PHB/TC90/TGIC	167	78	54	172	73	55	118	79	166	85	64

The melting behavior and crystallinity index during first heating scans of the composites are affected in different extents by the different components. However, it must be considered that the crystal morphologies developed during cooling correspond to processing conditions, which implies higher cooling rates with respect to DSC-controlled cooling at 10 °C/min.

Neat processed PHB presents a melting peak temperature of 175 °C and a crystallinity index (X_c) of 49% at 0 days. After aging, X_c increases to 59%, and the melting peak temperature changes to 170 °C, due to secondary crystallization [44]. After erasing thermal history, the cooling of PHB yields a crystallization peak temperature of 117 °C and ΔH_c of 91 J/g, which corresponds to an X_c value of 63% (for either aged or unaged samples).

Regarding the influence of the reactive agents on X_c, at 0 days, PHB/DCP and PHB/HMDI show similar crystallinity indexes than neat PHB, whereas in PHB/RDGE and PHB/TGIC compounds, X_c is slightly higher. The melting temperatures, on the other hand, are similar to that corresponding to neat PHB, with the exception of DCP, which is slightly inferior. After 100 days of aging, the crystallinity index of PHB with the different reactive agents is in all cases inferior with respect to neat PHB, especially in case of DCP, for which melting parameters remain practically unchanged compared to the unaged sample. This can be related with the crosslinking effect of DCP, which generates free radicals and disrupts the linearity of the PHB chains, thus limiting the maximum crystallinity that can be developed [45].

The presence of the reactive agents (with or without fibers) seems to partially hinder the secondary crystallization [46], as the crystallinity index achieved at 100 days is in all cases inferior to that corresponding to neat PHB. Indeed, it seems that the sole presence of the fibers restricts the mobility of polymer chains, partly hindering the development of crystallization during aging, since the increase in the crystallinity index is not observed over time for the PHB/TC90 composites. According to the literature, fillers can restrict the polymer chain mobility [24], which could result in a stabilized crystallinity index over time.

After erasing the thermal history, no remarkable differences in crystallization temperatures or enthalpies were observed among the compounds, except in the case of HMDI addition. Compounds with HMDI showed lower T_c values than the other compositions, finding a reduction of T_c from 117 °C to 106 °C in PHB/HMDI and 111°C in PHB/TC90/HMDI samples. These findings can be related with some hindered motion of the polymer chains, thus suggesting the interaction of HMDI with the polymer matrix and the fibers [47].

With respect to melting in second heating scans, after low cooling rates where polymer chains had enough time and mobility to develop high crystallinity (10 °C/min during DSC test conditions), the crystallinity indexes and melting temperatures of the different compositions were similar to those corresponding to neat PHB, except for the compositions containing DCP. For DCP-containing compounds, significant reductions of T_m and X_c was detected, being in agreement with some crosslinking of the PHB matrix with the peroxide initiator DCP [45].

3.1.3. Mechanical Properties

PHB is known by its physical aging and secondary crystallization [15,16,43]. So, the mechanical performance depends on time after its processing. For such a reason, tensile properties have been assessed after processing (0 day) and after 15 days stored at room temperature. According to Corre et. al., after such a period of time, the variations on the mechanical properties are so small that it can be said that the properties are stabilized [16]. The mechanical properties of all compounds were determined by uniaxial tensile tests up to failure. Representative stress versus strain curves of the composites with TC90 are shown in Figure 3. The average parameters obtained from the curves are summarized in Table 3, and selected values are represented in Figure 4 to illustrate the trends observed.

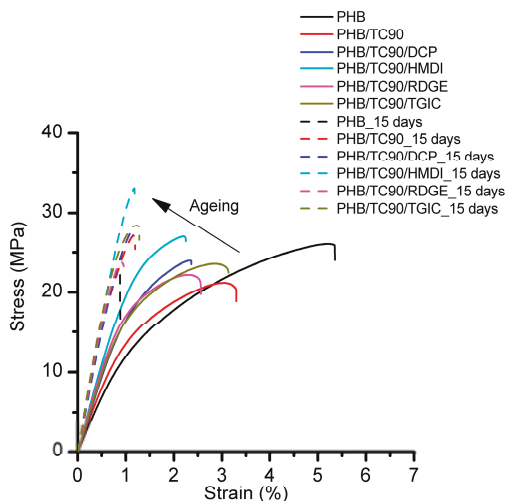


Figure 3. Representative stress–strain curves of neat PHB and PHB/TC90 composites at 0 days (solid lines) and after 15 days of aging (dashed lines).

Neat PHB shows a high variation in its tensile behavior due to aging. The elastic modulus increased more than 100% after 15 days, and the deformation at break decreased five times. In both cases, the failure mode is brittle, with unstable fracture and without showing necking nor evidence of shear yielding. The cause for such behavior is attributed to secondary crystallization and the physical aging of the amorphous region [15,16,43].

Table 3. Mechanical parameters corresponding to tensile tests.

	0 Days	15 Days	0 Days	15 Days	0 Days	15 Days	0 Days	15 Days
	Elastic Modulus (GPa)		Tensile Strength (MPa)		Elongation at Break (%)		Static Toughness (mj/m ³)	
PHB	1.41	3.04	25.89	23.03	4.96	0.98	0.84	0.13
P309/DCP	1.54	2.75	24.88	29.77	3.87	1.55	0.62	0.27
P309/HMDI	1.82	3.15	23.36	24.36	2.50	0.86	0.38	0.10
P309/RDGE	1.54	2.90	23.42	29.32	3.62	1.55	0.57	0.27
P309/TGIC	1.48	3.03	24.76	30.95	4.28	1.43	0.72	0.25
P309/TC90	1.71	3.44	21.27	27.14	3.49	1.21	0.53	0.19
P309/TC90/DCP	1.92	3.19	23.64	26.83	2.23	1.15	0.34	0.18
P309/TC90/HMDI	2.31	3.49	26.75	32.11	2.04	1.16	0.35	0.20
P309/TC90/RDGE	2.10	3.40	21.71	25.06	2.42	1.07	0.37	0.16
P309/TC90/TGIC	2.02	3.59	23.89	28.06	3.22	1.22	0.56	0.21

When reactive agents are added to PHB, at 0 days, there is a minimum increase in elastic modulus in the case of addition of DCP, RDGE, and TGIC and a more pronounced one with HMDI (Table 3). However, after 15 days, PHB/DCP elastic modulus is 9% lower than neat PHB. The reactivity with the polymer matrix can account for this behavior. For DCP, the generation of some crosslinking is in agreement with lower development in crystallinity and hence a reduction on elastic modulus [45]. With respect to RDGE and TGIC, some reactivity is also evidenced, but in a way that it seems to affect the amorphous region, since after 15 days, they are able to withstand higher deformations prior to rupture and show higher tensile strength before a crack generates and propagates through the PHB. It could be hypothesized that more voluminous RDGE and TGIC disrupt the pseudo-order in the rigid amorphous phase region. This is not observed in PHB/HMDI compounds, probably because of the small and linear geometry of the HMDI molecule, which does not prevent the rearrangements of the amorphous phase that take place during physical aging [16,17,43,48].

When cellulose (TC90) is added to neat PHB (at 0 days), an increase in elastic modulus and a reduction of tensile strength and ductility is observed (Figure 3). The increase in modulus of elasticity is attributed to the reinforcement effect of the cellulose fibers. However, the addition of TC90 promotes rupture at even lower stress than in the case of Neat PHB (and therefore, much lower than yielding). Along with the increase of elastic modulus, this behavior suggests that cellulose acts as a reinforcement in PHB matrix at low strains, but after a certain point, it promotes the appearance of large defects that nucleate cracks that lead to brittle fracture, explaining the low values of tensile strength and elongation at break.

When reactive agents are added, the elastic modulus rises in all cases with respect to either cellulose without reactive agents or PHB with reactive agents. Similarly, the tensile strength also rises; both suggest an increase of affinity between the matrix and reinforcement. However, deformation at break does not increase, and it remains at a similar value as uncompatibilized TC90.

To better understand the role of TC90 and the different reactive agents on the mechanical behavior of PHB after aging (15 days), the elastic modulus, tensile strength, and elongation at break values of the composites are depicted in Figure 4.

After aging, the incorporation of TC90 fibers to PHB results in a slight improvement of elastic modulus and tensile strength, while showing a comparable elongation at break. In Figure 4a, it can be appreciated that the elastic modulus of all the composites is improved with respect to neat PHB (about 13% for PHB/TC90). This behavior can be reasonably ascribed to the affinity between the rigid cellulose fibers and the PHB matrix. The addition of the reactive agents to the PHB/TC90 compounds did not show any remarkable additional improvement of the elastic modulus at 15 days with respect to the composites without them. However, in the case of tensile strength values, an interesting increase of about 18% with respect to PHB/TC90 is detected in the PHB/TC90/HMDI compound. This rise suggests

that HMDI had an effective compatibilizer role, strengthening the bonding of the cellulose fibers with the PHB matrix.

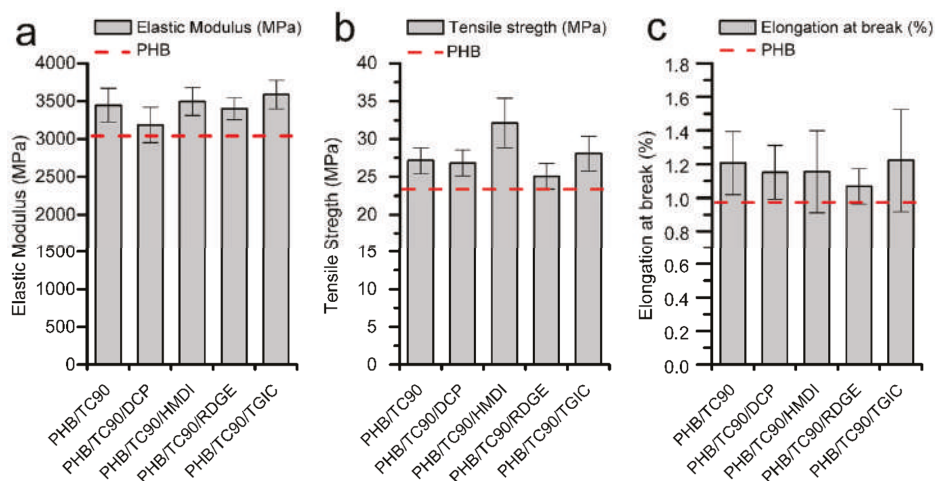


Figure 4. (a) Elastic modulus, (b) tensile strength, and (c) elongation at break of aged samples of neat PHB and PHB/TC90 composites with and without reactive agents.

The mechanical characterization of the composites was completed by DMA testing. Their storage modulus (G') and the damping factor ($\tan \delta$) evolution with temperature are represented in Figure 5.

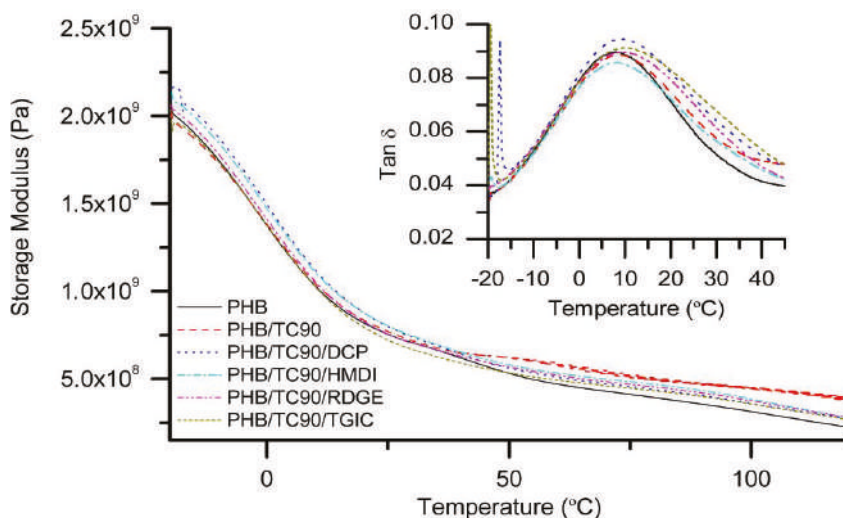


Figure 5. Storage modulus (G') and $\tan \delta$ (inset) evolution with temperature for neat PHB and PHB/TC90 composites with reactive agents.

No appreciable differences in storage modulus among the different samples are observed. These results are in agreement with the elastic modulus observed in mechanical tests. The $\tan \delta$ represents the energy dissipated during the dynamic tests, and the $\tan \delta$ peak is usually used to determine glass transition (T_g) in semicrystalline polymers [49]. In this case, all the samples present T_g

values around 10 °C. Nevertheless, the $\tan \delta$ versus temperature plot suggest certain restricted mobility of the polymer chains in composites, since the $\tan \delta$ peaks are broader than neat PHB [50]. Moreover, the height of the $\tan \delta$ peak corresponding to PHB/TC90/HMDI is reduced compared to the rest of composites, indicating the further hindered motion of the polymer chains. This can be related with a better interaction between PHB and TC90 fibers due to the compatibilization effect of HMDI [30].

3.2. Influence of Fiber Purity

3.2.1. Morphological Analysis

As it has been discussed above, HMDI has demonstrated its efficiency at improving the interfacial adhesion between PHB and highly purified commercial cellulose fibers (TC90). In this section, the compatibilization ability of HMDI is tested using an unpurified rice husk fiber (U_RH) and a chemically treated rice husk fiber (T_RH) to study the combined effect of purification treatment and compatibilizer on the interfacial PHB/fiber interactions.

SEM micrographs (shown in Figure 6) allow visualizing qualitatively the matrix/fiber interface interactions of PHB/ U_RH and PHB/T_RH composites, with and without HMDI.

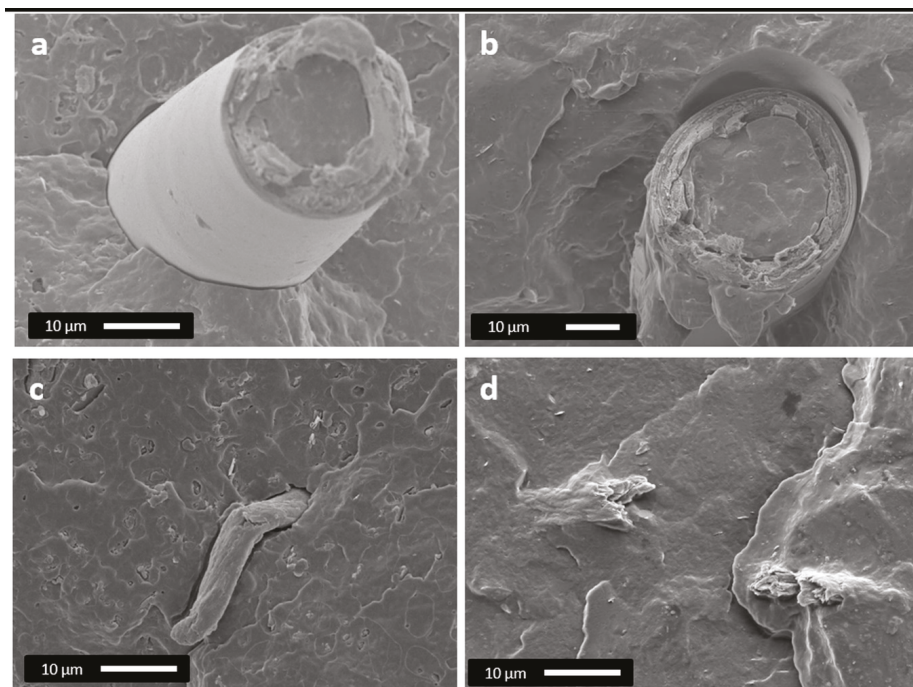


Figure 6. (a) SEM micrographs of PHB/U_RH, (b) PHB/U_RH/HMDI, (c) PHB/T_RH, and (d) PHB/T_RH/HMDI.

As it can be observed in Figure 6a, U_RH fibers within the compound present a smooth surface and show a gap between the fiber and the polymer matrix. A similar gap between these two components is also observed in PHB/U_RH/HMDI composition (Figure 6b). In case of treated fibers (PHB/T_RH), the fibers present a smaller diameter and a rougher surface than the untreated ones, but detachment of the fibers is also detected, thus indicating a certain lack of adhesion (Figure 6c). In the case of treated and compatibilized fibers (Figure 6d), they appear well covered by the polymer and no gap or signs of detachment at the interphase are detected, suggesting an improved adhesion.

3.2.2. Mechanical Properties

Uniaxial tensile tests of PHB/U_RH and PHB/T_RH with and without HMDI were performed on 15-day aged samples at room temperature. Elastic modulus, tensile strength, elongation at break, and the static toughness obtained from the area below the stress–strain representative curves for each composite are depicted in Figure 7. The mechanical parameters corresponding to neat PHB are also represented as a reference.

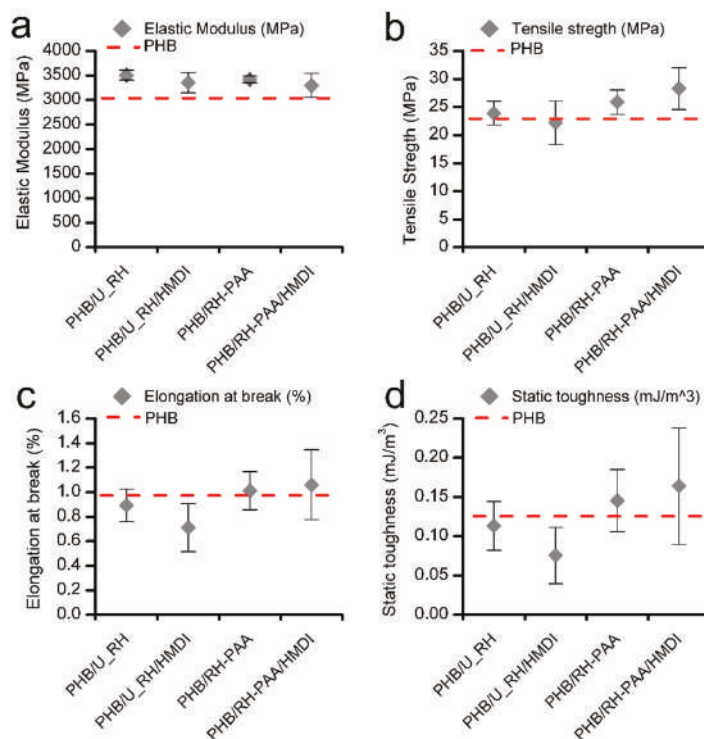


Figure 7. (a) Elastic modulus, (b) tensile strength, (c) elongation at break, and (d) static toughness of neat PHB, PHB/U_RH, and PHB/T_RH composites with and without reactive agents.

The addition of either U_RH or T_RH fibers produces a reinforcement effect with respect to neat PHB, since an increment of the modulus of elasticity is detected in all cases. On the other hand, the tensile strength seems to increase only when the treated fibers are the ones added, where the use of HMDI on such treated fibers produced an additional improvement of this parameter. For composites with treated fibers, the elongation at break remains similar to that of neat PHB, whereas for the untreated ones, this parameter is reduced (especially in the case with HMDI, in agreement with values reported for PHB/HMDI samples in Table 3). These results suggest that in the case of the untreated fibers, there is no interaction of HMDI between the polymer and the reinforcement.

Despite the fact that in all cases, the samples present a brittle behavior, the addition of the treated fibers leads to a visible trend of improvement of the static toughness, compared with neat PHB, especially with the addition of HMDI. Nevertheless, the enhancement of the mechanical performance was not as pronounced as in the case of the compound prepared in the previous section, with high-purity commercial cellulose (PHB/TC90/HMDI).

3.2.3. Thermoforming Ability

PHB-based composites reinforced with fibers are considered an attractive alternative to commodities for short-term life applications such as packaging. For this reason, it is of particular interest to test their processability by thermoforming, which is a conventional technique that is usually applied in this industrial field. In this regard, PHB/T_RH/HMDI films have been thermoformed into trays following the procedure described in the experimental section, and the best results obtained are presented in Figure 8.



Figure 8. PHB/T_RH/HMDI thermoformed tray: (a) bottom-side view, (b) top-side view and (c) bottom view.

As it can be observed in Figure 8, thermoformed trays with good mold reproducibility and relatively good thickness distribution (punctual thickening is observed in Figure 8c) can be obtained by adjusting the operational parameters. In our case, the best results were obtained for a heat resistance temperature fixed at 600 °C, a heating time of 35 s, and 7 s applying vacuum. The difficulties of thermoforming semicrystalline polymers [18,51,52] and even more filled with fibers are well recognized, so the results obtained here are very promising.

3.2.4. Biodisintegration in Composting Conditions

One of the strengths of the PHB/fiber composites that make them especially attractive for packaging applications is their biodegradability and specifically their compostability. For this reason, it is of special interest to evaluate the effect of the reactive agents on the behavior under normalized composting conditions of the composites. Biodisintegration tests were conducted according to the ISO 20200 standard. The weight loss over time of the tested materials is represented in Figure 9, and pictures of the samples at different composting times are depicted in Figure 10.

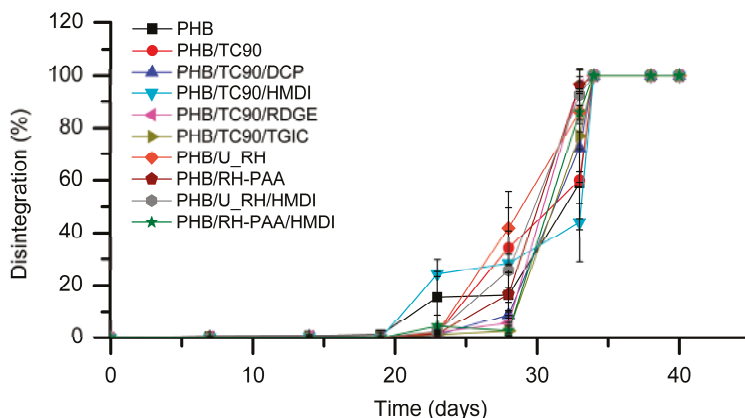


Figure 9. Disintegration of neat PHB and the studied composites over time under standard composting conditions (ISO 20200).

As shown in Figure 9, in neat PHB, the biodisintegration process occurs with an incubation period of about 23 days. From this time, appreciable weight loss is detected, and total disintegration (considered when fragments >2 mm are not detectable) is reached at 35 days of composting. For PHB/TC90 composites containing DCP, RDGE, and TGIC, the incubation period seems to be slightly longer. At intermediate composting times, some differences in weight loss among the samples were detected. However, these differences do not reveal a clear trend related with the presence or not of the different fibers or reactive agents. In any case, all the compositions reached total biodisintegration in the same period than neat PHB (35 days). Some authors have reported an accelerated biodegradation of biopolyesters with the incorporation of lignocellulosic fibers [23,25]. In our case, no remarkable differences were observed, as we had already previously noticed in PHBV/TC90 [53] and PHB/lignocellulosic composites [54].

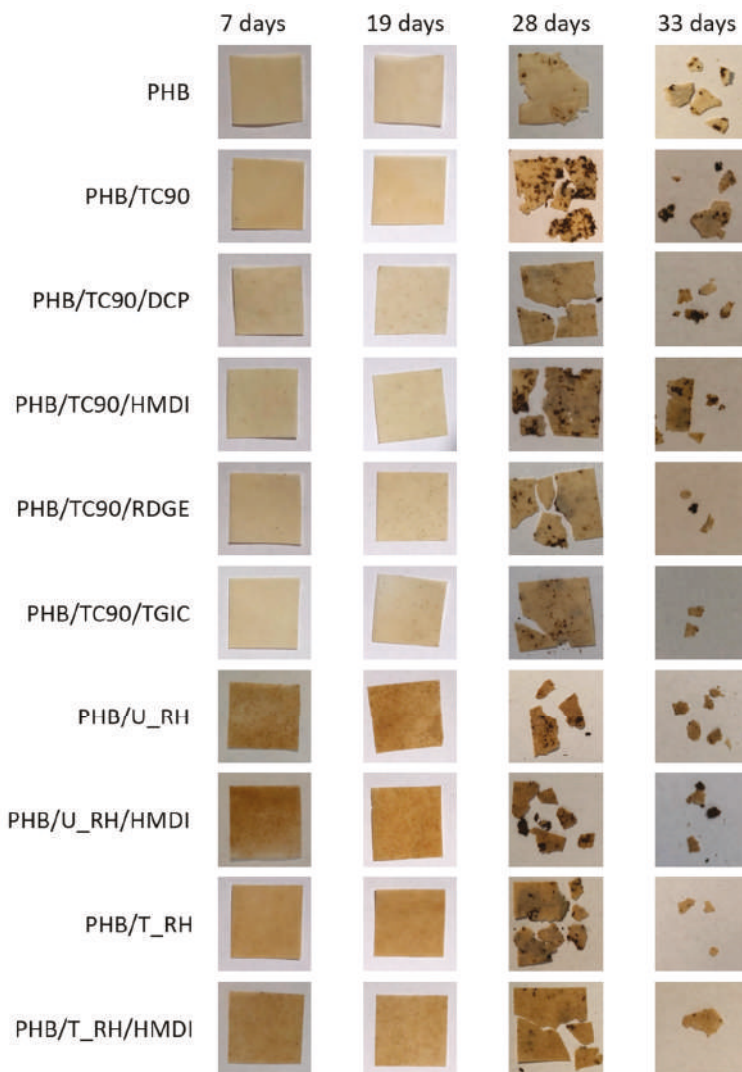


Figure 10. Pictures of neat PHB and the studied composites at different composting times.

As shown in Figure 10, no remarkable physical changes can be visually detected in the samples during the incubation period (pictures corresponding to 7 and 19 days of composting). At 28 days, clear deterioration of the samples is observed. The specimens are eroded and broken. As it has been reported in the literature, the biodisintegration process of PHB occurs by erosion from the surface to the bulk being the amorphous regions degraded in first place [55,56]. This leads to embrittlement and breakage of the samples. At 33 days of composting, all the samples appear broken into very small fragments.

According to these results, it can be concluded that neither the fibers nor the reactive agents have a negative effect on the biodisintegrability of PHB in composting conditions.

4. Discussion

Analyzing together the results obtained for the composites prepared with TC90, U_RH, and T_RH fibers with and without HMDI, it seems clear that the compatibility efficiency of the HMDI depends to a large extent on the purity of the fibers. Probably, this dependence is due to a greater presence of OH groups on the surface of the purified fibers, since it is assumed that compatibilization occurs through the formation of urethane bonds between the isocyanate groups of the HMDI and the hydroxyl groups of the fibers [33]. Tran et al. [57] also showed better results in PLA composites filled with rice and einkorn wheat husks using silane coupling agents, when fibers were previously submitted to an alkaline treatment.

As reported in previous works [54], U_RH fibers present waxes and impurities on their surface, which could be responsible for their poor adhesion with the PHB matrix. In addition, in lignocellulosic fibers, the cellulose is embedded in a matrix of non-cellulosic components (mainly composed by lignin, hemicelluloses, and pectin). All this limits the exposition of the reactive –OH groups of the cellulose for compatibilization. The purification treatment applied removed those waxes and impurities on the fibers surface, as well as most of the non-cellulosic components, leaving a greater amount of reactive –OH groups at the surface that could react with the compatibilizer. In addition, the treatment resulted in fibers with more favorable morphology and surface characteristics (i.e., a higher aspect ratio and roughness) that also contributed to improve the mechanical properties, even without the presence of a compatibilizer.

5. Conclusions

In this work, PHB/TC90 composites were obtained by reactive extrusion using four different reactive agents: dicumyl peroxide (DCP), hexamethylene diisocyanate (HMDI), resorcinol diglycidyl ether (RDGE), and triglycidyl isocyanurate (TGIC). The effect of aging attending on the influence of the reactive agents and the fibers on the mechanical and crystallization behavior of the composites was assessed. Aging produced a drastic embrittlement of the PHB characterized by increased elastic modulus and decreased tensile strength, elongation at break, and toughness. This embrittlement was attributed to secondary crystallization, which increased the value of X_c by about 17% in neat PHB samples, but also to the physical aging of the amorphous fraction. Both fibers and reactive agents partly hinder secondary crystallization, leading to lower crystallinity in aged composites with respect to neat PHB. The melting temperature and crystallinity index for the compositions containing DCP were reduced at high cooling rates (processing conditions) and low cooling rates (DSC conditions), suggesting crosslinking of the PHB matrix.

No clear compatibilization effect was found for the reactive agents DCP, RDGE, and TGIC. Elastic modulus, tensile strength, and elongation at break remained practically unchanged for PHB/TC90/DCP and PHB/TC90/TGIC compared with PHB/TC90. In the case of PHB/TC90/RDGE, those values were even lower than PHB/TC90. On the contrary, the tensile strength in PHB/TC90/HMDI was improved by about 40% with respect to neat PHB and around 18% with respect to the PHB/TC90 composite. The improved mechanical performance together with the SEM observations indicate enhanced interfacial adhesion between the TC90 fibers and PHB.

A clear influence of the purity of the fibers on the effectiveness of HMDI at improving interfacial adhesion was observed. HMDI only demonstrated effectiveness in purified cellulose fiber composites, the greatest improvements in the mechanical performance being the ones obtained with highly purified commercial cellulose fibers (TC90).

The different reactive agents did not negatively affect the compostability of PHB.

Finally, thermoformed trays with good mold reproducibility were successfully obtained for PHB/T_RH/HMDI composite.

Author Contributions: Conceptualization, J.G.-P., L.C. and J.M.L.; methodology, E.L.S.-S.; validation, J.G.-P., L.C. and J.M.L.; formal analysis, E.L.S.-S.; investigation, E.L.S.-S. and A.A.; resources, J.G.-P., L.C. and J.M.L.; data curation, E.L.S.-S. and A.A.; writing—original draft preparation, E.L.S.-S.; writing—review and editing, J.G.-P., L.C. and J.M.L.; supervision, J.G.-P., L.C. and J.M.L.; funding acquisition, J.G.-P., L.C. and J.M.L. All authors have read and agreed to the published version of the manuscript.

Funding: The authors would like to thank the financial support for this research from Ministerio de Ciencia e Innovación (RTI2018-097249-B-C22), Pla de Promoció de la Investigació de la Universitat Jaume I (UJI-B2019-44) and H2020 EU Project YPACK (H2020-SFS-2017-1, Reference 773872).

Acknowledgments: The authors would like to acknowledge the Instituto de Tecnología de Materiales of Universitat Politècnica de València-Campus de Alcoy, the Unidad Asociada IATA-UJI “Polymers Technology” and Servicios Centrales de Instrumentación Científica (SCIC) of Universitat Jaume I. We are also grateful to Raquel Oliver and Jose Ortega for experimental support.

Conflicts of Interest: The authors declare no conflict of interest.

References

1. Muneer, F.; Rasul, I.; Azeem, F.; Siddique, M.H.; Zubair, M.; Nadeem, H. Microbial Polyhydroxyalkanoates (PHAs): Efficient Replacement of Synthetic Polymers. *J. Polym. Environ.* **2020**, *28*, 2301–2323. [[CrossRef](#)]
2. Kumar, M.; Rathour, R.; Singh, R.; Sun, Y.; Pandey, A.; Gnansounou, E.; Andrew Lin, K.Y.; Tsang, D.C.W.; Thakur, I.S. Bacterial polyhydroxyalkanoates: Opportunities, challenges, and prospects. *J. Clean. Prod.* **2020**, *263*, 121500. [[CrossRef](#)]
3. Rujnić-Sokele, M.; Pilipović, A. Challenges and opportunities of biodegradable plastics: A mini review. *Waste Manag. Res.* **2017**, *35*, 132–140. [[CrossRef](#)] [[PubMed](#)]
4. Albuquerque, P.B.S.; Malafaia, C.B. Perspectives on the production, structural characteristics and potential applications of bioplastics derived from polyhydroxyalkanoates. *Int. J. Biol. Macromol.* **2018**, *107*, 615–625. [[CrossRef](#)] [[PubMed](#)]
5. Peelman, N.; Ragaert, P.; Ragaert, K.; De Meulenaer, B.; Devlieghere, F.; Cardon, L. Heat resistance of new biobased polymeric materials, focusing on starch, cellulose, PLA, and PHA. *J. Appl. Polym. Sci.* **2015**, *132*. [[CrossRef](#)]
6. Keskin, G.; Kizil, G.; Bechelany, M.; Pochat-Bohatier, C.; Öner, M. Potential of polyhydroxyalkanoate (PHA) polymers family as substitutes of petroleum based polymers for packaging applications and solutions brought by their composites to form barrier materials. *Pure Appl. Chem.* **2017**, *89*, 1841–1848. [[CrossRef](#)]
7. Bugnicourt, E.; Cinelli, P.; Lazzeri, A.; Alvarez, V. Polyhydroxyalkanoate (PHA): Review of synthesis, characteristics, processing and potential applications in packaging. *Express Polym. Lett.* **2014**, *8*, 791–808. [[CrossRef](#)]
8. Wang, Y.; Yin, J.; Chen, G.Q. Polyhydroxyalkanoates, challenges and opportunities. *Curr. Opin. Biotechnol.* **2014**, *30*, 59–65. [[CrossRef](#)]
9. Keshavarz, T.; Roy, I. Polyhydroxyalkanoates: Bioplastics with a green agenda. *Curr. Opin. Microbiol.* **2010**, *13*, 321–326. [[CrossRef](#)]
10. Możejko-Ciesielska, J.; Kiewisz, R. Bacterial polyhydroxyalkanoates: Still fabulous? *Microbiol. Res.* **2016**, *192*, 271–282. [[CrossRef](#)]
11. Dilkes-Hoffman, L.S.; Lant, P.A.; Laycock, B.; Pratt, S. The rate of biodegradation of PHA bioplastics in the marine environment: A meta-study. *Mar. Pollut. Bull.* **2019**, *142*, 15–24. [[CrossRef](#)] [[PubMed](#)]
12. Arcos-Hernandez, M.V.; Laycock, B.; Pratt, S.; Donose, B.C.; Nikolić, M.A.; Luckman, P.; Werker, A.; Lant, P.A. Biodegradation in a soil environment of activated sludge derived polyhydroxyalkanoate (PHBV). *Polym. Degrad. Stab.* **2012**, *97*, 2301–2312. [[CrossRef](#)]

13. Hermann, B.G.; Debeer, L.; De Wilde, B.; Blok, K.; Patel, M.K. To compost or not to compost: Carbon and energy footprints of biodegradable materials' waste treatment. *Polym. Degrad. Stab.* **2011**, *96*, 1159–1171. [[CrossRef](#)]
14. De Koning, G.J.M.; Scheeren, A.H.C.; Lemstra, P.J.; Peeters, M.; Reynaers, H. Crystallization phenomena in bacterial poly[(R)-3-hydroxybutyrate]: 3. Toughening via texture changes. *Polymer* **1994**, *35*, 4598–4605. [[CrossRef](#)]
15. Alata, H.; Aoyama, T.; Inoue, Y. Effect of Aging on the Mechanical Properties of Poly(3-hydroxybutyrate-co-3-hydroxyhexanoate). *Macromolecules* **2007**, *40*, 4546–4551. [[CrossRef](#)]
16. Corre, Y.-M.; Bruzaud, S.; Audic, J.-L.; Grohens, Y. Morphology and functional properties of commercial polyhydroxyalkanoates: A comprehensive and comparative study. *Polym. Test.* **2012**, *31*, 226–235. [[CrossRef](#)]
17. Esposito, A.; Delpouve, N.; Causin, V.; Dhotel, A.; Delbreilh, L.; Dargent, E. From a Three-Phase Model to a Continuous Description of Molecular Mobility in Semicrystalline Poly(hydroxybutyrate-co-hydroxyvalerate). *Macromolecules* **2016**, *49*, 4850–4861. [[CrossRef](#)]
18. González-Ausejo, J.; Sanchez-Safont, E.; Lagaron, J.M.; Olsson, R.T.; Gamez-Perez, J.; Cabedo, L. Assessing the thermoformability of poly(3-hydroxybutyrate-co-3-hydroxyvalerate)/poly(acid lactic) blends compatibilized with diisocyanates. *Polym. Test.* **2017**, *62*, 235–245. [[CrossRef](#)]
19. Pereira, P.H.F.; de Freitas, M.R.; Cioffi, M.O.H.; de Carvalho, K.C.C.B.; Milanese, A.C.; Voorwald, H.J.C.; Mulinari, D.R. Vegetal fibers in polymeric composites: A review. *Polímeros* **2015**, *25*, 9–22. [[CrossRef](#)]
20. Mohanty, A.K.; Misra, M.; Hinrichsen, G. Biofibres, biodegradable polymers and biocomposites: An overview. *Macromol. Mater. Eng.* **2000**, *276–277*, 1–24. [[CrossRef](#)]
21. Lagarón, J.M.; Lopez-Rubio, A.; Fabra, M.J. Bio-based packaging. *J. Appl. Polym. Sci.* **2015**, *133*. [[CrossRef](#)]
22. Bhardwaj, R.; Mohanty, A.K.; Drzal, L.T.; Pourboghra, F.; Misra, M. Renewable resource-based green composites from recycled cellulose fiber and poly(3-hydroxybutyrate-co-3-hydroxyvalerate) bioplastic. *Biomacromolecules* **2006**, *7*, 2044–2051. [[CrossRef](#)] [[PubMed](#)]
23. Gunning, M.A.; Geever, L.M.; Killion, J.A.; Lyons, J.G.; Higginbotham, C.L. Mechanical and biodegradation performance of short natural fibre polyhydroxybutyrate composites. *Polym. Test.* **2013**, *32*, 1603–1611. [[CrossRef](#)]
24. Torres-Tello, E.V.; Robledo-Ortiz, J.R.; González-García, Y.; Pérez-Fonseca, A.A.; Jasso-Gastinel, C.F.; Mendizábal, E. Effect of agave fiber content in the thermal and mechanical properties of green composites based on polyhydroxybutyrate or poly(hydroxybutyrate-co-hydroxyvalerate). *Ind. Crops Prod.* **2017**, *99*, 117–125. [[CrossRef](#)]
25. Batista, K.C.; Silva, D.A.K.; Coelho, L.A.F.; Pezzin, S.H.; Pezzin, A.P.T. Soil Biodegradation of PHBV/Peach Palm Particles Biocomposites. *J. Polym. Environ.* **2010**, *18*, 346–354. [[CrossRef](#)]
26. Barkoula, N.M.; Garkhail, S.K.; Peijs, T. Biodegradable composites based on flax/polyhydroxybutyrate and its copolymer with hydroxyvalerate. *Ind. Crops Prod.* **2010**, *31*, 34–42. [[CrossRef](#)]
27. Michel, A.T.; Billington, S.L. Characterization of poly-hydroxybutyrate films and hemp fiber reinforced composites exposed to accelerated weathering. *Polym. Degrad. Stab.* **2012**, *97*, 870–878. [[CrossRef](#)]
28. Rastogi, V.K.; Samyn, P. Novel processing of polyhydroxybutyrate with micro-to nanofibrillated cellulose and effect of fiber morphology on crystallization behaviour of composites. *Express Polym. Lett.* **2020**, *14*, 115–133. [[CrossRef](#)]
29. Wei, L.; McDonald, A. A Review on Grafting of Biofibers for Biocomposites. *Materials* **2016**, *9*, 303. [[CrossRef](#)]
30. Anderson, S.; Zhang, J.; Wolcott, M.P. Effect of Interfacial Modifiers on Mechanical and Physical Properties of the PHB Composite with High Wood Flour Content. *J. Polym. Environ.* **2013**, *21*, 631–639. [[CrossRef](#)]
31. Muthuraj, R.; Misra, M.; Mohanty, A.K. Reactive compatibilization and performance evaluation of miscanthus biofiber reinforced poly(hydroxybutyrate-co-hydroxyvalerate) biocomposites. *J. Appl. Polym. Sci.* **2017**, *134*. [[CrossRef](#)]
32. Jiang, L.; Chen, F.; Qian, J.; Huang, J.; Wolcott, M.; Liu, L.; Zhang, J. Reinforcing and Toughening Effects of Bamboo Pulp Fiber on Poly(3-hydroxybutyrate-co-3-hydroxyvalerate) Fiber Composites. *Ind. Eng. Chem. Res.* **2010**, *49*, 572–577. [[CrossRef](#)]
33. Nagarajan, V.; Misra, M.; Mohanty, A.K. New engineered biocomposites from poly(3-hydroxybutyrate-co-3-hydroxyvalerate) (PHBV)/poly(butylene adipate-co-terephthalate) (PBAT) blends and switchgrass: Fabrication and performance evaluation. *Ind. Crops Prod.* **2013**, *42*, 461–468. [[CrossRef](#)]

34. Hao, M.; Wu, H. Effect of in situ reactive interfacial compatibilization on structure and properties of polylactide/sisal fiber biocomposites. *Polym. Compos.* **2017**, *39*, E174–E187. [[CrossRef](#)]
35. Hao, M.; Wu, H.; Qiu, F.; Wang, X. Interface Bond Improvement of Sisal Fibre Reinforced Polylactide Composites with Added Epoxy Oligomer. *Materials* **2018**, *11*, 398. [[CrossRef](#)]
36. Wei, L.; Stark, N.M.; McDonald, A.G. Interfacial improvements in biocomposites based on poly(3-hydroxybutyrate) and poly(3-hydroxybutyrate-co-3-hydroxyvalerate) bioplastics reinforced and grafted with α -cellulose fibers. *Green Chem.* **2015**, *17*, 4800–4814. [[CrossRef](#)]
37. Sánchez-Safont, E.L.; Aldureid, A.; Lagarón, J.M.; Gamez-Perez, J.; Cabedo, L. Effect of the Purification Treatment on the Valorization of Natural Cellulosic Residues as Fillers in PHB-Based Composites for Short Shelf Life Applications. *Waste Biomass Valorization* **2020**, *1*, 3. [[CrossRef](#)]
38. Zhao, X.; van der Heide, E.; Zhang, T.; Liu, D. Delignification of sugarcane bagasse with alkali and peracetic acid and characterization of the pulp. *BioResources* **2010**, *5*, 1565–1580.
39. Mariano, M.; Cerená, R.; Soldi, V. Thermal characterization of cellulose nanocrystals isolated from sisal fibers using acid hydrolysis. *Ind. Crops Prod.* **2016**, *94*, 454–462. [[CrossRef](#)]
40. Carli, L.N.; Crespo, J.S.; Mauler, R.S. PHBV nanocomposites based on organomodified montmorillonite and halloysite: The effect of clay type on the morphology and thermal and mechanical properties. *Compos. Part A Appl. Sci. Manuf.* **2011**, *42*, 1601–1608. [[CrossRef](#)]
41. UNE-EN ISO UNE-EN ISO 20200. *Determinación del Grado de Desintegración de Materiales Plásticos Bajo Condiciones de Compostaje Simuladas en un Laboratorio*; Amigos Museo del Prado: Madrid, Spain, 2006.
42. Zhang, K.; Misra, M.; Mohanty, A.K. Toughened sustainable green composites from poly(3-hydroxybutyrate-co-3-hydroxyvalerate) based ternary blends and miscanthus biofiber. *ACS Sustain. Chem. Eng.* **2014**, *2*, 2345–2354. [[CrossRef](#)]
43. Crétois, R.; Chenal, J.M.; Sheibat-Othman, N.; Monnier, A.; Martin, C.; Astruz, O.; Kurusu, R.; Demarquette, N.R. Physical explanations about the improvement of PolyHydroxyButyrate ductility: Hidden effect of plasticizer on physical ageing. *Polymers* **2016**, *102*, 176–182. [[CrossRef](#)]
44. De Koning, G.J.M.; Lemstra, P.J. Crystallization phenomena in bacterial poly[(R)-3-hydroxybutyrate]: 2. Embrittlement and rejuvenation. *Polymer* **1993**, *34*, 4089–4094. [[CrossRef](#)]
45. Fei, B.; Chen, C.; Chen, S.; Peng, S.; Zhuang, Y.; An, Y.; Dong, L. Crosslinking of poly[(3-hydroxybutyrate)-co-(3-hydroxyvalerate)] using dicumyl peroxide as initiator. *Polym. Int.* **2004**, *53*, 937–943. [[CrossRef](#)]
46. Crist, B.; Schultz, J.M. Polymer spherulites: A critical review. *Prog. Polym. Sci.* **2016**, *56*, 1–63. [[CrossRef](#)]
47. Berthet, M.-A.; Angellier-Coussy, H.; Machado, D.; Hilliou, L.; Staebler, A.; Vicente, A.A.; Gontard, N. Exploring the potentialities of using lignocellulosic fibres derived from three food by-products as constituents of biocomposites for food packaging. *Ind. Crop. Prod.* **2015**, *69*, 110–122. [[CrossRef](#)]
48. Srubar, W.V.; Wright, Z.C.; Tsui, A.; Michel, A.T.; Billington, S.L.; Frank, C.W. Characterizing the effects of ambient aging on the mechanical and physical properties of two commercially available bacterial thermoplastics. In *Polymer Degradation and Stability, Proceedings of the 3rd International Conference on Biodegradable and Biobased Polymers (BIOPOL-2011), Strasbourg, Austria, 29–31 August 2011*; Elsevier: Amsterdam, The Netherlands, 2012; Volume 97, pp. 1922–1929.
49. Saba, N.; Jawaid, M.; Alothman, O.Y.; Paridah, M.T. A review on dynamic mechanical properties of natural fibre reinforced polymer composites. *Constr. Build. Mater.* **2016**, *106*, 149–159. [[CrossRef](#)]
50. Yu, L. *Biodegradable Polymer Blends and Composites from Renewable Resources*; John Wiley and Sons: Hoboken, NJ, USA, 2009; ISBN 9780470146835.
51. Giménez, E.; Lagarón, J.M.; Cabedo, L.; Gavara, R.; Saura, J.J. Study of the thermoformability of ethylene-vinyl alcohol copolymer based barrier blends of interest in food packaging applications. *J. Appl. Polym. Sci.* **2004**, *91*, 3851–3855. [[CrossRef](#)]
52. Giménez, E.; Lagarón, J.M.; MasPOCH, M.L.; Cabedo, L.; Saura, J.J. Uniaxial tensile behavior and thermoforming characteristics of high barrier EVOH-based blends of interest in food packaging. *Polym. Eng. Sci.* **2004**, *44*, 598–608. [[CrossRef](#)]
53. Sánchez-Safont, E.L.; González-Ausejo, J.; Gámez-Pérez, J.; Lagarón, J.M.; Cabedo, L. Poly(3-Hydroxybutyrate-co-3-Hydroxyvalerate)/Purified Cellulose Fiber Composites by Melt Blending: Characterization and Degradation in Composting Conditions. *J. Renew. Mater.* **2016**, *4*, 123–132. [[CrossRef](#)]

54. Sánchez-Safont, E.L.; Aldureid, A.; Lagarón, J.M.; Gámez-Pérez, J.; Cabedo, L. Biocomposites of different lignocellulosic wastes for sustainable food packaging applications. *Compos. Part B Eng.* **2018**, *145*, 215–225. [[CrossRef](#)]
55. Weng, Y.-X.; Wang, Y.-Z.Y.; Wang, X.-L.; Wang, Y.-Z.Y. Biodegradation behavior of PHBV films in a pilot-scale composting condition. *Polym. Test.* **2010**, *29*, 579–587. [[CrossRef](#)]
56. Arrieta, M.P.; López, J.; Rayón, E.; Jiménez, A. Disintegrability under composting conditions of plasticized PLA–PHB blends. *Polym. Degrad. Stab.* **2014**, *108*, 307–318. [[CrossRef](#)]
57. Tran, T.P.T.; Bénézet, J.-C.; Bergeret, A. Rice and Einkorn wheat husks reinforced poly(lactic acid) (PLA) biocomposites: Effects of alkaline and silane surface treatments of husks. *Ind. Crops Prod.* **2014**, *58*, 111–124. [[CrossRef](#)]



© 2020 by the authors. Licensee MDPI, Basel, Switzerland. This article is an open access article distributed under the terms and conditions of the Creative Commons Attribution (CC BY) license (<http://creativecommons.org/licenses/by/4.0/>).

Article

Injection Molding of Coir Coconut Fiber Reinforced Polyolefin Blends: Mechanical, Viscoelastic, Thermal Behavior and Three-Dimensional Microscopy Study

Miguel A. Hidalgo-Salazar ^{1,*}, Juan P. Correa-Aguirre ¹, Serafín García-Navarro ² and Luis Roca-Blay ²

¹ Research Group for Manufacturing Technologies GITEM, Universidad Autónoma de Occidente, Cali, DC 760030, USA; jpcorrea@uao.edu.co

² AIMPLAS, Gustave Eiffel 4 (València Parc Tecnològic), 46980 Paterna, Spain; sgarcia@aimplas.es (S.G.-N.); lroca@aimplas.es (L.R.-B.)

* Correspondence: mahidalgo@uao.edu.co; Tel.: +57-2-3188000

Received: 14 May 2020; Accepted: 23 June 2020; Published: 7 July 2020

Abstract: In this study, the properties of a polyolefin blend matrix (PP-HDPE) were evaluated and modified through the addition of raw coir coconut fibers-(CCF). PP-HDPE-CCF biocomposites were prepared using melt blending processes with CCF loadings up to 30% (*w/w*). CCF addition generates an increase of the tensile and flexural modulus up to 78% and 99% compared to PP-HDPE blend. This stiffening effect is caused by a decrease in the polymeric chain mobility due to CCF, the higher mechanical properties of the CCF compared to the polymeric matrix and could be an advantage for some biocomposites applications. Thermal characterizations show that CCF incorporation increases the PP-HDPE thermal stability up to 63 °C, slightly affecting the melting behavior of the PP and HDPE matrix. DMA analysis shows that CCF improves the PP-HDPE blend capacity to absorb higher external loads while exhibiting elastic behavior maintaining its characteristics at higher temperatures. Also, the three-dimensional microscopy study showed that CCF particles enhance the dimensional stability of the PP-HDPE matrix and decrease manufacturing defects as shrinkage in injected specimens. This research opens a feasible opportunity for considering PP-HDPE-CCF biocomposites as alternative materials for the design and manufacturing of sustainable products by injection molding.

Keywords: biocomposites; mechanical properties; thermal properties; natural fibers; injection molding

1. Introduction

A polymeric blend is a material formed from the physical combination of at least two polymers. These materials are used in various technological applications due to the possibility of modifying several properties considering the main characteristics of the polymers in the blend and their mixing ratio. Some studies estimated that currently, a large quantity of the polymers in the global market are sold as polymeric blends [1]. In the research context, these materials have been studied by several authors in the last years [2–4]. According to these studies, polymeric blends can be classified as immiscible (heterogeneous), compatible, or miscible (homogeneous), been most of these materials (around 90%) immiscible or multiphase systems with partial miscibility [1,3,4].

According to a Colombian non-profit organization that represents the companies related to chemical sector including plastics, rubber, paints, inks (coatings), and fibers, ACOPLASTICOS, the Colombian production of plastic resins was about 1.34 million tons in 2017 and polyolefins (low density polyethylene—LDPE, high density polyethylene and polypropylene—PP) represent around 42% of this production capacity [5]. Also, those polymers represent most of the post-consumer plastic

wastes and the separation into the individual polymer and complete sorting during mechanical recycling processes are expensive and sometimes impossible. However, valorization of these polyolefins is possible because they can be easily recycled by converting them into good performance polymer blends [6,7].

PP-PE blends have been studied for several researchers in the last years. Some of these studies show the limited miscibility of PP-LDPE blends [8]. However, most of the revised literature shows that PP and PE are immiscible, resulting in phase separation during melt blending, low adhesion between the constituents' phases, and poor mechanical properties [9–11]. Nonetheless, due to their availability, recyclability, sustainable character, and low-cost, PP-PE blends could become strategic materials for several industry applications facing a circular plastics economy [7,12–14].

The reinforcement of polymeric matrices with natural fibers as coir coconut fiber, hemp, sisal, pineapple, sugarcane bagasse, fique, wood flour and their combinations has been studied during the last years [15–22]. These materials are known as natural fiber reinforced polymer composites (NFRPCs) or biocomposites and have the potential to be used in several applications as automobile parts, construction, and furniture due to the lower cost of natural fibers in comparison with traditional fibers and the enhancement of the polymeric matrices properties induced by natural fibers incorporation [22,23]. Also, biocomposites provide some advantages such as reduction overweight, less dependence on oil resources, lower costs and CO₂ emissions, recycling, among others [24–26].

The coconut fruit constituents are the white meat (28% wt), which is protected by the shell (12% wt) and the coir (35% wt). Also, the raw coconut husk is formed by coir fibers (30% wt) and a cork-like material called pith (70% wt). Coir Coconut Fibers (CCF) main constituents are cellulose (42% wt), hemicellulose (0.25% wt), lignin (47% wt), ashes (2% wt), pectin (3% wt) and about 5% wt of moisture [17]. According to Alvarado [27], estimated coconut production in Colombia was around 139,000 metric tons, which generates at least 50,000 metric tons of coconut husks mainly used in the hydroponic industry, soil stabilization, compost, and fuel.

Several studies exploring the characterization of thermoplastic polymers-CCF biocomposites have been reported. The term biocomposite is often used to name polymeric reinforced composites, where the reinforcing phase and/or the matrix are derived from materials of biological origin [28,29]. According to the reviewed literature, several studies have reported the formulation and characterization of biocomposites, which have a status of renewable and sustainable materials since they are composed of natural fibers embedded in non-degradable and biodegradable polymeric matrices [30–33].

Mir et al. [33] studied the incorporation of CCF (up to 20% wt) in a PP matrix using thermocompression. The CCF were chemically treated with chromium sulfate and sodium bicarbonate in hydrochloric acid media to improve the compatibility between fibers and PP. Their results show that the tensile properties of PP-CCF biocomposites change with the fiber load. For the biocomposite PP-CCF 10% wt, the tensile strength increases 11% as compared with PP, whereas for PP-CCF 20% wt, the tensile strength drops to values lower than those of PP.

Haque et al. explored the effect of fiber content (up to 30% wt) and chemical modification of the fibers with sodium hydroxide and a benzene diazonium salt on the mechanical properties of biocomposites based on abaca fiber, CCF, and PP obtained by extrusion and injection molding [34]. The results showed that CCF generates better mechanical properties in biocomposites than abaca fiber. Tensile tests show that chemically modified CCF increases tensile strength up to 10% and tensile modulus up to 250% compared to PP. Finally, the authors conclude that based on fiber loading, biocomposites with 30% wt of fibers had the best set of mechanical properties among the materials studied. In another study, Perez-Fonseca et al. report the effect of the hybridization of CCF with agave fiber (up to 30%) and the addition of a coupling agent (maleated polyethylene, MAPE) on the water absorption and mechanical properties on HDPE based biocomposites obtained by extrusion and injection molding. Their results show that fibers and MAPE combination generates biocomposites with enhanced tensile and flexural strengths while lowering water absorption of the biocomposites.

The reviewed literature presents an overview of the characterization of biocomposites based on chemically modified CCF [17,35]. However, less effort has been focused on the study and production

of biocomposites based on untreated CCF and polyolefin blends using high-volume manufacturing processes such as extrusion and injection molding, which could be an advantage for the development of these materials in conventional plastic processing companies. In the present study, biocomposites based on a PP-HDPE blend and untreated CCF were prepared using extrusion following by injection molding. The thermal, mechanical, viscoelastic and morphological properties of the obtained materials were studied in order to evaluate CCF addition effect on the PP-HDPE blend behavior. Also, the analysis of the shrinkage and the dimensional stability of the injected specimens were studied through a novel three-dimensional microscopy study.

2. Materials and Methods

2.1. Materials

The polymeric materials used were an injection grade PP reference 575P and an injection grade HDPE reference M80064s with melt flow indexes (MFI) of 4.8 and 8.8 g/10 min respectively (measured at 190 °C, 2.16 kg). Both polymeric materials were purchased from SABIC (Al-Jubail, Saudi Arabia). The raw CCF, shown in Figure 1, were kindly supplied by “Super de Alimentos” (Manizales, Colombia) and were generated in the coconut candies production process. Before PP-HDPE-CCF biocomposites formulation, the CCF was grinded and sieved through a 400 µm sieve.



Figure 1. Raw coir coconut.

2.2. Methodology

Neat Polymers and Biocomposites Processing

The extrusion process of the different materials was performed in a co-rotating twin-screw extruder with a L:D ratio 40:1 and a screw diameter of 22 mm, equipped with two volumetric feeders and a pelletizer located next to the die zone. During the extrusion, the following parameters were fixed:

- Neat PP, HDPE and a 50–50 (% *w/w*) PP-HDPE blend pellets were fed in the extruder feeding zone using a volumetric feeder
- For PP-HDPE-CCF biocomposites, the CCF was fed with another volumetric side feeder at L/D 20. The side feeder speed was varied to obtain PP-HDPE-CCF biocomposites with CCF loadings of 10%, 20%, and 30% (*w/w*)
- Temperature: 165 (feeding zone) to 185 °C (die)
- Twin-screw rotation speed: 50 rpm

Then the pellets of the different materials were dried in an X-DRY AIR mini dryer (Moretto, Massanzago, Italy) at 60 °C and a dew point of −52 °C. The specimens used for mechanical characterizations (described in Section 2.3.2) were injected in a microinjection molding machine BOY XS (BOY Machines Inc., Exton, PA, USA) with the following parameters:

- Temperature: 180 (feeding zone) and 185 °C (nozzle).

- Filling pressure: 60 to 80 bars
- Holding pressure: 60 bars
- Clamping force: 30 kN

Figure 2 shows the injected flexural specimens of each material. The processing temperatures were set below 200 °C to avoid thermal degradation of the CCF (see Section 3.1), the remaining processing parameters were set based on reviewed literature regarding the processing optimization of natural fiber-polyolefin biocomposites [16,36].

The injection molding process allows to obtain complex geometric parts with fast function elements and in large quantities [37]. It offers several advantages over other manufacturing process as compression molding. According to Pickering [37], the content of natural fibers that can be incorporated during the injection process is between 20 to 40% by weight. A higher content is not recommended since an increase in fiber clearly reduces the flow capacity of the melt, generating instabilities during the process. Besides this, natural fibers have a similar morphology, but differ from each other by factors such as the internal area of the lumens, the number of lumens, the number and size of the fiber cells, the thickness of the secondary cell walls and the actual cross section [38]. These characteristics influence different fiber properties such as mechanical properties and bulk density which is related to the packing capacity of the fiber and the maximum throughput of the fibers [36]. In our case, the CCF throughput within the extruder was optimized to obtain PP-CCF biocomposites with a maximum fiber weight percentage of 30% and considerable flow properties to successfully apply in the injection molding process.



Figure 2. Injected specimens of neat PP, HDPE, PP-HDPE blend, and their biocomposites.

2.3. Materials Characterization

2.3.1. Melt Flow Index (MFI)

Melt flow index tests of neat PP and HDPE were performed at 190 °C and 2.16 kg using a plastics melt flow indexer.

2.3.2. Mechanical Properties

Tensile tests and three-point bending flexural tests were performed in a universal testing machine INSTRON Model 3366 (INSTRON, Norwood, MA, USA) equipped with an axial extensometer Epsilon model 3555 BP (Epsilon Tech, Jackson, WY, USA). Before being testing, the specimens were conditioned at 23 °C and 50% relative humidity for seven days. Tensile tests were performed on type V specimens (according to standard ASTM-D 638-14) at 23 °C, using a cross-head speed of 5 mm/min while flexural tests were carried out on bars with a rectangular cross-section at 23 °C, using a cross head speed of 1.3 mm/min, a distance between support spans of 50 mm and were performed up to 5% strain under standard ASTM D 790-17. The results were taken as the average of five samples. The impact strength of neat PP, HDPE, PP-HDPE blend, and their biocomposites was determined with an impact machine equipped with a 2.5 Joules pendulum. Notched IZOD impact tests were carried out at 23 °C and a starting angle of 150° under standard ASTM D 256-10 (2018). The results were taken as the average value of five samples.

2.3.3. Thermal Characterization

DSC tests were carried out using a TA Q2000 differential scanning calorimeter (Texas Instruments, Dallas, TX, USA) under nitrogen atmosphere at a scanning speed of 10 °C/min, with a sample of 10 mg in aluminum pans from 20 to 200 °C at a scanning speed of 10 °C/min, with a sample of 10 mg in aluminum pans. First, the samples were subjected to heating cycles at 10 °C/min from 20 to 200 °C to erase the thermal history related to processing events, following by cooling cycles at 10 °C/min from 200 to 0 °C. Finally, second heating cycles were performed at 10 °C/min from 0 to 200 °C. The samples were analyzed in aluminum crucibles under a N₂ atmosphere. On the other hand, thermogravimetric analysis (TGA) tests were performed using a TA Q500 thermogravimeter (Texas Instruments, Dallas, TX, USA) from 25 to 600 °C at a heating rate of 10 °C/min. The samples were analyzed in aluminum crucibles under a N₂ atmosphere.

2.3.4. Dynamic Mechanical Analysis (DMA)

DMA tests were performed using a DMA RSA-G2 (Texas Instruments, Dallas, TX, USA) in three-point bending mode from −80 to 150 °C, a frequency of 1 Hz, a constant heating rate of 3 °C/min and 0.01% of strain (taken from the linear viscoelastic domain of the plot E' vs. strain reported earlier for PP and PE [31,32] and PP-natural fiber biocomposites [16,33]). Changes in storage modulus (E'), loss modulus (E''), and tan delta (loss factor) were recorded.

2.3.5. Morphology

Scanning electronic microscopy (SEM) of the PP, HDPE, PP-HDPE blend, and their biocomposites was performed using a Quanta FEG 250 microscope (ThermoFisher Scientific, Hillsboro, OR, USA) operating at a voltage of 10 kV. To obtain a brittle fracture on the visualized surfaces, the samples were immersed in a container with liquid nitrogen for 15 min. Later, the fracture was generated inside the container using two steel forceps. Finally, with the aim of increasing their electric conductivity, the samples were previously sputter-coated with gold.

2.3.6. Particle Size and Roughness Measurements

The particle size of the milled and sieved CCF was measured with a Three-dimensional microscope VR-3000 Series with a wide-area three-dimensional measurement system from Keyence (Keyence Corporation of America, Itasca, IL, USA). The roughness measurements were also performed twenty single milled fibers with this measurement system. The reported results were Ra (arithmetical mean height) and Rz (maximum height of profile).

2.3.7. Statistical Analysis

Tensile, flexural, and impact properties of the materials were subject to analyses of variance (ANOVA), and Tukey’s test was applied at the 0.05 level of significance. All statistical analyses were performed using Minitab Statistical Software Release 14 (Minitab LLC, State College, PA, USA).

3. Results and Discussion

3.1. CCF Characterization

The milled CCF (Figure 3) contains fibers and cork-like particles with an average length (l) of and 0.94 ± 0.22 mm and 0.38 ± 0.10 mm respectively. The average width (w) was 0.22 ± 0.04 mm for fibers and 0.29 ± 0.07 mm for particles. The average aspect ratio (l/w) of the milled CCF was 4.27 and 1.3 for fibers and particles. As shown in Figure 4, the wide-area three-dimensional measurement system allows to perform several measurements as the length, diameter and the roughness profile of a single natural fiber. Ra and Rz values obtained as the average value of twenty samples were 0.011 ± 0.004 mm and 0.055 ± 0.021 mm. The natural fibers surface roughness is an important parameter to measure because it plays a significant role in the mechanical interlocking between the fibers and matrix, which is related to biocomposites mechanical properties [18,26,39,40].

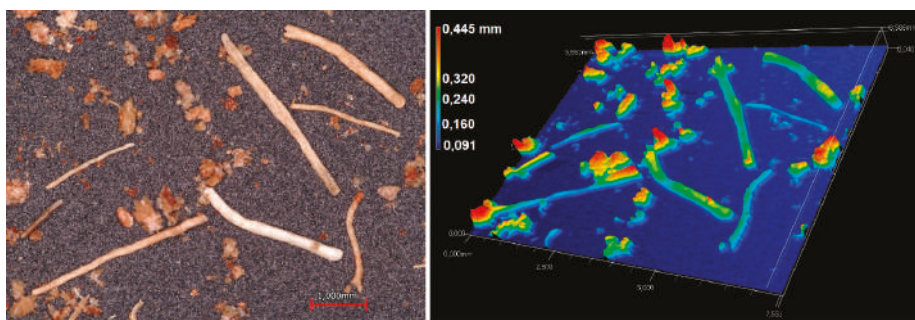


Figure 3. Optical micrograph and 3D height map of milled CCF.

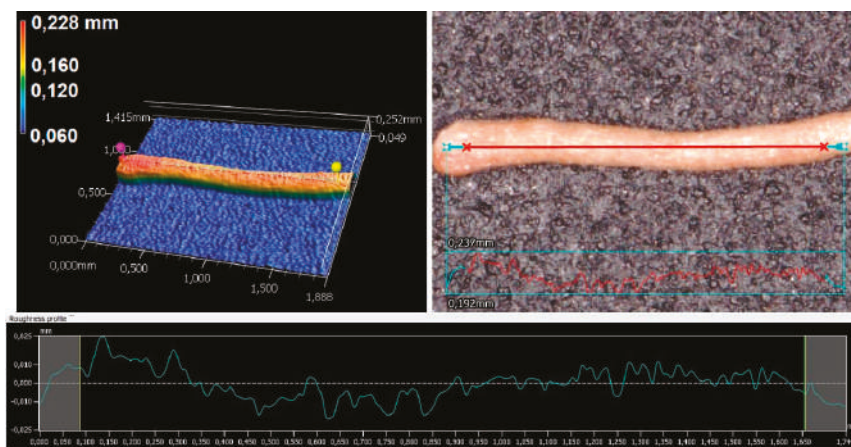


Figure 4. Roughness profile, optical micrograph and 3D height map of a single CCF.

Figure 5 shows the TGA and DTG thermograms of CCF under N_2 . Also, the degradation steps, onset temperature (T_o) and the maximum weight loss rate temperature of the sample (T_{max}) are

summarized in Table S1 supplementary information. For CCF, the TG curve shows four principal mass loss regions (Figure 5a). These regions are located around 30–100 °C, 100–200 °C, 200–300 °C, and 300–600 °C. The first region is related to the moisture evaporation of the sample with a weight loss of 9.2%. The second region is stable, without weight loss observed related to volatiles or CCF degradation by-products. This region shows that window processing of CCF based biocomposites should be below 200 °C (as indicates in the red circle in Figure 5b) to avoid thermal degradation of the fibers [41]. The third region between 200 °C and 300 °C presents a T_o of 253 °C and T_{max} of 283 °C (Figure 5b), which is related to released elements from the sample like hemicellulose. The last region starts from 323 °C and with a T_{max} 336 °C is related to α -cellulose decomposition.

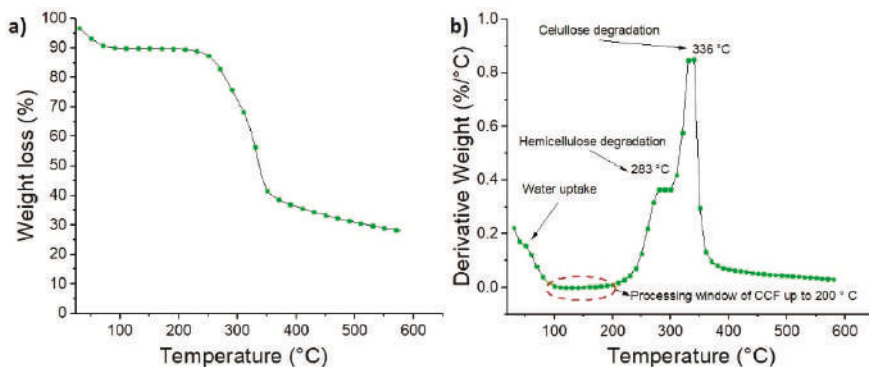


Figure 5. (a) TG and (b) DTG curves of coir coconut fibers at a heating rate of 10 °C/min.

3.2. Biocomposites Characterization

3.2.1. Mechanical Properties

The effect of CCF incorporation on the mechanical properties of the PP-HDPE blend was evaluated. The stress vs. strain graphs obtained from tensile and flexural tests for each material are shown in Figure 6. Also, the mechanical properties calculated from these tests are summarized in Supplementary Table S2.

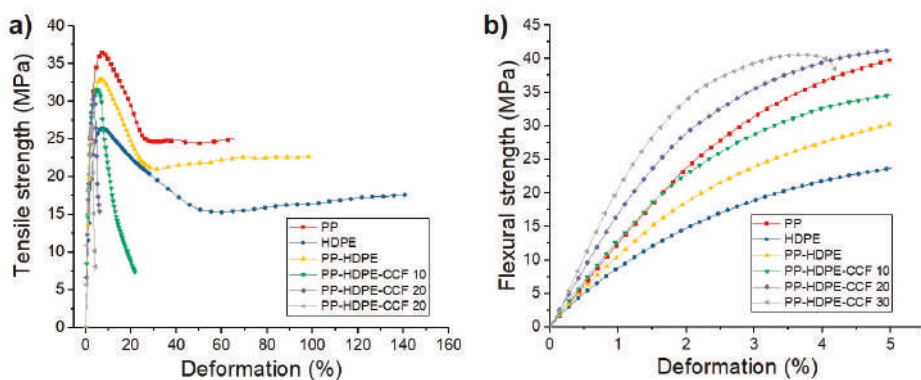


Figure 6. Average tensile stress vs deformation (a) and flexural stress vs deformation (b) of PP, HDPE, PP-HDPE blend, and their biocomposites.

Regarding neat polymers, it is observed that PP tensile modulus (TM) and tensile strength (TS) values are higher than those of HDPE. However, HDPE deformation at break (ϵ_b) is higher compared to PP. For PP-HDPE binary blend, TM was not significantly different from PP ($p \geq 0.05$) and its TS and

ϵ_b values were between neat polymers values. In the case of biocomposites, the results of the test show that CCF addition generates significant increases ($p < 0.05$) in TM values of 16, 35, and 78% compared to the PP-HDPE blend for the biocomposites PP-HDPE-CCF 10, 20 and 30%.

On the other hand, TS values of PP-HDPE- CCF 10, 20 and 30% decrease 6%, 7%, and 20%, respectively, in comparison with PP- HDPE blend ($p < 0.05$). Also, a CCF content increase generates a significant decrease in ϵ_b of the PP-HDPE matrix. This decrease in the TS and ϵ_b values have already been observed in some biocomposites [16,22,34] and could be related to the weak interfacial bonding between CCF (hydrophilic) and PP-HDPE (hydrophobic) or interface discontinuities that affect the biocomposites deformation capacity (see Section 3.2.4). With CCF loading increase, the weak interfacial area between the polymeric matrix and CCF increases, as a result, TS and ϵ_b values decreases.

Flexural test results also show that biocomposites modulus values (FM) increase around 13 and 99% for biocomposites PP-CCF 10 and 30 respectively, compared with PP-HDPE. This stiffening effect is caused by a decrease in the polymeric chain mobility due to CCF and the higher mechanical properties of the CCF compared to the polymeric matrix and could become a decisive property in product applications where the rigidity (related to tensile and flexural modulus) is an essential factor. Also, the FS values of PP-HDPE and biocomposites presents significant differences ($p < 0.05$). FS values of the biocomposites increases between 14% and 35% for PPP-HDPE-CCF 10 and 30 respectively [42]. These differences observed in the strength values of both mechanical tests were also observed on PP-Rice Husk and PP-CCF biocomposites and can be due to a higher interaction natural fiber-polymeric matrix under compression stresses generates during bending [16,34].

The results of the Notched IZOD impact tests (Supplementary Table S2) shows that HDPE has a better impact performance than PP and could be related to its higher deformation and energy absorption capability. As expected, the PP-HDPE blend impact strength was 67% greater than that of neat PP ($p < 0.05$). On the other hand, CCF addition leading to a reduction of impact strength between 44 and 64% for PP-HDPE-CCF 10 and 30% respectively in comparison with PP-HDPE ($p < 0.05$), these results are in the range of those published by other authors for PP-CCF biocomposites [42,43]. This reduction in impact strength in the biocomposites with CCF load could be due to the stiffening effect of the matrix observed earlier in the tensile test and a weak interfacial adhesion between the CCF and polymeric matrix. Also, the increase of CCF generates fibers clusters within the biocomposites that could act as crack initiation sites [44].

3.2.2. Thermal Properties

DSC thermograms for each material are shown in Figure 7. Also, the thermal properties obtained from these thermograms were included in Supplementary Table S3. The degree of crystallinity (χ_c) of each material was estimated from Equation (1):

$$\chi_c = \left(\frac{\Delta H_m}{[\Delta H_m^0 * (1 - W_{fiber}) * (w_{pol})]} \right) * 100 \quad (1)$$

where w_{fiber} is the CCF fraction, w_{pol} is the fraction of each polymer of the blend, ΔH_m is the normalized melting enthalpy of each sample, and ΔH_m^0 is the specific melting enthalpy of 100% crystalline PP and HDPE. These values are 207 and 293 J/g, respectively [45].

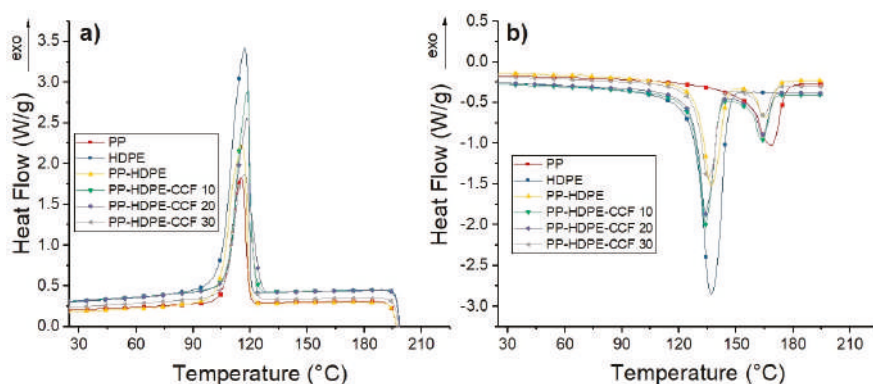


Figure 7. (a) Cooling and (b) Second heating DSC curves of PP, HDPE, PP-HDPE blend, and their biocomposites.

The cooling cycle of PP, HDPE, and PP-HDPE blend (Figure 7a) shows an exothermic peak located between 115 and 117 °C, which corresponds to PP and HDPE chains crystallization. Regarding biocomposites, it is observed that during cooling CCF addition induces an increase of the PP-HDPE chains crystallization temperature around 2 to 4 °C. This increase indicates that CCF could act as a nucleating agent for polyolefin blends.

The second heating curves (Figure 7b) show single melting endotherms located at 137 and 168 °C for neat PP and HDPE, respectively. These single peaks are associated with the melting temperature (T_m) of PP and HDPE crystals formed during the cooling stage. On the other hand, the PP-HDPE blend show two peaks located at 137 and 166 °C, related to the melting temperatures of each polymer when the blend is formed. This decrease has been observed in PP-PE blends and are related to a lack of miscibility between these polymers [9]. PP-HDPE-CCF biocomposites also exhibit two endothermic peaks around 135 and 165 °C related to the melting of the HDPE and PP phases.

Considering Figure 7b, it is observed that there were small decreases in relation to the T_m of PP-HDPE-CCF biocomposites compared to neat PP-HDPE blend. This thermal behavior has been already observed in several studies regarding biocomposites as PLA-Ramie [46] and PP-NBr-Bagasse fibers [47]. This decrease (albeit small), is due to the incompatibility between non-polar hydrophobic matrices and polar hydrophilic untreated CCF fiber which leads to poor interfacial properties and thus lowering the melting point. Also, the presence of CCF could also disturb the chain arrangement in PP-HDPE blend, thereby decreasing the T_m of the corresponding biocomposites.

TG and DTG thermograms of each material are shown in Figure 8. Also, the thermal parameters obtained are summarized in Supplementary Table S1.

PP and HDPE degradation occur in a one-step process with onset temperatures (T_o) located at 420 and 464 °C for PP and HDPE, respectively. Also, T_{max} values were 457 °C for PP and 485 °C for HDPE. This result shows that HDPE has higher thermal stability than PP. PP-HDPE blend presents a single step degradation with a T_o located at 413 °C and two T_{max} peaks located at 430 and 461 °C. These T_{max} peaks are related to PP and HDPE phases of the blend. The residual char after 600 °C was 0.4 and 0.6% for neat polymers and PP-HDPE blend; this low residual char indicates that constituent atoms of the polyolefins (carbon and hydrogen) were volatilized during TGA test.

On the other hand, the thermal degradation of biocomposites takes place in a multi-step process. The first step is related to CCF degradation and presents a T_o located between 266 and 275 °C, whereas the second step is associated with PP-HDPE thermal degradation. It is observed that CCF addition increases the polymeric matrix thermal stability, to values of PP-HDPE matrix increase between 28 and 40 °C and T_{max} increases between 9 and 12 °C as compared to PP-HDPE blend. This increase of the polymeric matrix thermal stability given by CCF addition has already been observed

in polyolefins-natural fibers biocomposites. This can be due to the increase of crystallinity and thermal properties of the matrix (as shown in Supplementary Table S3) generated by natural fibers nucleating effect [16,22]. Also, it is observed that the residual char of PP-HDPE-CCF biocomposites increases with the CCF content.

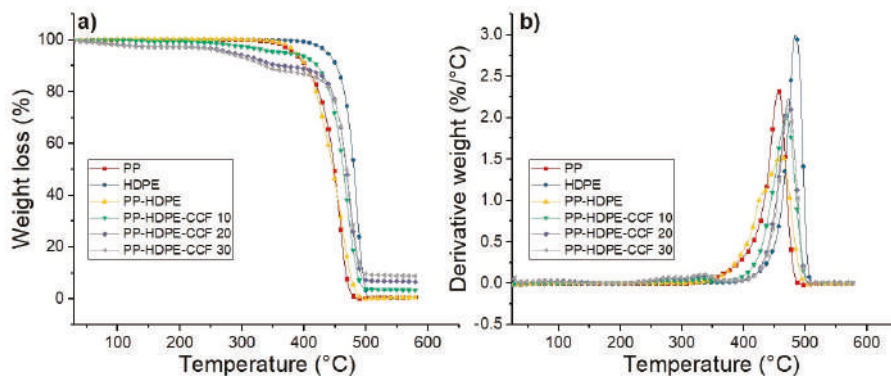


Figure 8. (a) TG and (b) DTG curves of PP, HDPE, PP-HDPE blend, and their biocomposites.

3.2.3. Dynamic Mechanical Analysis

Figure 9 and Table S4 presents the storage modulus values (E') of each material vs. temperature. Regarding neat polymer matrices, E' values of PP are higher than HDPE values in the entire temperature range, whereas, E' of the PP-HDPE blend values were between neat polyolefins values. Also, E' values decrease progressively with temperature increase for all materials. This could be due to the softening and the beginning of relaxation processes within the polymer matrix [48]. The CCF addition generates an increase of PP-HDPE blend stiffness, proportionally to the CCF content. This increase in E' values are related to the stiffening effect given by rigid CCF and is consistent with the results obtained by tensile and flexural tests (Section 3.2.1).

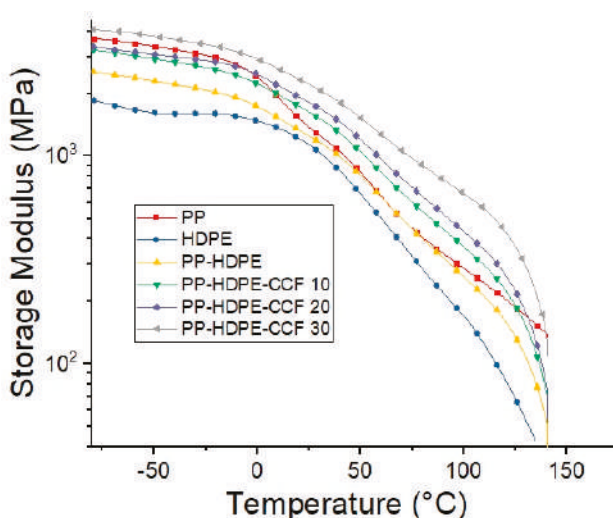


Figure 9. Temperature dependence of storage modulus of PP, HDPE, PP-HDPE blend, and their biocomposites.

However, this stiffening effect is dependent on the glass transition temperature (T_g) of the PP phase. Below T_g ($T = 0$ °C), E' increases 28% with 10% wt of CCF and shows a maximum increase of 65% with 30% wt of CCF compared to the PP-HDPE blend. At temperatures above T_g , for example $T = 25$ °C, this increase was between 31 and 78% for PP-HDPE-CCF 10 and 30% and is greater for temperatures above ambient ($T = 80$ °C) where the increase ranges from 35% to 125% with CCF content of 10% and 30% of respectively. This result suggests that at temperatures lower than T_g , the contribution of the fibers to the matrix rigidity is low since the matrix is in a glassy state. As the temperature increases, the drop in the matrix E' values is compensated by the stiffness of the CCF fibers. In this case the E' values is controlled by the percentage of fiber and increases with the fiber load in the biocomposite.

On the other hand, loss modulus (E'') vs. temperature of HDPE, PP, PP-HDPE blend, and their biocomposites is shown in Figure 10. E'' plot of neat PP shows a β relaxation around 6 °C related to the glass transition temperature or T_g and a shoulder around 60 °C related to an α relaxation [49,50]. On the other hand, E'' plot of HDPE exhibit a broad α relaxation around 40 °C which is associated with the beginning of the molecular movement of the HDPE crystalline phase. The PP-HDPE blend reveal two peaks related to PP β relaxation and HDPE α relaxation which decline and shift towards high temperatures with 10% wt of CCF. These shifts to higher temperatures are caused by a decrease in the molecular movement of the PP and HDPE chains generated by the presence of the CCF and a dispersed phase on the matrix. With fiber loading increase, the E'' peaks intensity gradually increases and becomes broader. This behavior has been observed in polymer-natural fibers biocomposites [51,52] and reveal that CCF effectively suppress the polymeric chains mobility resulting in a broadening of the T_g range.

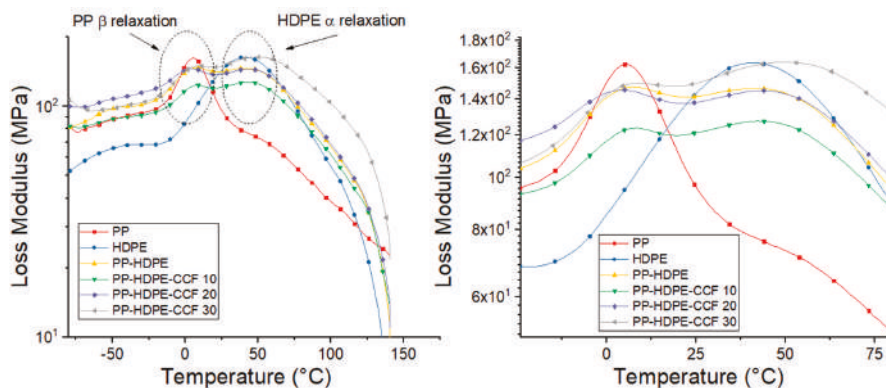


Figure 10. Temperature dependence of loss modulus of PP, HDPE, PP-HDPE blend, and their biocomposites.

Figure 11 shows the variation of $\tan \delta$ with temperature. According to Saba et al. [51], $\tan \delta$ is the ratio between E'' and E' , and is related with the damping behavior of the polymeric matrix. This graph confirms that neat PP exhibit a β relaxation which corresponds to the glass transition (T_g) and a α relaxation between 60 °C to 75 °C [50], also neat HDPE present the α relaxation observed in E'' graphs (Figure 10). Regarding biocomposites, $\tan \delta$ peaks height related to the T_g of the PP phase and the α relaxation of the HDPE phase were observed to gradually decreases and shifts towards higher temperatures with CCF content increase (Supplementary Table S4). This result could be due to the amplified stiffness imparted by the CCF and confirms that fiber addition hinder the molecular movement related to the damping and could be an advantage in some applications where a better performance against mechanical loads is required. Also, the broadness of $\tan \delta$ peaks, measured as the width at half maximum (FWHM), can be an indicator of the composite homogeneity and the interaction between the matrix and the fibers. In this sense, some author established that larger FWHM values

implies heterogeneity and more contact between the phases of a biocomposite [46,53]. Table S4 shows that FWHM values of $\tan \delta$ peaks is found to be the lowest for PP-HDPE blend and increases gradually with CCF content. This suggests that the heterogeneity of the biocomposite and the interaction between fibers and polymeric matrix increases with CCF content.

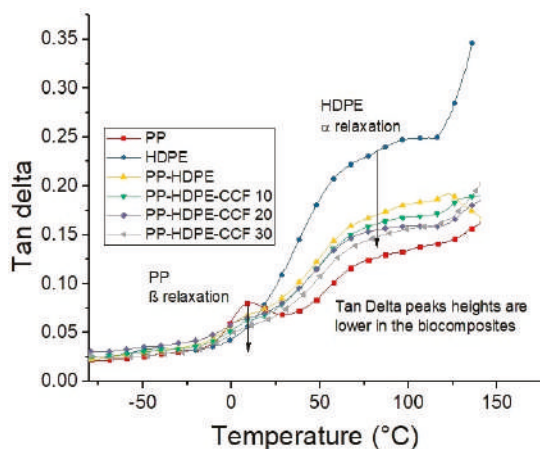


Figure 11. Temperature dependence of tan delta of neat PP, HDPE, PP-HDPE blend, and their biocomposites.

With the aim to further understand the viscoelastic and structural behavior of the studied materials, Cole–Cole diagrams were evaluated. These diagrams are obtained by drawing E'' vs. E' , and can describe the nature of polymeric and composite materials [54,55]. A homogeneous material with a single relaxation time shows a semicircle diagram while a multiphase system with different relaxation times will show two irregularly shaped modified circles [54]. Figure 12 shows the Cole–Cole diagrams for PP, HDPE, PP-HDPE blend, and its biocomposites. The Cole–Cole curves shows that PP and HDPE are homogeneous systems with a concave shape (semicircles), while the PP-HDPE blend is a heterogeneous system which exhibit two semicircles due to two different relaxation mechanisms corresponding to the immiscibility between the polymeric phases. This result is in good agreement with the data obtained from the DSC test (Section 3.2.2). Regarding biocomposites, the Cole–Cole diagram also display two semicircles and a progressive increase in the values of the E' and E'' with CCF loading [56]. This result show that CCF effectively suppresses the polymeric chains mobility and is an indicative of materials heterogeneity associated with greater differences in relaxation processes of the polymeric matrix when more CCF is incorporated. Also, the Cole–Cole diagram show that among the biocomposites, the one with 30% wt of CCF showed the highest E' and E'' values. Therefore, it can be inferred that PP-HDPE-30 CCF biocomposite can absorb higher external loads while exhibiting elastic behavior maintaining its characteristics at higher temperatures [57].

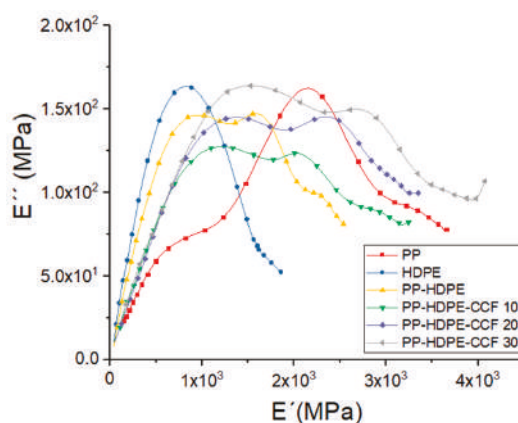


Figure 12. Cole-Cole plots of PP, HDPE, PP-HDPE blend, and their biocomposites.

3.2.4. Morphology

SEM micrographs of neat polymers and PP-HDPE blend are shown in Figure 13a–c, respectively. For PP and HDPE, the fracture surface is smooth, and only one phase is observed in each sample. The PP-HDPE blend micrographs (Figure 13c,d) show a two-phase morphology due to PP and HDPE immiscibility [11]. This phase-separated morphology is consistent with the results obtained in DSC and DMA tests. According to the measured melt flow indexes (MFI values in Section 2.1), PP viscosity is higher in comparison with HDPE viscosity. Thus, PP is not efficiently sheared and separated during melt blending and is the dispersed phase of the blend. Also, HDPE with lower viscosity is the continuous phase [11]. The average diameter of the dispersed phase for the PP-HDPE blend was $0.32 \pm 0.06 \mu\text{m}$.

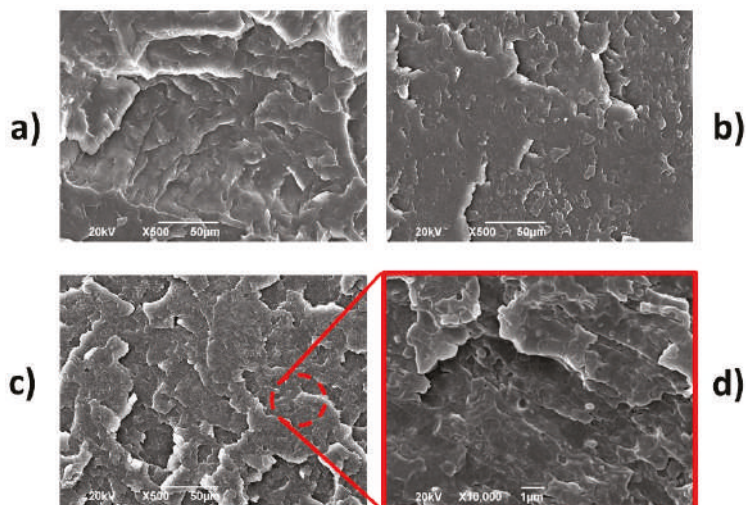


Figure 13. SEM micrographs for (a) PP, (b) HDPE and PP-HDPE blend (c,d).

The biocomposite PP-HDPE-CCF 10 presents a rough fracture surface with a dispersed phase morphology (average diameter of $0.34 \pm 0.08 \mu\text{m}$) and dispersed CCF (Figure 14a,b). This result shows that 10% of CCF addition did not disturb the dispersed phase formation. Also, the interphase

gaps between the CCF and the matrix (yellow circles in Figure 14c) indicate a poor interfacial adhesion between the polymeric matrix and CCF and could be related to the decreasing of tensile and impact properties (Section 3.2.1) [14,16,22]. On the other hand, for biocomposite PP-HDPE-CCF 30 (Figure 14d,e), the dispersed phase presents an oriented and elongated shape. In this case, a higher CCF proportion increases the contact surface between the polymeric phases and could reduce the surface tension between them. This behavior can change the spherical shape of the dispersed phase into the irregular spheroidal shape observed.

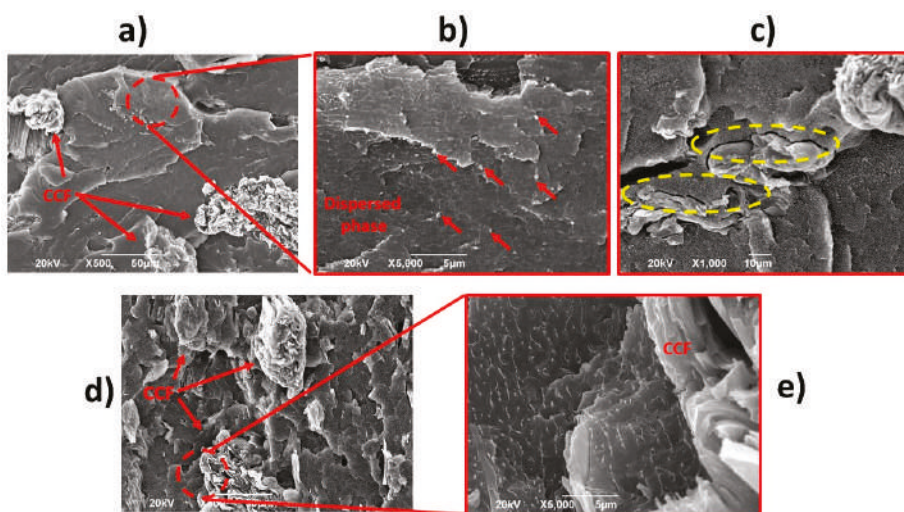


Figure 14. SEM micrographs for PP-HDPE-CCF 10 (a–c) and PP-HDPE-CCF 30 (d,e).

3.2.5. Linear Shrinkage and 3D Surface Characterization

In this study, the shrinkage was determined as the difference among the linear magnitudes of the mold cavity and that of the injected specimen at room temperature two days after the injection [58]. Also, the following equations were applied to calculate the shrinkage of the molded specimens.

$$Sf(\%) = \frac{L_f \text{ specimen} - L_f \text{ mold}}{L_f \text{ mold}} * 100 \quad (2)$$

$$St(\%) = \frac{L_t \text{ specimen} - L_t \text{ mold}}{L_t \text{ mold}} * 100 \quad (3)$$

where $L_f \text{ mold}$ and $L_t \text{ mold}$ are the cavity mold dimensions, measured at the flow and transverse direction (as indicated in Figure 15a), $L_f \text{ specimen}$ and $L_t \text{ specimen}$ are the dimensions of the injected specimen in the two directions (Figure 15b).

Linear shrinkage results of the specimens are shown in Table S5. These values are similar to those observed by Crawford et al., [59] for several polyolefins and show that all specimens present some degree of linear shrinkage during the injection process. However, it is observed that linear shrinkage decreases proportionally with the CCF content. Shrinkage is a frequent defect resulting from the injection molding process that can affect the quality and functionality of the final product. Some studies reported that overall shrinkage is affected by several parameters as the thermodynamic behavior of the injected polymer, the geometry of the injected part, the mold design, and the processing parameters among others [58,60].

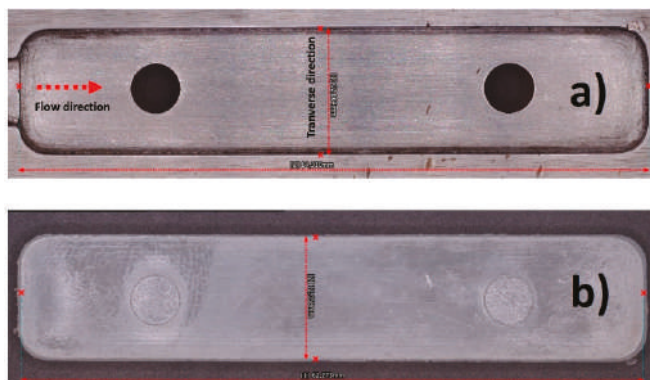


Figure 15. (a) mold cavity and (b) injected flexural specimen.

On the other hand, the surface characterization performed on the PP-HDPE blend and PP-HDPE-CCF 10, PP-HDPE-CCF 30 flexural specimens is shown in Figure 16. These measures were taken from the edge to the center of the specimen (as indicates in the yellow circle in Figure 16). For the specimen PP-HDPE (Figure 16a), the three-dimensional heights map shows a progressively decrease of the thickness values next to the edge of the specimen (blue and green zones) with a lower height value located at 0.541 mm. This effect is related to the shrinkage of the PP-HDPE matrix during the injection molding. Regarding biocomposites, a decrease in the shrinking with CCF addition was observed. For PP-HDPE-CCF 10 (Figure 16b) the lower height value was 0.250 mm whereas PP-HDPE-CCF 30 specimens present a lower height value located at the edge of 0.193 mm, which is uniform over the studied surface of the specimen (Figure 16c).

This result shows that CCF particles addition enhance the dimensional stability of the PP-HDPE matrix and decrease manufacturing defects as shrinkage in injected specimens and could be an alternative for other additives commonly used to reduce injection molding defects in polyolefins such as talc, calcium carbonate or foaming agents [61]. Also, this behavior is in good agreement with those obtained by several researchers which studied the injection molding of biocomposites with engineering simulation and 3D design software and concluded that natural fibers addition reduces the appearance of processing defects as volumetric shrinkage and warpage in injection molding products [62–64].

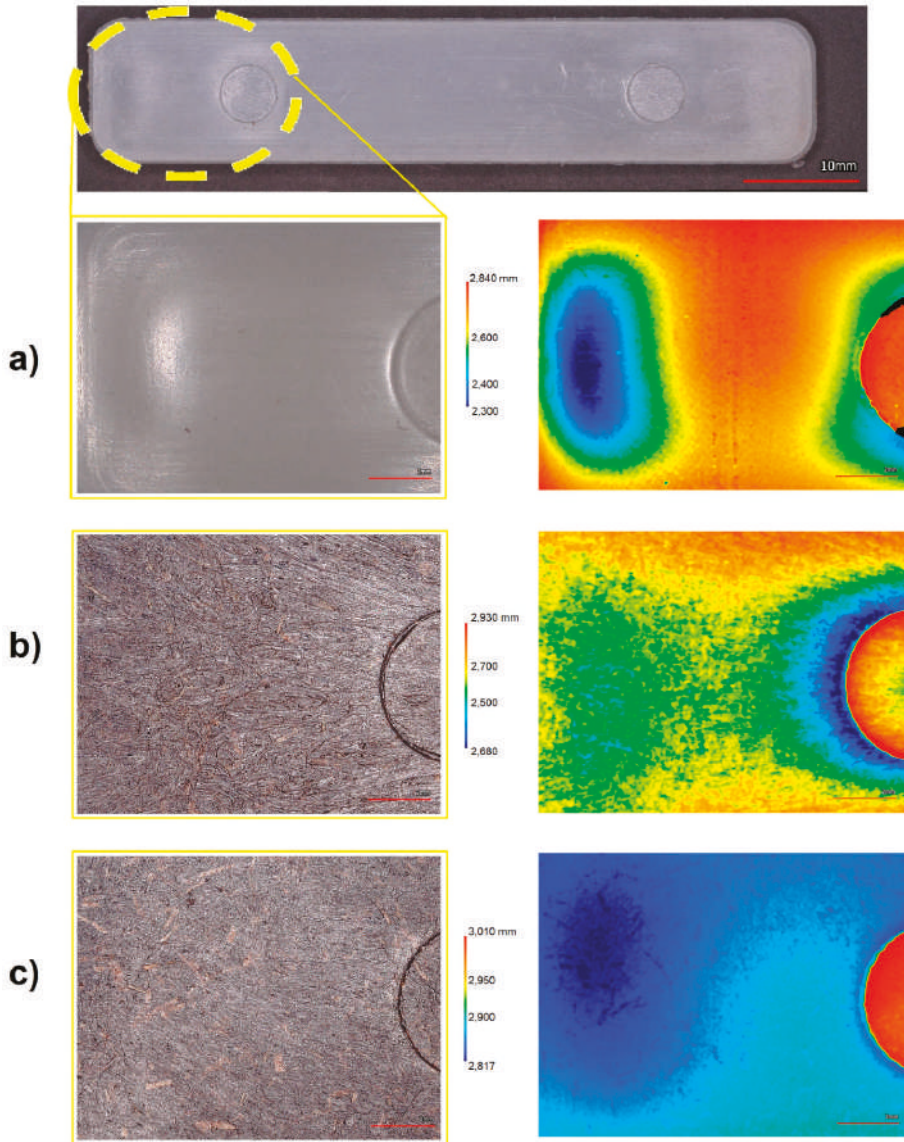


Figure 16. Surface characterization of (a) PP-HDPE blend (b) PP-HDPE-CCF 10 and (c) PP-HDPE-CCF 30 flexural specimens.

4. Conclusions

In this research, PP-HDPE-CCF biocomposites (up to 30% CCF by weight) were processed using extrusion following by injection molding. The objective was to valorize the CCF for their use in polyolefin-natural fiber biocomposites. This CCF is an agro-industrial by-product of the Colombian food industry generated after the separation process of the coconut pulp. The characterization results show that CCF addition generates mechanical properties and thermal stability improvements without affecting the PP-HDPE melting behavior. Also, the dynamic mechanical analysis combined with the three-dimensional microscopy study analysis were sensitive tools for data generation that defines

the dynamic mechanical properties, service temperatures and dimensional stability of polymers and biocomposites that support product development, particularly in construction and automotive applications. This study shows that CCF could be an alternative for other additives used to reduce injection molding defects such as talc, calcium carbonate or foaming agents. Finally, PP-HDPE-CCF biocomposites are alternative materials for the design and manufacture of products by injection molding that due to their availability and recyclability potential could generate some economic and environmental benefits in the search for sustainability in the plastics industry facing a circular plastics economy.

Supplementary Materials: The following are available online at <http://www.mdpi.com/2073-4360/12/7/1507/s1>, Table S1: Thermogravimetric data of the studied materials, Table S2: Mechanical properties of the studied materials, Table S3: Differential scanning calorimetry data of the studied materials, Table S4: DMA results of the studied materials, Table S5: Linear shrinkage of injected specimens at flow (Sf) and transverse (St) directions.

Author Contributions: Conceptualization, M.A.H.-S.; Data curation, M.A.H.-S.; Formal analysis, M.A.H.-S., and J.P.C.-A.; Funding acquisition, M.A.H.-S.; Investigation, M.A.H.-S., J.P.C.-A., S.G.-N. and L.R.-B.; Methodology, M.A.H.-S. and J.P.C.-A.; Supervision, M.A.H.-S.; Writing—original draft, M.A.H.-S. and J.P.C.-A.; Writing—review & editing, M.A.H.-S., J.P.C.-A., S.G.-N. and L.R.-B. All authors have read and agreed to the published version of the manuscript.

Funding: This research received no external funding.

Acknowledgments: The authors acknowledge the Autónoma de Occidente University (Cali- Colombia) and Colombian Ministry of Science for technical and financial support; Research Group of New Solids with Industrial Application-GINSAI (Autónoma de Occidente University) for its support in the thermal characterization; AIMPLAS (Valencia-Spain) for its academic and processing advice in the development of this work; Servicio Nacional de Aprendizaje-SENA (Cali-Colombia) for its technical support through injection molds manufacturing; University del Valle (Cali- Colombia) for SEM microscopy. Also, the authors wish to thank “Super de Alimentos” (Manizales, Colombia) for providing the raw coir coconut fibers (CCF).

Conflicts of Interest: The authors declare no conflict of interest.

References

1. Robeson, L.M. Emerging Technology Involving Polymer Blends. In *Polymer Blends*; Carl Hanser Verlag GmbH & Co. KG: München, Germany, 2007; pp. 415–438.
2. Xavier, S.F.; Xavier, S.F. Properties and performance of polymer blends. In *Polymer Blends Handbook*; Springer: Amsterdam, The Netherlands, 2014; pp. 1031–1201. ISBN 9789400760646.
3. Utracki, L.A.; Wilkie, C.A. *Polymer Blends Handbook*; Springer: Amsterdam, The Netherlands, 2014; ISBN 9789400760646.
4. Mittal, V. *Functional Polymer Blends Synthesis, Properties, and Performances*; CRC Press: Boca Raton, FL, USA, 2012; ISBN 9781138074347.
5. ACOPLASTICOS Plastics in Colombia. Available online: <http://www.acoplasticos.org/index.php/mnu-nos/mnu-pyr/pec> (accessed on 27 August 2018).
6. Hubo, S.; Delva, L.; Van Damme, N.; Ragaert, K. Blending of recycled mixed polyolefins with recycled polypropylene: Effect on physical and mechanical properties. *AIP Conf. Proc.* **2016**, *1779*, 140006.
7. Aummate, C.; Rudolph, N.; Sarmadi, M. Recycling of polypropylene/polyethylene blends: Effect of chain structure on the crystallization behaviors. *Polymers* **2019**, *11*, 1456. [[CrossRef](#)] [[PubMed](#)]
8. Bertin, S.; Robin, J.-J. Study and characterization of virgin and recycled LDPE/PP blends. *Eur. Polym. J.* **2002**, *38*, 2255–2264. [[CrossRef](#)]
9. Vranjes, N.; Rek, V. Effect of EPDM on Morphology, Mechanical Properties, Crystallization Behavior and Viscoelastic Properties of iPP+HDPE Blends. *Macromol. Symp.* **2007**, *258*, 90–100. [[CrossRef](#)]
10. Rachtanapun, P.; Selke, S.E.M.; Matuana, L.M. Microcellular foam of polymer blends of HDPE/PP and their composites with wood fiber. *J. Appl. Polym. Sci.* **2003**, *88*, 2842–2850. [[CrossRef](#)]
11. Lin, J.-H.; Pan, Y.-J.; Liu, C.-F.; Huang, C.-L.; Hsieh, C.-T.; Chen, C.-K.; Lin, Z.-I.; Lou, C.-W. Preparation and Compatibility Evaluation of Polypropylene/High Density Polyethylene Polyblends. *Materials* **2015**, *8*, 8850–8859. [[CrossRef](#)]
12. Van Eygen, E.; Laner, D.; Fellner, J. Circular economy of plastic packaging: Current practice and perspectives in Austria. *Waste Manag.* **2018**, *72*, 55–64. [[CrossRef](#)]

13. Curtzwiler, G.W.; Schweitzer, M.; Li, Y.; Jiang, S.; Vorst, K.L. Mixed post-consumer recycled polyolefins as a property tuning material for virgin polypropylene. *J. Clean. Prod.* **2019**, *239*. [[CrossRef](#)]
14. Dikobe, D.G.; Luyt, A.S. Comparative study of the morphology and properties of PP/LLDPE/wood powder and MAPP/LLDPE/wood powder polymer blend composites. *Express Polym. Lett.* **2010**, *4*, 729–741. [[CrossRef](#)]
15. Tanguy, M.; Bourmaud, A.; Beaugrand, J.; Gaudry, T.; Baley, C. Polypropylene reinforcement with flax or jute fibre; Influence of microstructure and constituents properties on the performance of composite. *Compos. Part B Eng.* **2018**, *139*, 64–74. [[CrossRef](#)]
16. Hidalgo-Salazar, M.A.; Salinas, E. Mechanical, thermal, viscoelastic performance and product application of PP- rice husk Colombian biocomposites. *Compos. Part B Eng.* **2019**, 107135. [[CrossRef](#)]
17. Verma, D.; Gope, P.C. The use of coir/coconut fibers as reinforcements in composites. *Biofiber Reinf. Compos. Mater.* **2015**, 285–319. [[CrossRef](#)]
18. Radoor, S.; Karayil, J.; Rangappa, S.M.; Siengchin, S.; Parameswaranpillai, J. A review on the extraction of pineapple, sisal and abaca fibers and their use as reinforcement in polymer matrix. *Express Polym. Lett.* **2020**, *14*, 309–335. [[CrossRef](#)]
19. Mochane, M.J.; Mokhena, T.C.; Mokhothu, T.H.; Mtibe, A.; Sadiku, E.R.; Ray, S.S.; Ibrahim, I.D.; Daramola, O.O. Recent progress on natural fiber hybrid composites for advanced applications: A review. *Express Polym. Lett.* **2019**, *13*, 159–198. [[CrossRef](#)]
20. Muñoz-Vélez, M.; Hidalgo-Salazar, M.; Mina-Hernández, J.; Muñoz-Vélez, M.F.; Hidalgo-Salazar, M.A.; Mina-Hernández, J.H. Effect of Content and Surface Modification of Fique Fibers on the Properties of a Low-Density Polyethylene (LDPE)-Al/Fique Composite. *Polymers* **2018**, *10*, 1050. [[CrossRef](#)]
21. Hidalgo, M.A.; Muñoz, M.F.; Quintana, K.J. Mechanical behavior of polyethylene aluminum composite reinforced with continuous agro fique fibers. *Rev. Lat. Met. Mat.* **2011**, *31*, 187–194.
22. Hidalgo Salazar, M.A.; Muñoz Velez, M.F.; Quintana Cuellar, K.J. Análisis mecánico del compuesto polietileno aluminio reforzado con fibras cortas de fique en disposición bidimensional (Mechanical analysis of polyethylene aluminum composite reinforced with short fique fibers available a in two-dimensional arrangement). *Rev. Latinoam. Metal. y Mater.* **2012**, *32*, 89–95.
23. Siengchin, S. Editorial corner—A personal view Potential use of ‘green’ composites in automotive applications. *Express Polym. Lett.* **2017**, *11*, 600. [[CrossRef](#)]
24. Correa, J.P.; Montalvo-Navarrete, J.M.; Hidalgo-Salazar, M.A. Carbon footprint considerations for biocomposite materials for sustainable products: A review. *J. Clean. Prod.* **2019**, *208*, 785–794. [[CrossRef](#)]
25. Väisänen, T.; Das, O.; Tomppo, L. A review on new bio-based constituents for natural fiber-polymer composites. *J. Clean. Prod.* **2017**, *149*, 582–596. [[CrossRef](#)]
26. Pickering, K.L.; Efendy, M.G.A.; Le, T.M. A review of recent developments in natural fibre composites and their mechanical performance. *Compos. Part A Appl. Sci. Manuf.* **2016**, *83*, 98–112. [[CrossRef](#)]
27. Alvarado, K.; Blanco, A.; Taquechel, A. Fibra de coco: Una alternativa ecológica como sustrato agrícola. *Agric. Org.* **2008**, *3*, 30–31.
28. Beigbeder, J.; Socalingame, L.; Perrin, D.; Bénétet, J.C.; Bergeret, A. How to manage biocomposites wastes end of life? A life cycle assessment approach (LCA) focused on polypropylene (PP)/wood flour and polylactic acid (PLA)/flax fibres biocomposites. *Waste Manag.* **2019**, *83*, 184–193. [[CrossRef](#)] [[PubMed](#)]
29. Sapuan, S.M. Materials Selection for Composites: Concurrent Engineering Perspective. In *Composite Materials*; Butterworth-Heinemann: Oxford, UK, 2017; Chapter 6.
30. Mohan Bhasney, S.; Kumar, A.; Katiyar, V. Microcrystalline cellulose, polylactic acid and polypropylene biocomposites and its morphological, mechanical, thermal and rheological properties. *Compos. Part B Eng.* **2020**, *184*, 107717. [[CrossRef](#)]
31. Essabir, H.; Raji, M.; Laaziz, S.A.; Rodrique, D.; Bouhfid, R.; Qaiss, A. el kacem Thermo-mechanical performances of polypropylene biocomposites based on untreated, treated and compatibilized spent coffee grounds. *Compos. Part B Eng.* **2018**, *149*, 1–11. [[CrossRef](#)]
32. Bledzki, A.K.; Franciszczak, P.; Osman, Z.; Elbadawi, M. Polypropylene biocomposites reinforced with softwood, abaca, jute, and kenaf fibers. *Ind. Crops Prod.* **2015**, *70*, 91–99. [[CrossRef](#)]
33. Mir, S.S.; Nafsin, N.; Hasan, M.; Hasan, N.; Hassan, A. Improvement of physico-mechanical properties of coir-polypropylene biocomposites by fiber chemical treatment. *Mater. Des.* **2013**, *52*, 251–257. [[CrossRef](#)]
34. Haque, M.; Rahman, R.; Islam, N.; Huque, M.; Hasan, M. Mechanical properties of polypropylene composites reinforced with chemically treated coir and abaca fiber. *J. Reinf. Plast. Compos.* **2010**, *29*, 2253–2261. [[CrossRef](#)]

35. Adeniyi, A.G.; Onifade, D.V.; Ighalo, J.O.; Adeoye, A.S. A review of coir fiber reinforced polymer composites. *Compos. Part B Eng.* **2019**, *176*, 107305. [[CrossRef](#)]
36. Burgstaller, C. A comparison of processing and performance for lignocellulosic reinforced polypropylene for injection moulding applications. *Compos. Part B Eng.* **2014**, *67*, 192–198. [[CrossRef](#)]
37. Pickering, K.L. *Properties and Performance of Natural-Fibre Composites*; Woodhead Publishing Limited-CRC Press: Boca Raton, FL, USA, 2008; ISBN 9781855737396.
38. Alves Fidelis, M.E.; Pereira, T.V.C.; Gomes, O.D.F.M.; De Andrade Silva, F.; Toledo Filho, R.D. The effect of fiber morphology on the tensile strength of natural fibers. *J. Mater. Res. Technol.* **2013**, *2*, 149–157. [[CrossRef](#)]
39. Kalagi, G.R.; Patil, R.; Nayak, N. Experimental Study on Mechanical Properties of Natural Fiber Reinforced Polymer Composite Materials for Wind Turbine Blades. In *Materials Today: Proceedings*; Elsevier Ltd.: Amsterdam, The Netherlands, 2018; Volume 5, pp. 2588–2596.
40. Latif, R.; Wakeel, S.; Zaman Khan, N.; Noor Siddiquee, A.; Lal Verma, S.; Akhtar Khan, Z. Surface treatments of plant fibers and their effects on mechanical properties of fiber-reinforced composites: A review. *J. Reinf. Plast. Compos.* **2019**, *38*, 15–30. [[CrossRef](#)]
41. Saheb, D.N.; Jog, J.P. Natural fiber polymer composites: A review. *Adv. Polym. Technol.* **1999**, *18*, 351–363. [[CrossRef](#)]
42. Sudhakar, P.; Jagadeesh, D.; Wang, Y.; Venkata Prasad, C.; Devi, A.P.K.; Balakrishnan, G.; Kim, B.S.; Song, J.I. Fabrication of Borassus fruit lignocellulose fiber/PP composites and comparison with jute, sisal and coir fibers. *Carbohydr. Polym.* **2013**, *98*, 1002–1010. [[CrossRef](#)] [[PubMed](#)]
43. Zainudin, E.S.; Yan, L.H.; Haniiffah, W.H.; Jawaid, M.; Alothman, O.Y. Effect of coir fiber loading on mechanical and morphological properties of oil palm fibers reinforced polypropylene composites. *Polym. Compos.* **2014**, *35*, 1418–1425. [[CrossRef](#)]
44. Sohn, J.S.; Cha, S.W. Effect of chemical modification on mechanical properties of wood-plastic composite injection-molded parts. *Polymers* **2018**, *10*, 1391. [[CrossRef](#)]
45. Blaine, R.L. Thermal Applications Note—Polymer Heat of Fusion. Available online: <http://www.tainstruments.com/pdf/literature/TN048.pdf> (accessed on 15 July 2019).
46. Xu, H.; Liu, C.Y.; Chen, C.; Hsiao, B.S.; Zhong, G.J.; Li, Z.M. Easy alignment and effective nucleation activity of ramie fibers in injection-molded poly(lactic acid) biocomposites. *Biopolymers* **2012**, *97*, 825–839. [[CrossRef](#)]
47. Zainal, M.; Santiago, R.; Ayob, A.; Ghani, A.A.; Mustafa, W.A.; Othman, N.S. Thermal and mechanical properties of chemical modification on sugarcane bagasse mixed with polypropylene and recycle acrylonitrile butadiene rubber composite. *J. Thermoplast. Compos. Mater.* **2019**, 089270571983207. [[CrossRef](#)]
48. Hassaini, L.; Kaci, M.; Touati, N.; Pillin, I.; Kervoelen, A.; Bruzaud, S. Valorization of olive husk flour as a filler for biocomposites based on poly(3-hydroxybutyrate-co-3-hydroxyvalerate): Effects of silane treatment. *Polym. Test.* **2017**, *59*, 430–440. [[CrossRef](#)]
49. Guo, C.; Song, Y.; Wang, Q.; Shen, C. Dynamic-mechanical analysis and SEM morphology of wood flour/polypropylene composites. *J. For. Res.* **2006**, *17*, 315–318. [[CrossRef](#)]
50. Hidalgo-Salazar, M.; Luna-Vera, F.; Pablo Correa-Aguirre, J. Biocomposites from Colombian Sugarcane Bagasse with Polypropylene: Mechanical, Thermal and Viscoelastic Properties. In *Characterizations of Some Composite Materials*; IntechOpen: London, UK, 2019.
51. Saba, N.; Jawaid, M.; Alothman, O.Y.; Paridah, M.T. A review on dynamic mechanical properties of natural fibre reinforced polymer composites. *Constr. Build. Mater.* **2016**, *106*, 149–159. [[CrossRef](#)]
52. Chaitanya, S.; Singh, I.; Song, J. II Recyclability analysis of PLA/Sisal fiber biocomposites. *Compos. Part B Eng.* **2019**, *173*, 106895. [[CrossRef](#)]
53. Manikandan Nair, K.C.; Thomas, S.; Groeninckx, G. Thermal and dynamic mechanical analysis of polystyrene composites reinforced with short sisal fibres. *Compos. Sci. Technol.* **2001**, *61*, 2519–2529. [[CrossRef](#)]
54. Bagotia, N.; Sharma, D.K. Systematic study of dynamic mechanical and thermal properties of multiwalled carbon nanotube reinforced polycarbonate/ethylene methyl acrylate nanocomposites. *Polym. Test.* **2019**, *73*, 425–432. [[CrossRef](#)]
55. Mohana Krishnudu, D.; Sreeramulu, D.; Venkateshwar Reddy, P. A study of filler content influence on dynamic mechanical and thermal characteristics of coir and luffa cylindrica reinforced hybrid composites. *Constr. Build. Mater.* **2020**, *251*, 119040. [[CrossRef](#)]

56. Romanzini, D.; Ornaghi, H.L.; Amico, S.C.; Zattera, A.J. Influence of fiber hybridization on the dynamic mechanical properties of glass/ramie fiber-reinforced polyester composites. *J. Reinf. Plast. Compos.* **2012**, *31*, 1652–1661. [[CrossRef](#)]
57. Sathyaseelan, P.; Sellamuthu, P.; Palanimuthu, L. Dynamic mechanical analysis of areca/kenaf fiber reinforced epoxy hybrid composites fabricated in different stacking sequences. *Mater. Today Proc.* **2020**. [[CrossRef](#)]
58. Fischer, J.M. *Handbook of Molded Part Shrinkage and Warpage*, 2nd ed.; Elsevier Inc.: Amsterdam, The Netherlands, 2012; ISBN 9781455730575.
59. Crawford, R.J.; Throne, J.L. Mechanical Part Design. In *Rotational Molding Technology*; Elsevier Inc.: Amsterdam, The Netherlands, 2002; pp. 307–365.
60. Masato, D.; Rathore, J.; Sorgato, M.; Carmignato, S.; Lucchetta, G. Analysis of the shrinkage of injection-molded fiber-reinforced thin-wall parts. *Mater. Des.* **2017**, *132*, 496–504. [[CrossRef](#)]
61. Tolinski, M. *Additives for Polyolefins: Getting the Most Out of Polypropylene, Polyethylene and TPO*, 2nd ed.; William Andrew: Oxford, UK, 2015; ISBN 9780323371773.
62. Azaman, M.D.; Sapuan, S.M.; Sulaiman, S.; Zainudin, E.S.; Khalina, A. Shrinkages and warpage in the processability of wood-filled polypropylene composite thin-walled parts formed by injection molding. *Mater. Des.* **2013**, *52*, 1018–1026. [[CrossRef](#)]
63. Azaman, M.D.; Sapuan, S.M.; Sulaiman, S.; Zainudin, E.S.; Abdan, K. An investigation of the processability of natural fibre reinforced polymer composites on shallow and flat thin-walled parts by injection moulding process. *Mater. Des.* **2013**, *50*, 451–456. [[CrossRef](#)]
64. Santos, J.D.; Fajardo, J.I.; Cuji, A.R.; García, J.A.; Garzón, L.E.; López, L.M. Experimental evaluation and simulation of volumetric shrinkage and warpage on polymeric composite reinforced with short natural fibers. *Front. Mech. Eng.* **2015**, *10*, 287–293. [[CrossRef](#)]



© 2020 by the authors. Licensee MDPI, Basel, Switzerland. This article is an open access article distributed under the terms and conditions of the Creative Commons Attribution (CC BY) license (<http://creativecommons.org/licenses/by/4.0/>).

Article

The Effects of Reprocessing and Fiber Treatments on the Properties of Polypropylene-Sugarcane Bagasse Biocomposites

Juan P. Correa-Aguirre ¹, Fernando Luna-Vera ², Carolina Caicedo ², Bairo Vera-Mondragón ² and Miguel A. Hidalgo-Salazar ^{1,*}

¹ Research Group for Manufacturing Technologies GITEM, Universidad Autónoma de Occidente, Cali 760030, Colombia; jpcorrea@uao.edu.co

² Research Group for Development of Materials and Products GIDEMP, National Center for Technical Assistance to Industry (ASTIN-SENA), Cali 760003, Colombia; fernandolunavera@gmail.com (F.L.-V.); ccaicedo60@misena.edu.co (C.C.); bvera@sena.edu.co (B.V.-M.)

* Correspondence: mahidalgo@uao.edu.co; Tel.: +57-2-3188-000

Received: 16 April 2020; Accepted: 22 June 2020; Published: 27 June 2020

Abstract: This study explores the reprocessing behavior of polypropylene-sugarcane bagasse biocomposites using neat and chemically treated bagasse fibers (20 wt.%). Biocomposites were reprocessed 5 times using the extrusion process followed by injection molding. The mechanical properties indicate that microfibers bagasse fibers addition and chemical treatments generate improvements in the mechanical properties, reaching the highest performance in the third cycle where the flexural modulus and flexural strength increase 57 and 12% in comparison with neat PP. differential scanning calorimetry (DSC) and TGA characterization show that bagasse fibers addition increases the crystallization temperature and thermal stability of the biocomposites 7 and 39 °C respectively, without disturbing the melting process of the PP phase for all extrusion cycles. The rheological test shows that viscosity values of PP and biocomposites decrease progressively with extrusion cycles; however, Cole–Cole plots, dynamic mechanical analysis (DMA), width at half maximum of tan delta peaks and SEM micrographs show that chemical treatments and reprocessing could improve fiber dispersion and fiber–matrix interaction. Based on these results, it can be concluded that recycling potential of polypropylene-sugarcane bagasse biocomposites is huge due to their mechanical, thermal and rheological performance resulting in advantages in terms of sustainability and life cycle impact of these materials.

Keywords: biocomposites; recycling; rheological properties; DMA; injection molding

1. Introduction

The reinforcement of polymers with natural fibers such as coir coconut, hemp, sisal, pineapple leaf fibers, sugarcane bagasse, fique and their combinations to create biocomposites has been studied in recent years [1–7]. The term biocomposites refers here to polymeric reinforced composites, where the reinforcing phase and/or the matrix are derived from materials of biological origin. In this sense, several studies have reported the formulation and characterization of biocomposites, which have a status of renewable and sustainable materials since they are composed of natural fibers embedded in non-degradable (i.e., polypropylene, polyethylene, polyamides, etc.) and biodegradable polymeric matrices (starch, polylactic acid, and polyhydroxialkanoates) [8,9].

These materials have the potential to replace traditional plastics in commercial applications such as car parts, toys, furniture, reusable cutlery, among others due to their low cost in comparison with traditional fibers and the enhancement of the polymeric matrices properties induced by natural

fibers incorporation. These improvements include weight reduction, better specific properties, dimensional stability, biodegradability, recyclability, decrease in the embodied energy of the products, carbon emissions, and costs due to the polymeric substitution fraction that reduces the amount of plastic material needed to manufacture products [3,10–14].

Sugarcane is one of the most important crops for sugar production around the world. According to the Food and Agriculture Organization located in Rome, Italy (FAO), Colombia is the second-largest producer of sugarcane in South America, with an estimated 220,000 ha planted in 2019 [15], which produces approximately 6 million tons of bagasse by year [16]. This agro-industrial by-product is generated in sugar factories after the cane stem has been crushed and pressed. Sugarcane fiber is mainly composed of cellulose (37 wt.%), hemicellulose (21 wt.%), lignin (22 wt.%) and pectin (10 wt.%) [17]. The availability of this by-product, its low cost and the possibility of valorization are competitive advantages for the development of bagasse fibers based biocomposites at the regional level.

The combination of natural fibers with polymeric matrices generates a problem associated with the incompatibility between the polar and hygroscopic cellulose of the fibers and the non-polar and hydrophobic polymers. Additionally, other components of the natural fiber like hemicellulose, lignin, pectin and waxes generate a smooth surface that hinders the interlocking and the interfacial bonding between the matrix and the reinforcing phase [2,17].

For this reason, several researchers have performed surface treatments over the natural fibers to improve their compatibility with the polymeric matrix. These surface treatments could exhibit physical or chemical nature according to the mechanism applied to improve the interfacial bonding. The most used surface treatment methods included molecular interdiffusion, electrostatic bonding, mechanical interlocking and chemical modification through bleaching, acetylation, alkaline treatments and chemical bonding by coupling agents such as silanes or maleic anhydride [2,17,18].

Anggono et al. [19] studied the incorporation of bagasse (up to 30 wt.%) in a polypropylene (PP) matrix using injection molding processes. They perform alkali treatments on the fibers with calcium hydroxide ($\text{Ca}(\text{OH})_2$) and sodium hydroxide (NaOH) and evaluated the effect of those treatments on the mechanical properties of the biocomposites. The results showed that the tensile strength of the biocomposites increases proportionally with bagasse content and chemical modification of these fibers. Additionally, the biocomposites obtained from NaOH treated fibers present the highest mechanical performance results. Carvahlo et al. [20] studied the effect of bagasse content (up to 20 wt.%) and chemical modification (NaOH and acetylation) on the mechanical performance of recycled high-density polyethylene-(r-PE) biocomposites obtained by extrusion. Their results show that chemical modification increased the compatibility between r-PE and bagasse fibers and improves the mechanical properties of the biocomposites. Zainal et al. [21] studied the mechanical, thermal and morphological properties of biocomposites based on a recycled polypropylene-acrylonitrile rubber blend (PP-NBRr) and chemically modified bagasse fibers (up to 30 wt.%) with NaOH and silanes, prepared using melt blending techniques. Their results showed that chemical modification of the fibers enhances the thermal stability and tensile mechanical properties of the biocomposites. They also observed that among chemical treatments, silanization generate better results on the evaluated properties.

The reviewed literature showed that natural fiber-polyolefin based biocomposites could be processed using high-volume manufacturing processes such as extrusion and injection molding reproducibility and production capacity, advantages for the development of products using these materials. However, these manufacturing processes generate some scrap. In the case of injection molding, the overall process generates waste as gates, runners and sprues, which must be ground after the process. Thus, the recycling of wastes generated after products life cycle ending and during processing is an issue to study further and a lucrative option for the growing biocomposites industry that has not yet been fully explored.

Mechanical recycling of polyolefins like PP has been studied due to its ease of processing, property retention and availability [22]. Martín-Alfonso and Franco studied the recycling of PP using multiple extrusion cycles (up to 10 cycles) [23]. Their results showed that thermo-mechanical reprocessing

generates a scission of the PP chains, which generates a progressive decrease in thermal stability, melting temperature, viscosity and viscoelastic properties with reprocessing cycles increase.

Regarding biocomposites, Uitterhaegen et al. [13] studied the mechanical behavior of biocomposites based on polyolefins (PP and Bio-PE) and coriander straw (up to 40 wt.%) ground and reprocessed 5 times using injection molding. The authors reported that mechanical properties did not decrease more than 10% through the reprocessing cycles, giving a high recycling potential to these polyolefin-based biocomposites. In another study, Chaitanya et al. [12] explored the recycling of biodegradable biocomposites based on polylactic acid (PLA) and alkaline treated sisal fibers (30 wt.%). The biocomposites were recycled using extrusion (8 cycles) and it was observed that mechanical properties gradually decreased until the third recycling cycle. Beyond these cycles, a significant reduction in properties was observed due to the decrease in PLA molecular weight and fibers attrition. From these results, the authors conclude that PLA-Sisal biocomposites can be recycled up to 3 times to make low to medium strength commercial products.

In the present research, PP-bagasse microfibers (untreated and chemically modified with NaOH and silanes) biocomposites were obtained through extrusion followed by injection molding processes. The mechanical, thermal, rheological and viscoelastic properties were evaluated and compared in order to understand the effect of chemical modification and reprocessing cycles (up to 5 times) on the microfibers dispersion on the biocomposites properties. We consider that the study of the performance of recycled biocomposites is an excellent contribution that supports the novelty of this article, bearing in mind that the interest in the design and manufacture of sustainable and highly recyclable products by injection molding with biocomposites based on natural fibers is increasing around the world.

2. Materials and Methods

2.1. Materials

PP reference 01H41 was sourced from Essentia (Cartagena, Colombia). Untreated sugarcane bagasse fibers were provided by Sucromiles S.A. (Cali, Colombia). In order to perform the chemical modification of these fibers, analytical-grade reagents hexadecyltrimethoxysilane and NaOH were obtained from Sigma-Aldrich (Milwaukee, WI, USA).

2.2. Methodology

2.2.1. Preparation and Chemical Modification of Sugarcane Bagasse

The bagasse fibers were first washed with distilled water and dried at 60 °C for 48 h to remove soil and residues. Then, clean bagasse fibers were grounded with a lab mill and sieved through a 200 µm sieve. The bagasse fibers were separated into three groups: untreated bagasse, aqueous solution of 8% NaOH treated bagasse and aqueous solution of 8% NaOH following by silanized treated bagasse. The chemical surface treatments were performed according to the procedure described in detail in previous research work reported earlier by our group [6].

2.2.2. Processing of Biocomposites

The reprocessing of the biocomposites was simulated using a continuous extrusions methodology. For this technique, the PP and the bagasse fibers were physically mixed in a bag using 20 wt.% of bagasse. This formulation was selected based on experimental results of our group and reviewed literature regarding the microinjection optimization of PP-Bagasse biocomposites [24]. This mixture was fed into the feed zone of a co-rotating twin-screw extruder HAAKE™ PolyLab™ (Thermo Scientific-United States) with 16 mm diameter and 40 D total length, using a temperature gradient between 140 and 170 °C and a screw speed of 70 rpm. These processing parameters were selected from previously reported studies on polyolefin-based biocomposites [6,25]. Then, the extruded material was cooled in water and subsequently pelletized using a mechanical cutter that generated 5 mm long pellets.

These pellets were dried in an air oven at 85 °C for 8 h after each extrusion cycle. The granules of neat PP and biocomposites were extruded 5 times, generating a total of 20 batches of granules that led to the development of 5 biocomposites and 10 reprocessed biocomposites. For this study, the properties of the materials corresponding to processing cycles 1, 3 and 5 were evaluated. The nomenclature of the prepared biocomposites is listed in Table 1.

Table 1. Nomenclature of processed biocomposites.

Processing Cycle Number	Neat PP (wt.%)	Sugar Cane Bagasse (wt.%)	Chemical Treatment	Designation Along the Document
1	100	-	-	PP 1st cycle
	80	20	-	PP-Bag 1st cycle
			NaOH	PP-Bag +alk. 1st cycle
			NaOH + Silanes	PP-Bag +alk. +sil 1st cycle
3	100	-	-	PP 3rd cycle
	80	20	-	PP-Bag 3rd cycle
			NaOH	PP-Bag +alk. 3rd cycle
			NaOH + Silanes	PP-Bag +alk. +sil 3rd cycle
5	100	-	-	PP 5th cycle
	80	20	-	PP-Bag 5th cycle
			NaOH	PP-Bag +alk. 5th cycle
			NaOH + Silanes	PP-Bag +alk.+sil 5th cycle

Finally, a small quantity of the pellets of the different biocomposites was used for the development of injected specimens for flexural and impact tests using a BOY XS microinjection molding machine (BOY Machines Inc., United States) with a temperature gradient between 180 and 185 °C (from the feeding area to the nozzle), a filling pressure of 80 bars, a holding pressure of 60 bars and a mold clamping force of 30 kN. Figure 1 shows the injected PP specimens corresponding to 1st, 3rd and 5th processing cycles and the biocomposites of the 1st processing cycle. It is observed that after the 3rd processing cycle, the neat PP samples show a yellow shade that indicates thermal degradation of the matrix during reprocessing.

2.2.3. Mechanical Properties

The mechanical properties in terms of flexural and impact performance of the materials were determined following the ASTM D790-17 and D256-10 standards, respectively. Three-point bending tests were performed using an INSTRON 3366 universal testing machine, while impact tests were performed using a 2.5 Joules impact tester. Flexural tests were carried out up to 5% deformation using specimens with a rectangular cross-section and 3.2 mm of thickness. The crosshead speed was 1.36 mm/min and the distance between the support span was 50 mm, while the impact tests were carried out on notched specimens (IZOD). The results were taken as the average of 5 samples and were subjected to an analysis of variance (ANOVA). Post hoc comparison was performed to determine the individual means, which are significantly different from a set of means of each reprocessing group using Tukey's test at a 5% probability level.

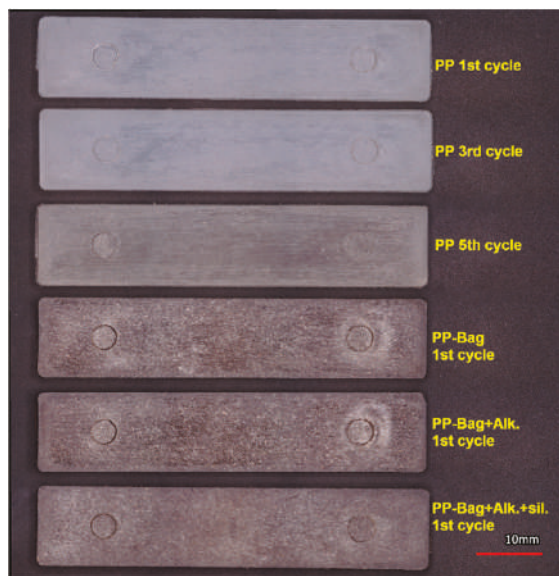


Figure 1. Injected specimens of PP and their bagasse fiber biocomposites.

2.2.4. Thermal Measurements

The thermal stability of the materials was evaluated by thermogravimetric analysis (TGA), measuring the weight loss (%) as a function of temperature using a TA Q500 thermogravimetric analyzer (Texas Instruments, Dallas, TX, USA). These tests were carried out from 25 to 600 °C at a heating rate of 10 °C/min in a nitrogen atmosphere to determine the onset degradation temperature (T_o) and the temperature at the maximum degradation rate (T_{max}). In order to explore the effect of reprocessing cycles and chemical modification of the fibers on the thermal properties of the material, differential scanning calorimetry (DSC) tests were performed. These tests were carried out at a heating–cooling rate of 10 °C/min in a nitrogen atmosphere in several steps: First, the samples were subjected to heating cycle from 20 to 190 °C to erase the thermal history related to processing events, following by a cooling cycle from 190 to 0 °C to determine crystallization temperature (T_c). Finally, a second heating cycle was performed from 0 to 200 °C to determine the melting temperature of the PP phase. Additionally, the degree of crystallinity (χ_c) of each material was calculated from Equation (1) [26]:

$$\chi_c = \left(\frac{\Delta H_m}{\Delta H_m^0 \times W} \times 100 \right) \quad (1)$$

where W represents the PP fraction by weight, ΔH_m is the normalized melting enthalpy of PP of each sample, and ΔH_m^0 (207 J/g) is the melting enthalpy of 100% crystalline PP [27].

2.2.5. Rheological Measurements

The rheological behavior was determined by a rotational rheometer DHR-2 (Texas Instruments, Dallas, TX, USA) equipped with a cone-plate configuration with a diameter of 25 mm and an angle of 5.7°. For this geometry, the cone was truncated to avoid contact between the cone and the plate, and to prevent damage to either with a calibrated distance of 145 µm at the center of the cone. The rheological measurements were performed at 195 °C, the shear rate between 0.1 and 10 s⁻¹ and a strain of 1%. Storage modulus (G'), loss modulus (G'') and complex viscosity (η^*) were measured.

2.2.6. Dynamic Mechanical Analysis (DMA)

The thermo-mechanical properties of the materials were evaluated using a dynamic mechanical analysis (DMA) RSA-G2 (Texas Instruments, Dallas, TX, USA) with a three-point bending clamp. The equipment was set up as follows: frequency of 1 Hz, 0.01% of strain, temperature range from -50 to 120 °C and a heating rate of 3 °C/min. Storage modulus (E'), loss modulus (E'') and $\tan \delta$ (loss factor) were measured.

2.2.7. Scanning Electronic Microscopy (SEM)

SEM of the different samples was carried out on the cryogenic fracture surfaces of non-tested injected specimens, operating at a voltage of 10 kV. The samples were previously sputter-coated with gold to increase their electric conductivity. Magnifications of $200\times$ of the fracture surfaces were taken.

3. Results and Discussion

3.1. Mechanical Properties

The influence of bagasse fibers addition and reprocessing cycles on the PP flexural properties were evaluated. With ever increasing demand for high quality and reliable materials and products, flexural tests have become an important tool in both the manufacturing process and research fields to define the material ability to resist deformation under load [28]. Some recent studies have been carried out to study the effects of reprocessing on the flexural and tensile properties of PP reinforced with natural fibers [13,24]. Their results show some differences between flexural and tensile properties, the latter being lower than the former.

During a tensile test, the entire sample is under tensile stress and the rupture begins through the propagation of the largest defect within the specimen. On the other hand, during a flexural test, the maximum stress occurs at the upper and lower surfaces of the specimen where the shear stress is minimum. If the largest defect in the sample is not located in these sections, its influence on the failure mechanism and, therefore, on the flexural strength of the material will be minimal [13]. Therefore, the tensile strength values will be lower as compared to flexural strength values. Despite these differences, in these studies, it was observed that the results of both characterization techniques follow a similar trend with reprocessing cycles. Therefore, the flexural test has been validated as a valuable tool for the mechanical characterization of biocomposites. Figure 2 presents the three-dimensional colormap surface of the flexural modulus and flexural strength of the materials, which are summarized in the Table 2.

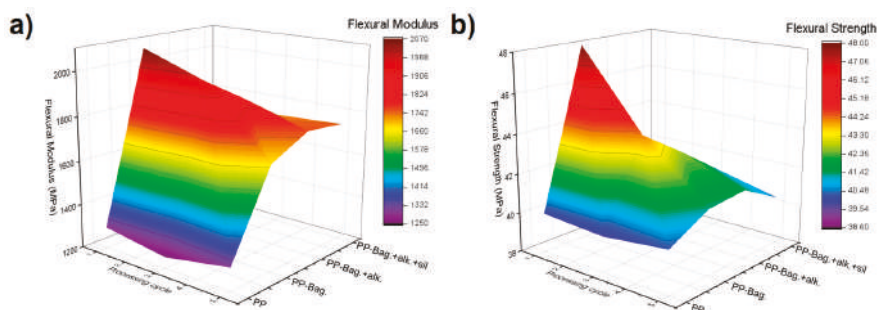


Figure 2. Three-dimensional colormap surface of flexural modulus (a) and flexural strength (b) of PP and PP-Bagasse biocomposites.

The 3D colormap surface indicates that successive reprocessing cycles did not affect the flexural behavior of the PP. However, bagasse fibers addition and chemical treatments performed on these fibers generate improvements in the flexural properties of the PP matrix. Additionally, it is observed

that flexural behavior of biocomposites are dependent on reprocessing cycles of the materials, reaching maximum values around the third cycle. With subsequent reprocessing, a decrease in flexural properties was observed.

Table 2. Flexural properties of PP and PP-Bagasse biocomposites.

Sample	Flexural Modulus (MPa)			Flexural Strength (MPa)		
	Processing Cycle Number					
	1	3	5	1	3	5
PP	1296 ± 70a	1251 ± 54a	1305 ± 36a	40.0 ± 0.7a	39.8 ± 0.9a	40.2 ± 0.4a
PP-Bag.	2069 ± 30b	1969 ± 48b	1673 ± 100b	48.0 ± 1.1b	44.1 ± 0.7b	41.3 ± 1.3a
PP-Bag.+alk.	1847 ± 114c	1853 ± 68c	1761 ± 78b	43.3 ± 0.5c	42.7 ± 0.3c	41.5 ± 1.2a
PP-Bag. +alk.+sil.	1505 ± 94d	1729 ± 66c	1742 ± 116b	38.6 ± 1.9a	41.2 ± 0.4d	40.4 ± 0.9a

(a–d) Different letters in the same column indicate significative differences from a set of means of each reprocessing group ($p < 0.05$).

The first processing cycle shows the flexural modulus (FM) of biocomposites PP-Bag. and PP-Bag. + Alk, increased by 60% and 42% compared to neat PP. Additionally, flexural strength values (FS) increased by 20% and 8%, respectively. For biocomposite PP-Bag. +alk. +sil. FM value increased by 16%; however, no significant differences in the FS value were observed ($p \geq 0.05$). Cerqueira et al. investigated the effect of untreated bagasse addition on the flexural properties of PP and found that FM and FS values increased by 32% and 35% respectively [29]. These improvements in flexural properties due to the addition of natural fibers have been observed in long [30] and short fibers [31,32]. However, it is essential to remark that our study demonstrated that this effect was also generated with the addition of microfibers.

For the third processing cycle, all FM and FS values of the biocomposites show significant differences compared to the FM value of the PP matrix. These increments were 57%, 48% and 38% for PP-Bag., PP-Bag. + Alk. and PP-Bag. +alk. +sil respectively. Additionally, FS values increased by 11%, 7% and 4% respectively. It is interesting to show that FM and FS values of the sample PP-Bag. +alk. +sil. increased by 15% and 7% in comparison with the first processing cycle values. This could be related to a better dispersion state of the silanized bagasse fibers within the PP matrix, the higher thermal stability of chemically modified fibers [6] and a better interaction fiber–matrix generated by the reprocessing cycles.

For the last reprocessing cycle, FM values of the biocomposites show significant differences in comparison with the PP matrix ($p < 0.05$); however, no significant differences were observed among the biocomposites. In the same way, the FS values of the samples were statistically equivalent. These results show that reprocessing could improve fiber dispersion and improve fiber–matrix interaction under compression stresses developed in the biocomposites during bending. However, these improvements seem to achieve a maximum point that in our study corresponded to the third cycle.

Similar behavior was reported by Chaitanya et al., [12], who studied the recyclability of polylactic acid-sisal biocomposites. They found that reprocessing generates a severe reduction in mechanical and viscoelastic properties due to fiber and matrix degradation; therefore, they concluded that recycling of PLA/Sisal biocomposites beyond third reprocessing cycle is not recommended. Figure 3 shows the effect of the addition of bagasse fibers and the reprocessing cycles on the impact strength values.

For the first processing cycle, no significant differences were observed in the impact strength values of the PP matrix and the biocomposites PP-Bag. and PP-Bag. + Alk. However, for the PP-Bag. + Alk. +sil. biocomposite the impact strength increased by around 40% compared to neat PP. This result shows that bagasse fibers treated by silanes agents had improved the capacity of the polymeric matrix to absorb energy. From the revised literature, it can be observed that several factors governed the impact behavior of natural fiber-reinforced biocomposites, for example, chemical treatment applied on the natural fibers, type of natural fiber, interfacial bonding, the composition of the biocomposite and

the toughness of the polymeric matrix. In the case of silanes treatments, it was found that this process may have different effects on the impact properties of biocomposite PE-Hemp and PE-Sisal [17].

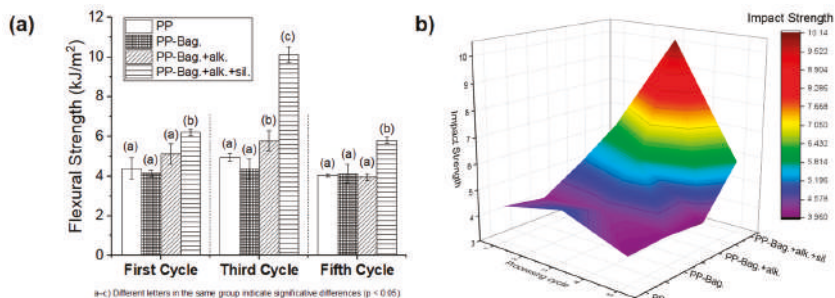


Figure 3. (a) Impact properties of PP and PP-Bagasse biocomposites and (b) 3D colormap surface of the impact properties.

Biocomposites reprocessing causes interesting changes in the impact properties studied. According to the 3D colormap surface (Figure 3b), the third reprocessing cycle generates a significant increase in the impact values of PP-Bag. + Alk. and PP-Bag. + Alk. +sil. biocomposites. These increases were between 17 and 103% in comparison with reprocessed PP. For the fifth processing cycle, the impact values have similar behavior to that observed in the first cycle. The impact value of biocomposite PP-Bag. + Alk. +sil. increased by 43% compared to the PP. These results are evidence that reprocessing improves the dispersion state of the silanized fibers, fiber–matrix interaction and promotes PP energy absorption. However, as observed in the flexural test these improvements reach their highest point around the third reprocessing cycle.

3.2. Thermal Properties

DSC curves for neat PP and their biocomposites with bagasse fibers at the 1st, 3rd and 5th processing cycles are shown in Figures 4–6. The numerical values of the thermal events of the samples are shown in Table 3. These thermograms do not show any indication of bagasse fibers because the peaks attributed to the different reactions or mechanisms involved in pyrolyzing of the bagasse appears at temperatures higher than those selected for our DSC tests (above 290 °C) [33,34]. However, the fibers effect on the crystallization and melting behavior of the PP phase are discussed in this work.

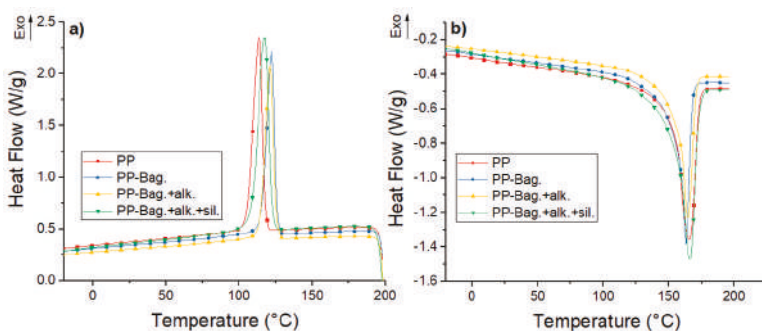


Figure 4. (a) Cooling and (b) second heating DSC curves for first processing cycle PP and PP-Bagasse biocomposites.

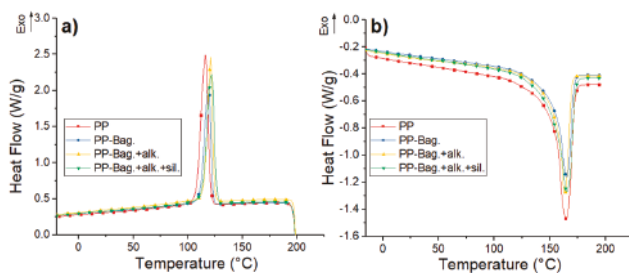


Figure 5. (a) Cooling and (b) second heating DSC curves for third processing cycle PP and PP-Bagasse biocomposites.

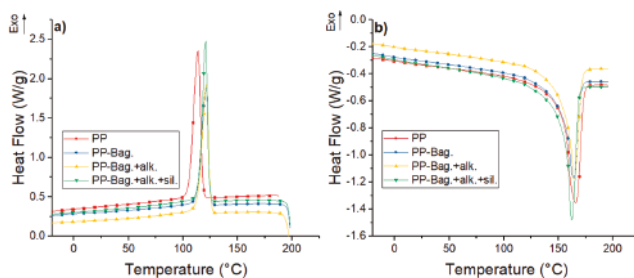


Figure 6. (a) Cooling and (b) second heating DSC curves for fifth processing cycle PP and PP-Bagasse biocomposites.

Table 3. Thermal properties on cooling and second heating differential scanning calorimetry (DSC) scans of the samples.

Processing Cycle Number	Sample	Cooling		Second Heating	
		T _c * (°C)	T _m * (°C)	ΔH _m (J/g)	X _c (%)
1	PP	114	166	91	44
	PP-Bag.	122	163	75	45
	PP-Bag. +alk.	121	165	74	44
	PP-Bag. +alk. +sil.	118	166	99	59
3	PP	116	165	101	49
	PP-Bag.	119	165	80	49
	PP-Bag. +alk.	121	163	84	50
	PP-Bag. +alk. +sil.	122	165	100	60
5	PP	114	166	95	46
	PP-Bag.	121	164	75	46
	PP-Bag. +alk.	121	164	78	47
	PP-Bag. +alk. +sil.	121	162	83	50

* T_c and T_m were taken at the maximum peak of crystallization and melting peaks.

Cooling thermograms of PP show exothermic peaks located between 114 and 116 °C. These peaks corresponded to the crystallization during the cooling of the PP chains. These crystallization peaks are also observed in PP-Bagasse biocomposites, however, these peaks are located at temperatures between 3 and 7 °C higher compared to the PP in the different extrusion cycles. This shows that bagasse fibers could act as nucleation points that allow the crystallization of PP chains at higher temperatures.

The second heating runs of PP and PP-Bagasse biocomposites present endothermic peaks between 163 and 166 °C related to the melting of the PP matrix. This indicates that bagasse fibers addition did not interfere with the melting process of the PP matrix. In this study, the maximum processing temperature was 185 °C, which is higher than PP melting temperature. This was done with the aim to ensure completely melting of PP crystals and improving the processing of the material without causing degradation to the bagasse fibers. In this aspect, some authors reported that biocomposites processing must be performed below 200 °C to avoid natural fibers degradation [2,17,35].

Additionally, melting enthalpy (ΔH_m) and crystallinity degree (χ_c) values of the biocomposites changed with the number of extrusion cycles and with the bagasse fiber type. For all extrusion cycles, a decrease in the ΔH_m values of PP-Bag and PP-Bag.-alk biocomposites were observed. However, the χ_c of the PP matrix remained similar when the ΔH_m was corrected, considering the weight fraction of bagasse (Equation (1)). This behavior was also observed in other natural fiber-polyolefin biocomposites [5,36]. On the other hand, for biocomposites with silanized bagasse fibers (extrusion cycles 1 and 3), an increase in the χ_c values of around 15% was observed in comparison with the χ_c of the PP matrix. This χ_c increase was slightly for cycle 5; however, it is concluded that the silanized process improved the nucleating effect of the bagasse fibers in the PP. Therefore, the mechanical strength improvement observed in the PP-Bagasse biocomposites could be related to the reinforcement effect of bagasse fibers in the PP and the crystallinity changes of the thermoplastic matrix. Similar results were reported by Zainal et al. [21] on polypropylene-acrylonitrile butadiene rubber-modified bagasse biocomposites. They reported that the chemical treatment of bagasse fibers using silanes increases the nucleation density and the crystallinity degree (%) of the polymeric matrix.

Thermogravimetry (TG) and Derivative Thermogravimetry (DTG) thermograms of PP and PP-Bagasse biocomposites at the 1st, 3rd and 5th processing cycles are shown in Figures 7–9. Additionally, the main thermal parameters obtained from these curves are summarized in Table 4.

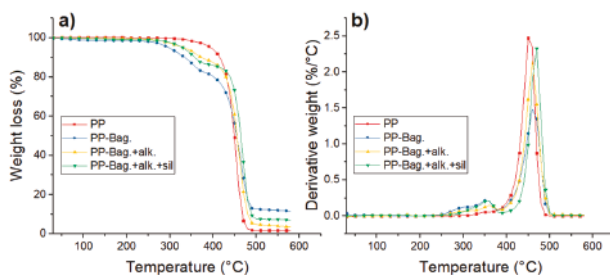


Figure 7. (a) TG and (b) DTG curves for first processing cycle PP and PP-Bagasse biocomposites.

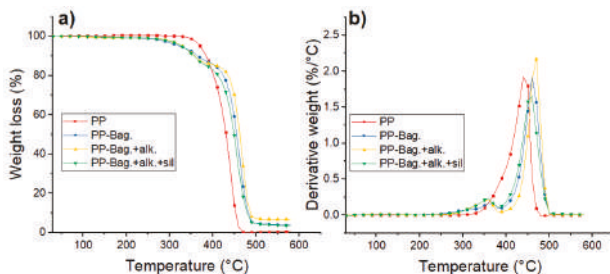


Figure 8. (a) TG and (b) DTG curves for third processing cycle PP and PP-Bagasse biocomposites.

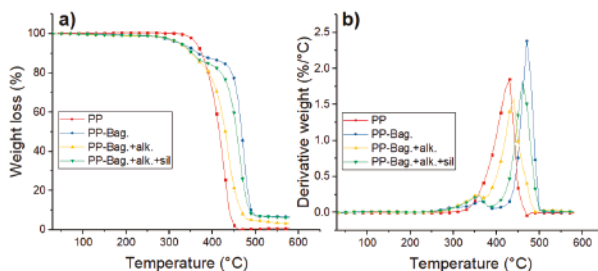


Figure 9. (a) TG and (b) DTG curves for fifth processing cycle PP and PP-Bagasse biocomposites.

Table 4. Thermal degradation data of PP and PP-Bagasse biocomposites.

Processing Cycle	Sample	Degradation Stage	T _O (°C)	T _{max} (°C)
First cycle	PP	1	408	455
		2	423	462
	PP-Bag.	1	271	354
		2	423	462
	PP-Bag. +alk.	1	314	363
		2	438	461
	PP-Bag. +alk. +sil.	1	317	360
		2	447	468
Third cycle	PP	1	373	445
		2	431	463
	PP-Bag.	1	271	363
		2	431	463
	PP-Bag. +alk.	1	309	358
		2	431	468
	PP-Bag. +alk. +sil.	1	310	358
		2	428	457
Fifth cycle	PP	1	371	431
		2	430	472
	PP-Bag.	1	287	366
		2	430	472
	PP-Bag. +alk.	1	318	360
		2	417	440
	PP-Bag. +alk. +sil.	1	322	360
		2	434	461

The thermal degradation of PP matrices occurs in a single step process. For the first cycle, a T_O of 408 °C and a T_{max} of 455 °C were observed. For reprocessing cycles 3 and 5, T_O values decreased by 35 and 37 °C while T_{max} decreased by 10 and 24 °C as compared with PP at the first extrusion cycle. This lowering in PP thermal stability with melt reprocessing has been already observed in other studies and could be related to the chain scission mechanism of PP during multiple extrusions [23,37]. Da costa et al. cited that scission of the PP chains during reprocessing generates small and defective molecules, a broader distribution of molecular weights and reduction in the onset degradation temperature of the polymer [38].

For biocomposites, degradation occurs in a two-step process. The first step is related to the decomposition of the bagasse fibers within the biocomposite, while the second step corresponds to the thermal degradation of the PP matrix [6]. The first degradation step show that thermal stability of the chemically treated bagasse fibers is higher than the exhibited by untreated fibers. According to a previous research work published recently by our group the performed chemical treatments could help to extract low thermal stability components of the bagasse fibers like hemicellulose, lignin, pectin and

waxes [6]. With only cellulose, the bagasse fibers gain some thermal stability. Additionally, the silanes presence increases thermal stability of the bagasse fibers within the biocomposite, mostly due to the formation of refractory siloxane networks between the fibers and PP after silanization as indicated by literature [39].

The second degradation stage shows that bagasse addition increases the thermal stability of the PP phase. For the first reprocessing cycle, T_g increased between 15 and 39 °C. Additionally, T_{max} increased between 13 and 6 °C in comparison to neat PP as shown in Table 4. This increment in the thermal stability of the biocomposites has been observed in several studies and could be related to the increase of the crystallinity with bagasse addition observed by DSC [40,41]. This behavior is more evident during reprocessing cycles 3 and 5 due to the observed decrease of the thermal stability of neat PP during melt reprocessing. This result shows that bagasse addition improves the thermal stability of the polymer matrix when reprocessing cycles, such as mechanical recycling, are carried out.

After 500 °C, the residue of the samples remains. These residues were composed mainly of ashes and had a weight of 12% for PP-Bag., 8% for PP-Bag. +alk. +sil. and 4% for PP-Bag. +alk. This difference could be related to lignin present on the untreated bagasse, which generates a large number of solid residues after the pyrolysis of the fiber [33].

3.3. Rheological Properties

The influence of bagasse fibers addition and reprocessing cycles on the PP storage modulus (G') and loss modulus (G'') modulus vs. a frequency is presented in Figure 10. According to Osswald and Rudolph, G' is a measure for the stored energy and is related to the rigidity and relative entanglement of polymeric chains. On the other hand, G'' is a measure for the lost energy dissipated, for example, as heat or used on the relative movement among polymeric chains [42].

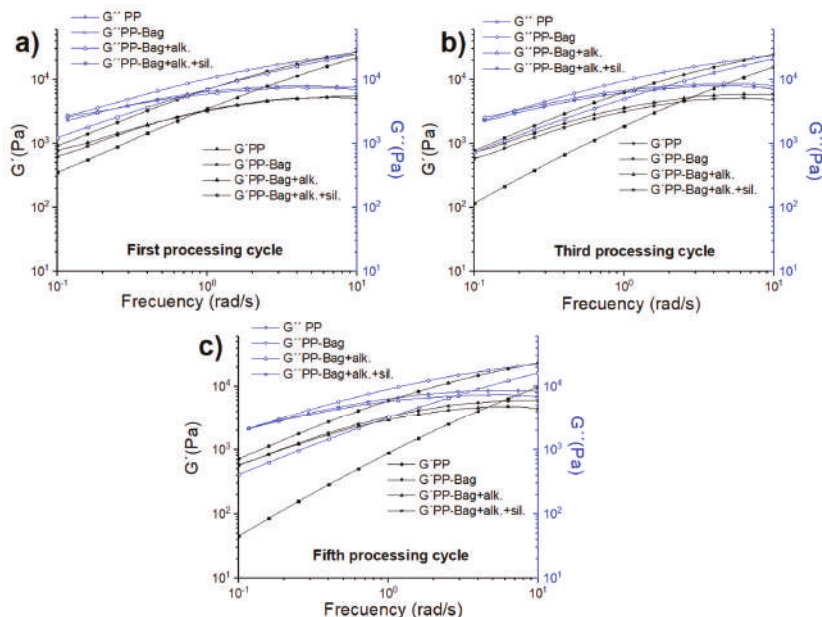


Figure 10. Storage and loss modulus as a frequency function of PP and PP-Bagasse biocomposites: (a) First, (b) Third and (c) Fifth processing cycles.

The results show that G'' is higher than G' for neat PP and all biocomposites, indicating that these materials present a dominant liquid viscoelastic behavior in the studied frequency range. This behavior

has previously been observed in another polyolefin-natural fiber biocomposites with fiber percentages up to 20% by weight [43,44]. Additionally, it is observed that G' and G'' values of neat PP and biocomposites decrease with successive reprocessing cycles. This decrease has been previously observed and could be related to changes in the length and entanglements of PP polymeric chains caused by multiple extrusion processes [23]. Therefore, the elastic behavior of the biocomposites would be lower with successive reprocessing cycles.

Besides this, a decrease in G' and G'' values are observed in biocomposites with chemically modified bagasse fibers. These chemical treatments modify the surface of the bagasse fibers; in general terms, these modifications reduce the particle agglomeration, improving the slip or flow between them inside the biocomposite. This is reflected in lower G' and G'' values. It is interesting to note that the biocomposites with silanized bagasse fibers present the lowest G' and G'' values for all reprocessing cycles. This could be due to short silane chains that could act as a lubricant at the PP-bagasse fibers interface and could reduce the internal stress generated by fibers agglomeration.

Figure 11 provides the complex viscosity vs. frequency of the neat PP and biocomposites. All materials show shear-thinning behavior, as had been previously observed in PP and PP-natural fiber biocomposites [43]. This behavior is related to the viscoelastic nature of the polymeric matrix and the interaction with the bagasse fibers. At the frequencies studied, the polymeric chains do not have enough recovery time due to the contact between the fibers leading to the non-Newtonian rheological characteristics observed.

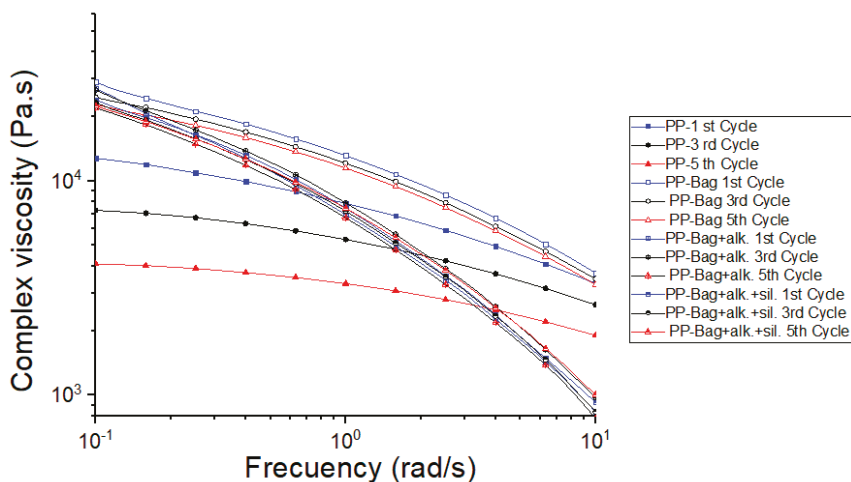


Figure 11. Complex viscosity as a frequency function of PP and PP-Bagasse biocomposites.

The results also show that PP-Bag. biocomposites present the higher viscosity values in the entire frequency range studied. For PP-Bag., the relative movement and disentanglement of bagasse fibers are impeded due to agglomeration of fibers, which hinders polymer chains flow and increasing the viscosity values. For biocomposites obtained from chemically modified bagasse fibers, the viscosity values are lower in comparison to PP-Bag. biocomposites. As mentioned above, the untreated fibers can agglomerate due to adhesive forces between fibers. The performed alkaline treatment aimed to extract the lignin, which is a hydrophobic layer that covers the bagasse fibers. This treatment exposed the cellulose of the bagasse and improved their dispersion within the polymeric matrix, thus decreased the particle–particle interactions, allowing the polymer chains to flow and decreased the viscosity. Furthermore, the silanes treatment produced a functionalized surface with covalent Si-O bonds, which hindered the agglomeration of the fibers and acted as a lubricant, which improved the fibers flowing within the polymeric matrix, causing a decrease in the viscosity values and eased the

processability of the biocomposites by conventional plastic transformation processes such as extrusion or injection molding.

Regarding the reprocessing cycles, it is observed that the viscosity values of PP and biocomposites decreased progressively with extrusion cycles. This decrease of the viscosity values was also reported on several PP reprocessing studies and can be related to a decrease of the PP matrix molecular weight due to polymeric chain scission during the multiple extrusion reprocessing steps [23,37,38].

With the aim of further investigate the effect of reprocessing and bagasse fibers addition on the rheological and structural behavior of the materials, Cole–Cole diagrams were used (Figure 12). In this diagram, the imaginary viscosity component (η'') is represented as a function of the real component of the viscosity (η'). The graph should be like a semicircle if the system describes a single relaxation. In heterogeneous melts containing agglomerated fibers, the semicircle shape of the Cole–Cole graph will be modified, the elastic component of the viscosity, and the relaxation time increases [42].

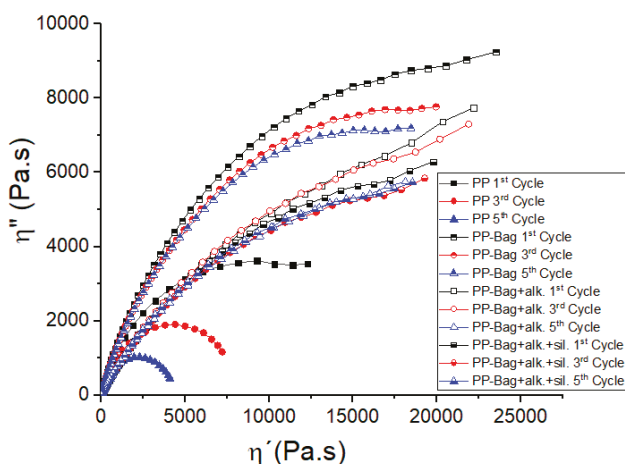


Figure 12. Cole–Cole plots of PP and PP-Bagasse biocomposites.

The Cole–Cole plots of neat PP revealed a semicircle related to single relaxation time. On the other hand, untreated bagasse fibers addition generated an increase in the elastic behavior and relaxation time of the structure, visualized in viscosity components values increments. This behavior indicates the presence of agglomerated fibers and decreased progressively with extrusion cycles. Finally, it is observed that chemical modification of bagasse fibers clearly generated a decrease in the elastic component of the viscosity (η'') and shorter relaxation times of the materials. These results could indicate that continuous extrusion processes and chemical modification generate a better dispersion of bagasse fibers within the polymeric matrix.

3.4. Dynamic Mechanical Analysis

According to Saba et al., [45], the storage modulus (E') is related to the ability of a material to store energy during a dynamic test and determine the stiffness of the sample. Additionally, E' is essential for the evaluation of the mechanical properties from the molecular basis because it is sensitive to structural changes within the polymeric matrix such as molecular weight and the interfacial bond between the fibers and the matrix.

Figure 13 shows the E' as a function of temperature for the first processing cycle. It can be observed that E' values of PP increase after the bagasse fibers incorporation. At room temperature, the E' value of neat PP (1481 MPa) increased to 18% with the addition of untreated bagasse fibers. This stiffness increase could be attributed to a decrease in the PP chains mobility generated by the rigid bagasse

fibers and indicates that PP-Bag biocomposite had a higher capacity to store energy in comparison with neat PP. This behavior was even more significant after the incorporation of chemically modified bagasse. E' value increased by 32 and 52% for PP-Bag. +alk. +sil. and PP-Bag. +alk. in comparison with neat PP, respectively. These results show that chemical modifications induced a better adhesion on the interface between bagasse fibers and PP matrix and increased the material capacity to absorb energy. This result was in good agreement with the data obtained from the impact test (Section 3.1).

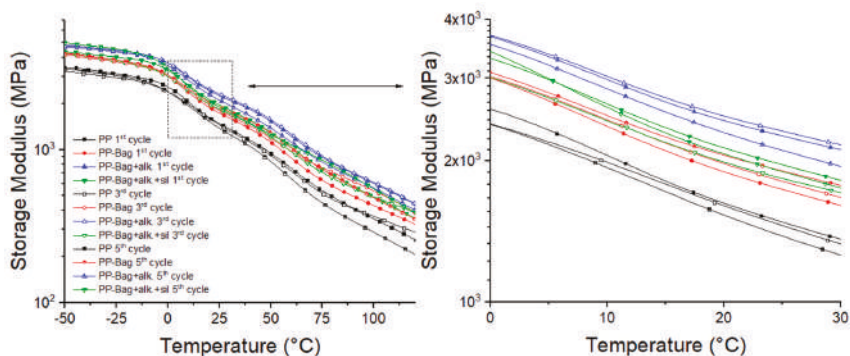


Figure 13. Temperature dependence of the storage modulus of PP and their biocomposites.

Regarding reprocessing cycles, it is observed that E' values of biocomposites increased progressively with extrusion cycles in comparison with neat PP. For the third reprocessing cycle, E' values increased up to 27 and 60% for PP-Bag and PP-Bag. +alk., whereas, for the fifth reprocessing cycle, this increment lay between 35 and 57% (again for PP-Bag and PP-Bag. +alk.). This processing event has been already observed during PLA-Sisal biocomposites recycling and indicates that thermo-mechanical reprocessing generate an improvement in the interfacial bonding between the bagasse fibers and the PP matrix [12].

Similar to the observed behavior in E' graphs, the E'' peaks of PP-bag biocomposites were higher as compared to neat PP (Figure 14). These increases indicate a reduction in the mobility of PP chains due to bagasse fibers. These increases of E'' peaks were higher upon chemically modified bagasse incorporation for all reprocessing cycles and could be related to the enhanced adhesion at the interphase given by the chemical treatments, which suppressed the molecular mobility of the polymeric matrix. This trend has been observed for several polymer-chemical treated fibers biocomposites [6,46,47].

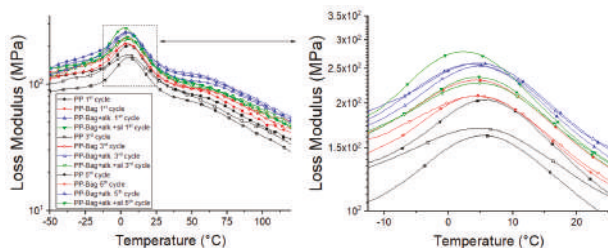


Figure 14. Temperature dependence of loss modulus of PP and their biocomposites.

$\tan \delta$ is defined as the ratio between the loss and storage modulus ($\tan \delta = E''/E'$) and is related to the damping properties of the polymeric matrix [45]. The variation of $\tan \delta$ with temperature is represented in Figure 15. According to this graph, PP shows two main relaxation peaks in the evaluated temperature range, a β relaxation, located around 7–9 °C, which corresponds to the glass transition (T_g) and an α relaxation between 60 and 75 °C [6].

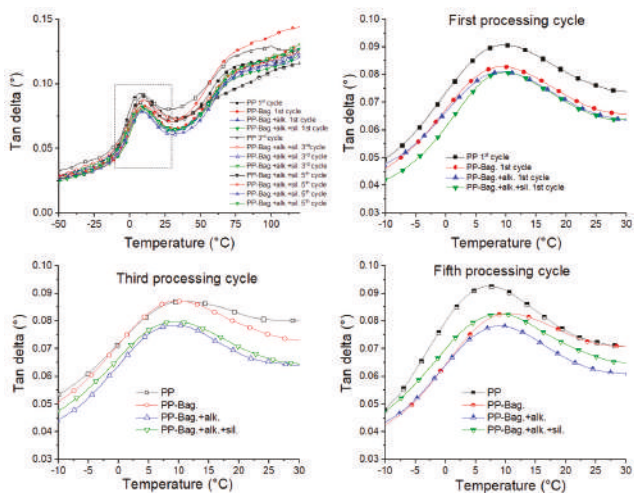


Figure 15. Temperature dependence of tan delta of neat PP and their biocomposites.

Table 5 shows that after untreated bagasse fibers addition into neat PP, $Tan \delta$ peaks height decreased for all reprocessing cycles. This is because bagasse fibers hinder the mobility of the polymer chains; also, these fibers support higher stresses fields, which generate less deformation of them at the interface, which causes more energy dissipation. Additionally, it is observed that bagasse fibers addition did not generate significant changes in PP relaxations values (Table 5). For biocomposites obtained from chemically modified bagasse fibers, the $Tan \delta$ peaks exhibited even lower magnitude when compared with untreated bagasse biocomposites for all reprocessing cycles. These results, albeit small, show that biocomposites with improved interfacial bonding between natural fibers and PP matrix, given by the chemical modification, will tend to dissipate less energy, showing the lower magnitude of the $Tan \delta$ peak in comparison with biocomposites with a weakly bonded interface and can be decisive in product applications that require better mechanical behavior under flexural loads.

To further understand the mobility of the chain segments and the state of dispersion, the full width at half maximum (FWHM) of $\tan \delta$ peaks was evaluated. Some studies on biocomposites viscoelastic properties have shown that FWHM is a measurement of $\tan \delta$ curve broadness and could be useful to evaluate the reduction of the molecular mobility during a relaxation like the glass transition [48,49]. According to Manikandan et al., a higher FWHM value implies more interaction and contact between the phases of the composite, which can be associated with low dispersion and a heterogeneous amorphous phase [49]. Among biocomposites, those based on untreated bagasse fibers present the higher FWHM values for all reprocessing cycles. This could be attributed to the suppressed effect of the poor dispersed fibers on the PP matrix molecular mobility. It is also observed that FWHM values decreased for all biocomposites with reprocessing, and it was found to be the lowest for chemically treated fiber-based biocomposites. This result shows that the successive reprocessing improved the homogeneity of the matrix and confirmed that chemical treatments improved the adhesion at the interface, which suppressed the molecular movement of the polymer matrix. This means that biocomposites obtained from chemically modified fibers acted more elastic and confirmed that under a load, these biocomposites had more potential to store energy instead of dissipating it.

Table 5. Dynamic mechanical analysis (DMA) results of the studied materials.

Processing Cycle Number	Sample	T _g (°C) *	E' (MPa) at 25 °C	Full Width at Half Maximum (FWHM) of Tan δ Peaks	Tan δ Peaks Height
1	PP	7.9	1481	24.4	0.091
	PP-Bag.	8.2	1741	23.3	0.083
	PP-Bag. +alk.	8.1	2261	21.9	0.081
	PP-Bag. +alk. +sil.	8.6	1962	22.2	0.081
3	PP	8.4	1453	24.9	0.087
	PP-Bag.	8.3	1810	22.5	0.087
	PP-Bag. +alk.	7.3	2319	20.7	0.078
	PP-Bag. +alk. +sil.	7.9	1835	20.5	0.080
5	PP	7.0	1383	23.4	0.093
	PP-Bag.	8.9	1905	22.7	0.083
	PP-Bag. +alk.	8.1	2111	21.1	0.080
	PP-Bag. +alk. +sil.	8.2	1899	21.8	0.078

* T_g values of the PP phase were taken at the maximum peak of the tan delta curves.

3.5. Morphology

Figure 16 shows the cryogenic fracture surface of neat PP (Figure 16a) and PP-bag. Biocomposites at the first (Figure 16b,c) and fifth reprocessing cycles (Figure 16d,e). Neat PP presents an irregular surface fracture, which is caused by the inherent semi-crystalline structure of this polymer whereas untreated bagasse incorporation generates a rough fracture surface.

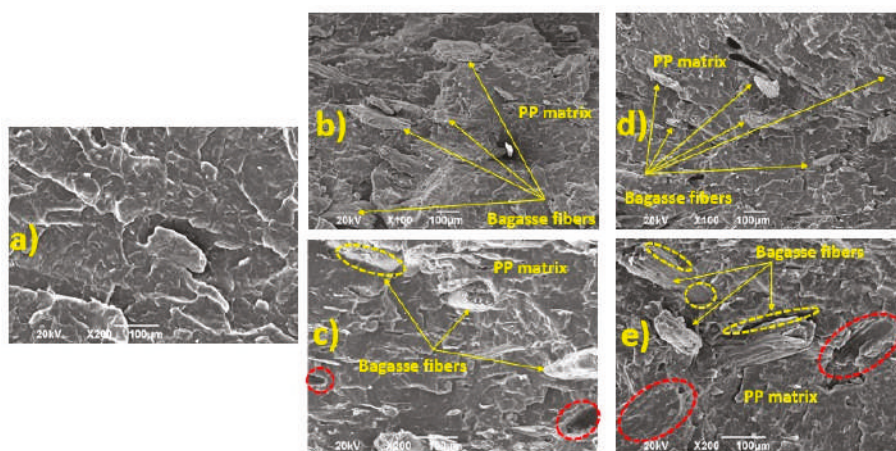


Figure 16. SEM micrograph of the fracture surface of (a) neat PP, (b,c) PP-Bag. 1st cycle and (d,e) PP-Bag. 5th cycle.

Regarding the first cycle, the lower magnification allows one to observe bundles of bagasse fibers within the PP matrix with an average length of 213 ± 24 micrometers (Figure 16b). On the other hand, higher magnification (Figure 16c) show some voids resulting from the fibers pulled out from the matrix (as shown in red circles) and well-delineated gaps at the interface between the bagasse fibers and the PP matrix (yellow circles). These gaps are evidence of the low interfacial adhesion between the PP and the untreated bagasse fibers. This microstructural behavior at the interface was observed

in different polymer matrix biocomposites and was related to the low chemical affinity between the inherent hydrophobic polyolefin matrix and the hydrophilic natural fiber.

After five reprocessing cycles, a better distribution of the fibers and a decrease in their length to 165 ± 17 micrometers was observed (Figure 16c). This result shows that during the five extrusion and injection cycles the fibers get crushed to some extent and their length was reduced by 20% and could be related to the decrease observed in the mechanical performance observed in PP-bag. biocomposites considering all reprocessing cycles (Table 2).

Several studies have shown that reprocessing of biocomposites generates a decrease of 60% in the fibers length. The fibers length decreasing is higher than that observed in our study, however the initial size of the fibers used must be considered. In these studies, the initial size of the fibers was 1–0.8 mm, while in our study, the initial average size was around 0.2 mm. However, the authors report that biocomposites retain its mechanical performance throughout cycles better than fiberglass reinforced composites due to the inherent flexibility of the natural fibers and the ability to resist external mechanical forces.

Reprocessing cycles will inevitably impact the mechanical properties of biocomposites; however, our study shows that PP-Bag. biocomposites' mechanical performance was maintained up to three reprocessing cycles without the addition of virgin material. Based on this result, it could be concluded that recycling potential of biocomposites was huge due to their mechanical performance retention resulting in advantages in terms of sustainability and life cycle impact of these materials.

Figure 17 shows the cryogenic fracture surface corresponding to the biocomposites of the fifth reprocessing cycle along with the optical micrograph of the surface of each sample at the same lighting level. For Figure 17b,c, chemical treatments reduced the gaps between the bagasse fibers and the PP matrix and improved the interface of the biocomposites. Additionally, the optical micrographs of chemically modified fibers based biocomposites show a decrease of the dark areas related to particles agglomeration on the surface of the sample. This behavior is observed in better detail in the sample with silanized bagasse and could be due to the lubricant effect given by silanes, which improved the dispersion of the fibers. This result was also consistent with the data obtained by rheology and DMA measurements and confirmed that chemical treatments generated a bonding effect at the PP and natural fibers interface and exposed the cellulose of the bagasse improving their dispersion within the polymeric matrix.

The scanning electronic microscopy gives valuable information about biocomposites morphological characterization. Several authors have made conclusions studying the fiber content (composition), the chemical treatment of natural fibers, and biocomposites reprocessing using SEM [12,20,21,44]. This technique, together with the performed rheological and dynamic mechanical characterization, could provide valuable evidence of the dispersion state of the fibers within the biocomposites. In our case, the Cole–Cole plots and FWHM of $\tan \delta$ peaks gave evidence for concluding that multiple extrusion cycles could decrease the particle agglomeration and generated a better dispersion of the fibers within the matrix.

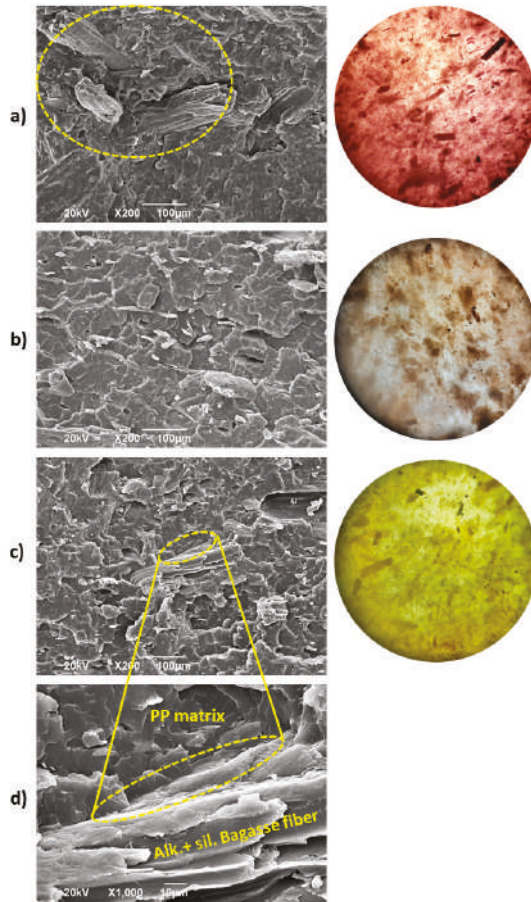


Figure 17. SEM (left) and optical micrographs (right) for 5th processing cycle: (a) PP-Bag., (b) PP-Bag + Alk. and PP-Bag + Alk. +sil. (c,d).

4. Conclusions

In this research, PP-bagasse biocomposites were prepared by incorporating 20% by weight of bagasse fibers treated by alkaline treatment with NaOH and silanization after the alkaline treatment.

These biocomposites were reprocessed 5 times using the extrusion process followed by injection molding after each reprocessing cycle in order to evaluate the effects of reprocessing and chemical treatments on the morphology, mechanical, thermal, as well as viscoelastic properties of these materials. Doing so, the following conclusions could be obtained from the present research:

- The mechanical properties indicate that reprocessing and chemical treatments performed to bagasse microfibers could improve fiber dispersion and fiber–matrix interaction under compression stresses developed in the biocomposites during bending, and promoted PP energy absorption. These mechanical improvements achieved a maximum point that, in our study, corresponded to the third cycle.
- Thermal characterization revealed that bagasse fibers addition increased the crystallization temperature and the thermal stability of the PP phase for all extrusion cycles without disturbing

the melting process of the PP matrix. Additionally, silanized fibers based biocomposites presented the highest thermal stability for all processing cycles.

- The rheological test shows that the viscosity values of PP and biocomposites decreased progressively with extrusion cycles. Additionally, biocomposites obtained from chemically modified bagasse particles presented lower viscosity values in comparison with neat bagasse based biocomposites. However, Cole–Cole plots indicates that continuous extrusion processes and chemical modification generated a better dispersion of bagasse fibers within the polymeric matrix.
- DMA results included a complete analysis of the height and broadness of $\tan \delta$ peaks and show that reprocessing and chemical modifications induced a better adhesion on the interface between bagasse fibers and PP matrix and increased the PP capacity to absorb energy.
- SEM micrographs show that during reprocessing the bagasse fibers got crushed to some extent and length was reduced around 20%. However it is important to remark that despite this decrease in fiber length, PP-Bag. biocomposites' mechanical performance was maintained up to three reprocessing cycles without the addition of virgin material. Additionally, chemical treatments generated a bonding effect at the PP and natural fibers interface and exposed the cellulose of the bagasse, improving their dispersion within the polymeric matrix.
- Based on these findings, it could be concluded that bagasse fibers show an interesting potential for biocomposites production with a high potential of application in the design and manufacture of sustainable and highly recyclable products by injection molding. This could generate some economic and environmental benefits in the search for sustainability in the plastics industry.

Author Contributions: Conceptualization, F.L.-V. and M.A.H.-S.; Formal analysis, J.P.C.-A., F.L.-V., C.C. and M.A.H.-S.; Funding acquisition, B.V.-M. and M.A.H.-S.; Investigation, J.P.C.-A., F.L.-V., C.C. and M.A.H.-S.; Methodology, J.P.C.-A., F.L.-V., C.C. and M.A.H.-S.; Project administration, B.V.-M. and M.A.H.-S.; Resources, B.V.-M. and M.A.H.-S.; Supervision, B.V.-M.; Writing—original draft, J.P.C.-A., F.L.-V. and M.A.H.-S.; Writing—review and editing, J.P.C.-A., F.L.-V., C.C., B.V.-M. and M.A.H.-S. All authors have read and agreed to the published version of the manuscript.

Funding: This research received no external funding.

Acknowledgments: The authors acknowledge the Autónoma de Occidente University (Cali-Colombia) for technical and financial support; Research Group of New Solids with Industrial Application-GINSAI (Autónoma de Occidente University) for its support in the thermal characterization; National Center for Technical Assistance to Industry-ASTIN SENA (Cali-Colombia) for its technical support through injection molds manufacturing and rheological measurements; University del Valle (Cali-Colombia) for SEM microscopy. Also, the authors wish to thank to the company “Sucromiles” (Cali-Colombia), for providing the raw sugarcane bagasse.

Conflicts of Interest: The authors declare no conflict of interest.

References

1. Mochane, M.J.; Mokhena, T.C.; Mokhothu, T.H.; Mtibe, A.; Sadiku, E.R.; Ray, S.S.; Ibrahim, I.D.; Daramola, O.O. Recent progress on natural fiber hybrid composites for advanced applications: A review. *Express Polym. Lett.* **2019**, *13*, 159–198. [[CrossRef](#)]
2. Pickering, K.L.; Efendy, M.G.A.; Le, T.M. A review of recent developments in natural fibre composites and their mechanical performance. *Compos. Part A Appl. Sci. Manuf.* **2016**, *83*, 98–112. [[CrossRef](#)]
3. Hidalgo-Salazar, M.A.; Correa-Aguirre, J.P.; Montalvo-Navarrete, J.M.; Lopez-Rodriguez, D.F.R.-G.A. Recycled Polypropylene-Coffee Husk and Coir Coconut Biocomposites: Morphological, Mechanical, Thermal and Environmental Studies. In *Thermosoftening Plastics*; IntechOpen: London, UK, 2020.
4. KC, B.; Faruk, O.; Agnelli, J.A.M.; Leao, A.L.; Tjong, J.; Sain, M. Sisal-glass fiber hybrid biocomposite: Optimization of injection molding parameters using Taguchi method for reducing shrinkage. *Compos. Part A Appl. Sci. Manuf.* **2016**, *83*, 152–159. [[CrossRef](#)]
5. Hidalgo-Salazar, M.A.; Correa, J.P. Mechanical and thermal properties of biocomposites from nonwoven industrial Figue fiber mats with Epoxy Resin and Linear Low Density Polyethylene. *Results Phys.* **2018**, *8*, 461–467. [[CrossRef](#)]

6. Hidalgo-Salazar, M.; Luna-Vera, F.; Pablo Correa-Aguirre, J. Biocomposites from Colombian Sugarcane Bagasse with Polypropylene: Mechanical, Thermal and Viscoelastic Properties. In *Characterizations of Some Composite Materials*; IntechOpen: London, UK, 2019.
7. Radoor, S.; Karayil, J.; Rangappa, S.M.; Siengchin, S.; Parameswaranpillai, J. A review on the extraction of pineapple, sisal and abaca fibers and their use as reinforcement in polymer matrix. *Express Polym. Lett.* **2020**, *14*, 309–335. [[CrossRef](#)]
8. Beigbeder, J.; Soccalingame, L.; Perrin, D.; Bénétet, J.C.; Bergeret, A. How to manage biocomposites wastes end of life? A life cycle assessment approach (LCA) focused on polypropylene (PP)/wood flour and polylactic acid (PLA)/flax fibres biocomposites. *Waste Manag.* **2019**, *83*, 184–193. [[CrossRef](#)] [[PubMed](#)]
9. Sapuan, S.M. Chapter 6 - Materials Selection for Composites: Concurrent Engineering Perspective. In *Composite Materials*; Butterworth-Heinemann: Oxford, UK, 2017.
10. Väisänen, T.; Das, O.; Tomppo, L. A review on new bio-based constituents for natural fiber-polymer composites. *J. Clean. Prod.* **2017**, *149*, 582–596. [[CrossRef](#)]
11. Correa, J.P.; Montalvo-Navarrete, J.M.; Hidalgo-Salazar, M.A. Carbon footprint considerations for biocomposite materials for sustainable products: A review. *J. Clean. Prod.* **2018**. [[CrossRef](#)]
12. Chaitanya, S.; Singh, I.; Song, J. II Recyclability analysis of PLA/Sisal fiber biocomposites. *Compos. Part B Eng.* **2019**, *173*, 106895. [[CrossRef](#)]
13. Uitterhaegen, E.; Parinet, J.; Labonne, L.; Mérian, T.; Ballas, S.; Véronèse, T.; Merah, O.; Talou, T.; Stevens, C.V.; Chabert, F.; et al. Performance, durability and recycling of thermoplastic biocomposites reinforced with coriander straw. *Compos. Part A Appl. Sci. Manuf.* **2018**, *113*, 254–263. [[CrossRef](#)]
14. Hidalgo Salazar, M.A.; Muñoz Velez, M.F.; Quintana Cuellar, K.J. Análisis mecánico del compuesto polietileno aluminio reforzado con fibras cortas de fique en disposición bidimensional (Mechanical analysis of polyethylene aluminum composite reinforced with short fique fibers available in a two-dimensional arrangement). *Rev. Latinoam. Metal. Mater.* **2011**, *32*, 89–95.
15. FAO Food Outlook: Sugar chapter. Available online: http://www.fao.org/fileadmin/templates/est/COMM_MARKETS_MONITORING/Sugar/Documents/sugar_assessment_food_outlook_may_2019.pdf (accessed on 3 April 2020).
16. Carlos Cueva-Orjuela, J.; Hormaza-Anaguano, A.; Merino-Restrepo, A. Sugarcane bagasse and its potential use for the textile effluent treatment. *Rev. DYNA* **2017**, *84*, 291–297. [[CrossRef](#)]
17. Latif, R.; Wakeel, S.; Zaman Khan, N.; Noor Siddiquee, A.; Lal Verma, S.; Akhtar Khan, Z. Surface treatments of plant fibers and their effects on mechanical properties of fiber-reinforced composites: A review. *J. Reinf. Plast. Compos.* **2019**, *38*, 15–30. [[CrossRef](#)]
18. Muñoz-Vélez, M.; Hidalgo-Salazar, M.; Mina-Hernández, J.; Muñoz-Vélez, M.F.; Hidalgo-Salazar, M.A.; Mina-Hernández, J.H. Effect of Content and Surface Modification of Fique Fibers on the Properties of a Low-Density Polyethylene (LDPE)-Al/Fique Composite. *Polymers* **2018**, *10*, 1050. [[CrossRef](#)]
19. Anggono, J.; Sugondo, S.; Sewucipto, S.; Purwaningsih, H.; Henrico, S. The use of sugarcane bagasse in PP matrix composites: A comparative study of bagasse treatment using calcium hydroxide and sodium hydroxide on composite strength. *AIP Conf. Proc.* **2017**, *1788*, 030055.
20. de Carvalho Neto, A.G.V.; Ganzerli, T.A.; Cardozo, A.L.; Fávaro, S.L.; Pereira, A.G.B.; Giroto, E.M.; Radovanovic, E. Development of composites based on recycled polyethylene/sugarcane bagasse fibers. *Polym. Compos.* **2014**, *35*, 768–774. [[CrossRef](#)]
21. Zainal, M.; Santiago, R.; Ayob, A.; Ghani, A.A.; Mustafa, W.A.; Othman, N.S. Thermal and mechanical properties of chemical modification on sugarcane bagasse mixed with polypropylene and recycle acrylonitrile butadiene rubber composite. *J. Thermoplast. Compos. Mater.* **2019**, 089270571983207. [[CrossRef](#)]
22. Achilias, D.S.; Antonakou, E.; Roupakias, C.; Megalokonomos, P.; Lappas, A. Recycling techniques of polyolefins from plastic wastes. *Glob. Nest J.* **2008**, *10*, 114–122. [[CrossRef](#)]
23. Martín-Alfonso, J.E.; Franco, J.M. Influence of polymer reprocessing cycles on the microstructure and rheological behavior of polypropylene/mineral oil oleogels. *Polym. Test.* **2015**, *45*, 12–19. [[CrossRef](#)]
24. Lila, M.K.; Singhal, A.; Banwait, S.S.; Singh, I. A recyclability study of bagasse fiber reinforced polypropylene composites. *Polym. Degrad. Stab.* **2018**, *152*, 272–279. [[CrossRef](#)]
25. Hidalgo-Salazar, M.A.; Salinas, E. Mechanical, thermal, viscoelastic performance and product application of PP- rice husk Colombian biocomposites. *Compos. Part B Eng.* **2019**, *176*, 107135. [[CrossRef](#)]

26. Mazian, B.; Bergeret, A.; Benezet, J.C.; Malhautier, L. Impact of field retting and accelerated retting performed in a lab-scale pilot unit on the properties of hemp fibres/polypropylene biocomposites. *Ind. Crops Prod.* **2020**, *143*, 111912. [CrossRef]
27. Blaine, R.L. Thermal Applications Note - Polymer Heat of Fusion. Available online: <http://www.tainstruments.com/pdf/literature/TN048.pdf> (accessed on 15 July 2019).
28. Hodgkinson, J.M. Testing the strength and stiffness of polymer matrix composites. In *Failure Mechanisms in Polymer Matrix Composites*; Elsevier: Amsterdam, The Netherlands, 2012; pp. 129–182.
29. Cerqueira, E.F.; Baptista, C.A.R.P.; Mulinari, D.R. Mechanical behaviour of polypropylene reinforced sugarcane bagasse fibers composites. *Procedia Eng.* **2011**, *10*, 2046–2051. [CrossRef]
30. Hidalgo, M.A.; Muñoz, M.F.; Quintana, K.J. Mechanical behavior of polyethylene aluminum composite reinforced with continuous agro fique fibers. *Rev. Lat. Met. Mat.* **2011**, *31*, 187–194.
31. Hidalgo, M.; Muñoz, M.; Quintana, K. Mechanical analysis of polyethylene aluminum composite reinforced with short fique fibers available a in two-dimensional arrangement. *Rev. Latinoam. Metal. Mater.* **2012**, *32*, 89–95.
32. Bourmaud, A.; Baley, C. Investigations on the recycling of hemp and sisal fibre reinforced polypropylene composites. *Polym. Degrad. Stab.* **2007**, *92*, 1034–1045. [CrossRef]
33. Yang, H.; Yan, R.; Chen, H.; Lee, D.H.; Zheng, C. Characteristics of hemicellulose, cellulose and lignin pyrolysis. *Fuel* **2007**, *86*, 1781–1788. [CrossRef]
34. Fernandes Pereira, P.H.; Cornelis, H.; Voorwald, J.; Odila, M.; Cioffi, H.; Mulinari, D.R.; Da Luz, S.M.; Lucia, M.; Pinto, C.; Silva, D. Sugarcane Bagasse Pulp and Bleaching: Thermal and Chemical Characterization. *BioRes* **2011**, *6*, 2471–2482.
35. Ramamoorthy, S.K.; Skrifvars, M.; Persson, A. A Review of Natural Fibers Used in Biocomposites: Plant, Animal and Regenerated Cellulose Fibers. *Polym. Rev.* **2015**, *55*, 107–162. [CrossRef]
36. Hidalgo-Salazar, M.A.; Muñoz, M.F.; Mina, J.H. Influence of Incorporation of Natural Fibers on the Physical, Mechanical, and Thermal Properties of Composites LDPE-Al Reinforced with Fique Fibers. *Int. J. Polym. Sci.* **2015**. [CrossRef]
37. Caicedo-Cano, C.; Crespo-Delgado Lina, M.; De La Cruz-Rodríguez Hever, Á.-J.N.A. Thermo-mechanical properties of Polypropylene: Effects during reprocessing. *Ing. Investig. Technol.* **2017**, *18*, 245–252. [CrossRef]
38. Da Costa, H.M.; Ramos, V.D.; Rocha, M.C.G. Rheological properties of polypropylene during multiple extrusion. *Polym. Test.* **2005**, *24*, 86–93. [CrossRef]
39. Kabir, M.M.; Wang, H.; Lau, K.T.; Cardona, F. Chemical treatments on plant-based natural fibre reinforced polymer composites: An overview. *Compos. Part B Eng.* **2012**, *43*, 2883–2892. [CrossRef]
40. Luz, S.M.; Gonçalves, A.R.; Del’arco, A.P.; Ferrão, P.M.C. Composites from Brazilian natural fibers with polypropylene: Mechanical and thermal properties. *Compos. Interfaces* **2008**, *15*, 841–850. [CrossRef]
41. Motaung, T.E.; Linganiso, L.Z.; John, M.; Anandjiwala, R.D.; Motaung, T.E.; Linganiso, L.Z.; John, M.; Anandjiwala, R.D. The Effect of Silane Treated Sugar Cane Bagasse on Mechanical, Thermal and Crystallization Studies of Recycled Polypropylene. *Mater. Sci. Appl.* **2015**, *6*, 724–733. [CrossRef]
42. Osswald, T.; Rudolph, N. *Polymer Rheology. Fundamentals and Applications*; Hanser Publications: Munich, Germany, 2015; ISBN 9781569905173.
43. Ares, A.; Bouza, R.; Pardo, S.G.; Abad, M.J.; Barral, L. Rheological, mechanical and thermal behaviour of wood polymer composites based on recycled polypropylene. *J. Polym. Environ.* **2010**, *18*, 318–325. [CrossRef]
44. Escócio, V.A.; Pacheco, E.B.A.V.; Silva, A.L.N.; da Cavalcante, A.d.P.; Visconte, L.L.Y. Rheological Behavior of Renewable Polyethylene (HDPE) Composites and Sponge Gourd (*Luffa cylindrica*) Residue. *Int. J. Polym. Sci.* **2015**, *2015*, 714352. [CrossRef]
45. Saba, N.; Jawaid, M.; Alothman, O.Y.; Paridah, M.T. A review on dynamic mechanical properties of natural fibre reinforced polymer composites. *Constr. Build. Mater.* **2016**, *106*, 149–159. [CrossRef]
46. Shinoj, S.; Visvanathan, R.; Panigrahi, S.; Varadharaju, N. Dynamic mechanical properties of oil palm fibre (OPF)-linear low density polyethylene (LLDPE) biocomposites and study of fibre-matrix interactions. *Biosyst. Eng.* **2011**, *109*, 99–107. [CrossRef]
47. Mohanty, S.; Verma, S.K.; Nayak, S.K. Dynamic mechanical and thermal properties of MAPE treated jute/HDPE composites. *Compos. Sci. Technol.* **2006**, *66*, 538–547. [CrossRef]

48. Xu, H.; Liu, C.Y.; Chen, C.; Hsiao, B.S.; Zhong, G.J.; Li, Z.M. Easy alignment and effective nucleation activity of ramie fibers in injection-molded poly(lactic acid) biocomposites. *Biopolymers* **2012**, *97*, 825–839. [[CrossRef](#)] [[PubMed](#)]
49. Manikandan Nair, K.; Thomas, S.; Groeninckx, G. Thermal and dynamic mechanical analysis of polystyrene composites reinforced with short sisal fibres. *Compos. Sci. Technol.* **2001**, *61*, 2519–2529. [[CrossRef](#)]



© 2020 by the authors. Licensee MDPI, Basel, Switzerland. This article is an open access article distributed under the terms and conditions of the Creative Commons Attribution (CC BY) license (<http://creativecommons.org/licenses/by/4.0/>).

Article

Characterization, Biocompatibility, and Optimization of Electrospun SF/PCL/CS Composite Nanofibers

Hua-Wei Chen * and Min-Feng Lin

Department of Chemical and Materials Engineering, National Ilan University, Yilan 26047, Taiwan; superlemi@gmail.com

* Correspondence: hwchen@niu.edu.tw

Received: 9 March 2020; Accepted: 25 June 2020; Published: 27 June 2020

Abstract: In this study, composite nanofibers (SF/PCL/CS) for the application of dressings were prepared with silk fibroin (SF), polycaprolactone (PCL), and chitosan (CS) by electrospinning techniques, and the effect of the fiber diameter was investigated using the three-stage Taguchi experimental design method (L9). Nanofibrous scaffolds were characterized by the combined techniques of scanning electron microscopy (SEM) and transmission electron microscopy (TEM), a cytotoxicity test, proliferation tests, the antimicrobial activity, and the equilibrium water content. A signal-to-noise ratio (S/N) analysis indicated that the contribution followed the order of SF to PCL > flow rate > applied voltage > CS addition, possibly owing to the viscosity and formation of the beaded fiber. The optimum combination for obtaining the smallest fiber diameter (170 nm) with a smooth and uniform distribution was determined to be a ratio of SF to PCL of 1:2, a flow rate of 0.3 mL/hr, and an applied voltage of 25 kV at a needle tip-to-collector distance of 15 cm (position). The viability of these mouse fibroblast L929 cell cultures exceeded 50% within 24 hours, therefore SF/PCL/CS could be considered non-toxic according to the standards. The results proposed that the hydrophilic structure of SF/PCL/CS not only revealed a highly interconnected porous construction but also that it could help cells promote the exchange of nutrients and oxygen. The SF/PCL/CS scaffold showed a high interconnectivity between pores and porosity and water uptake abilities able to provide good conditions for cell infiltration and proliferation. The results from this study suggested that SF/PCL/CS could be suitable for skin tissue engineering.

Keywords: chitosan; composite nanofibers; electrospinning; silk fibroin; polycaprolactone; Taguchi

1. Introduction

In recent decades, nanofiber membranes have been widely used in various fields and attracted more attention due to their unique properties, such as large specific surface areas, high porosity, interconnected pores, and high functionality. Electrospun composite nanofibers possess great potentialities in biomedical applications, such as tissue engineering [2–4], wound healing [5–7], and drug delivery [8–10], as well as other applications such as magnetism [11], photonics [12], filtration [13], composites [14], shape memory [15], and lithium batteries [16]. The diameter of electrospun nanofibers affects many important properties, such as the melting point, tensile modulus, hardness, drug delivery, biological factors, and cell growth of nonwoven fabrics [17,18]. Research [19] has demonstrated that fiber diameter plays a key role in cell adhesion, proliferation, and cell migration on the scaffold.

Silk fibroin (SF), which is extracted mainly from silkworms, has various properties, including good biocompatibility, biodegradability, morphological flexibility, mechanical properties, a low inflammatory response, non-toxicity, and non-carcinogenicity, and it can promote cell adhesion, migration, and the proliferation of cell ligands [8,20,21]. However, the β -sheet secondary structure of pure SF seems to impede the electrospinning process, and the mechanical properties of neat SF electrospun fibers were

poor [20]. Herein, polycaprolactone (PCL), the most commonly used synthetic polymer, was chosen to be blended with SF. PCL is widely used in tissue engineering and drug delivery applications due to its good mechanical properties and biodegradability. PCL has limitations to its biological activity, hydrophobicity, and bacterial degradation, therefore PCL cannot provide the adhesion environment required for cells [2]. PCL has renowned mechanical properties and does not have ionizable side groups in its structures, such as $-\text{COOH}$ and $-\text{NH}_2$, which occur on the natural polymer chitosan (CS) and on several anionic polysaccharides and proteins, respectively. The CS is an amino polysaccharide derived from chitin that has excellent biological properties, such as biocompatibility, biodegradability, hydrophilicity, non-toxicity, and antithrombotic and antimicrobial activities. Chitosan that possesses positively charged groups (amine groups) is likely to interact with negatively charged cell membranes via electrostatic interaction. Furthermore, the antimicrobial activity of chitosan effectively increases the permeability of negatively charged cell membranes to disrupt and release intracellular compounds [22]. Therefore, investigations of SF and its association with other components (PCL and CS) are carried out to give better mechanical properties to the smooth nanofibers for the tissue engineering. The Taguchi method is an effective method to find the influence of different factors on the target results, thereby improving the manufacturability, reliability, and quality of a product and reducing the number of experiments and calculation time [23,24].

Thus, SF/PCL/CS composite nanofiber scaffolds for the application of dressings and tissue engineering were fabricated with PCL polymer as a precursor using electrospinning techniques in this study. Further, the effect of chitosan additions on the nanofiber diameter was also investigated via the analysis of the antimicrobial activity and equilibrium water content. The optimum combination of parameters obtained from the ratio of silk fibroin to polycaprolactone, chitosan additions, flow rate, and applied voltage in response to minimizing diameter size and its variation for SF/PCL/CS composite nanofibers was determined by means of the Taguchi DoE method. Herein, the biocompatible properties were evaluated with cytotoxicity tests and proliferation tests so as to determine the optimal SF/PCL/CS scaffolds.

2. Experimental Method

2.1. Preparation of Regenerated Silk Fibroin (SF)

All the materials, solvents, and reagents were purchased from commercial suppliers and used as received. Cocoons were received from Paolun farm (Taiwan). Polycaprolactone (PCL, Mw = 80,000) was purchased from Sigma-Aldrich (St. Louis, MO). Polyethylene oxide (PEO, Mw = 60,000–100,000), chitosan (CS, Mw = 10,000–30,000), and formic acid were purchased from Acros Organics. The preparation of the silk fibroin (SF) used in this study made reference to previous research [1], with some modification. The cocoons were boiled in a 0.5% (w/v) Na_2CO_3 aqueous solution at a temperature of 100 °C for one hour. The silk fibers were rinsed with distilled water for 30 min to remove the Na_2CO_3 aqueous solution and then rinsed with deionized water for 30 min to remove the sericin. After being dried to a constant weight in an oven at 80 °C, the degummed silk fibers were dissolved in 40% aqueous CaCl_2 at 100 °C. The SF solution was replaced with a dialyzed membrane (molecular weight cut-off (MWCO) = 12,000–14,000 Da) for three days to eliminate small molecular impurities and calcium chloride. Lastly, the SF solution was lyophilized in a freeze dryer and stored at room temperature.

2.2. Preparation of the Electrospinning Solutions and Electrospinning

The SF and PCL were dissolved in formic acid to obtain 10 wt.% concentrations. Different ratios of SF/PCL (5.00%:5.00%, 3.33%:6.67%, and 2.50%:7.50%) were dissolved in formic acid and stirred at room temperature for two hours. Subsequently, 1 wt.% PEO as a thickener was added to the solution. Finally, from 0.5 to 1 wt.% CS was added to the electrospinning solutions.

The SF/PCL/CS composite nanofibers were obtained from the electrospinning of the prepared suspensions through a FES-COS electrospinning apparatus (Falco Co, Taipei, Taiwan). Briefly, the suspensions were drawn into a 10 mL syringe with a 21-gauge needle. The electrospinning was performed under ambient conditions (a temperature of 24.5 to 27.5 °C and a relative humidity of 45% to 50%). The following optimized electrospinning parameters were kept constant throughout the experiments: 100 rpm roller collector to collect fibers, 15 cm TCD (tip to collector distance), 15 kV–25 kV applied voltage, and 0.2 mL/h–0.4 mL/h feeding rate. The SF/PCL/CS homogeneous solutions were electrospun on a rotating cylindrical drum covered with an aluminum layer during the process. Finally, the collected membranes were taken from the surface of the collector and conserved in a sealed container for further experiments.

2.3. Taguchi DOE Parameter Setting

Numerous references [19–24] state that the ratio of silk fibroin to polycaprolactone, the chitosan content, the flow rate, and the applied voltage have significant effects on the average diameter and uniformity of fibers; thus, these four concentration and electrospinning parameters were selected for this experiment (Table 1).

Table 1. Actors and levels used in the experiment.

	Ratio of Silk Fibroin and Polycaprolactone	Chitosan Content (wt.%)	Flow Rate (mL/h)	Voltage (kV)
Level 1	1:1 (5.00%:5.00%)	0.50	0.2	15
Level 2	1:2 (3.33%:6.67%)	0.75	0.3	20
Level 3	1:3 (2.50%:7.50%)	1.00	0.4	25

The full factorial experiment of 81 (3⁴) trials could be completed in just 27 runs due to the slope collector; however, that would entail a large number of tests, which would be significant in both experimental cost and time. As a result, the Taguchi design of experiments (DoE) layouts were more applicable when compared to a traditional full-factorial counterpart because they reduced the number of tests to a practical level. The L9 DoE orthogonal array was selected with the assumption of no factorial interactions, resulting in nine trials, as illustrated in Table 2.

Table 2. Experimental results of the fiber fineness of the composite nanofibers planned by the L₉(3⁴) orthogonal table.

L ₉ (3 ⁴)	Ratio (SF: PCL)	Chitosan Addition (%)	Flow Rate (mL/h)	Voltage (kV)	S/N	Means of Diameter (nm)	Porosity (%)	WVTR (g m ⁻² ·24 h)
1	1:1	0.50	0.2	15	12.65	232.55±60.28	88.01±4.32	4417.29±87.27
2	1:1	0.75	0.3	20	12.71	229.09±60.66	83.10±4.21	4362.97±91.67
3	1:1	1.00	0.4	25	13.61	208.39±55.81	91.96±5.16	4641.38±19.21
4	1:2	0.50	0.3	25	15.37	170.00±55.76	92.05±3.70	4768.71±85.04
5	1:2	0.75	0.4	15	11.92	253.42±65.37	91.43±5.50	4636.29±25.46
6	1:2	1.00	0.2	20	13.11	220.67±62.13	85.37±4.04	4432.89±45.84
7	1:3	0.50	0.4	20	10.86	285.71±78.08	92.60±4.10	4581.97±92.58
8	1:3	0.75	0.2	25	11.47	266.75±76.71	84.74±5.70	4330.71±5.09
9	1:3	1.00	0.3	15	12.68	231.94±63.64	82.03±1.45	4405.41±74.86

In the “larger the better” characteristic, the formula for calculating the ratio of S/N as the best parameter for calculating the factors was calculated by the following Equation (1):

$$S/N = -10 \times \log \left(\frac{1}{n} \sum_{i=1}^n \frac{1}{y_i^2} \right) \tag{1}$$

where n and y denote the number of measurements and observed data, respectively.

2.4. Characterization of Nanofiber Scaffolds

The morphology of the nanofiber scaffold was detected using scanning electron microscopy (SEM; TS 5136MM, TESCAN, Czech Republic). The average fiber diameter was determined by measuring 100 fibers selected randomly from each sample. Chemical analysis was performed using a Fourier transform infrared spectrometer (FTIR; Spectrum 100, Perkin Elmer, USA) with a scan range of 4000 to 450 cm^{-1} and an accumulation of 16 scans.

According to standard method of Japanese Industrial Standards (JIS) 10099A, the water vapor transmission rate (WVTR) is a measure of the passage of water vapor through a substance. In addition to measurements of the permeability of the vapor barriers, the porosity of the SF/PCL/CS was also examined by the study [25]. For the antibacterial assay, the inhibitory effects of chitosan on bacterial growth were detected by the plate well diffusion method [26] via the formation of a zone of inhibition. To attain this figure, the sequential dilution was necessary (six for *E. coli* and for *S. aureus*) according to the simultaneous counting of plate colonies (CFU). The procedure used in this analysis followed the agar diffusion method according to the previous literature [27], in which small circular cavities were punctured in the culture medium for each chitosan concentration.

The equilibrium water content (EWC) was measured by the conventional gravimetric method. The pre-weighed dry samples were immersed in deionized water, and the excess surface water was blotted out with absorbent paper. The swelling procedure was repeated until there was no further weight increase. The EWC was calculated as the weight increase with respect to the weight of the swollen samples within 24 h using the following Equation (2):

$$EWC = \frac{W_{\text{wet}} - W_{\text{dry}}}{W_{\text{wet}}} \times 100\% \quad (2)$$

where W_{wet} and W_{dry} denote the weights of the swollen and dry samples, respectively.

A cytotoxicity assay is a test for analyzing the cytotoxic effects of materials and medical devices on living organisms [28]. The following cell culture-based tests, as recommended by ISO 10993-5, used a direct contact test. In all the tests (blank, negative control, positive control, and sample), the incubation time of the mouse fibroblast L929 cell cultures was 24 h. Cell culture is the process by which cells from human tissue are grown in an incubator under controlled conditions in order to provide sufficient material for testing. After solubilization, the solutions were transferred to fresh flat bottom 96-well plates, and the absorbance (570 nm) of each well was measured by spectrophotometry. The background absorbance at 650 nm was subtracted from the readings at 570 nm to obtain the final optical density (OD). The following Equation (3) was used to calculate the reduction in the culture viability of the cells exposed to a tested sample (i.e., SF/PCL/CS under optimal conditions) in comparison to the cell culture viability of group b:

$$\text{Viability (\%)} = \frac{OD_{570e}}{OD_{570b}} \times 100\% \quad (3)$$

where OD_{570e} is the average OD of the respective groups that were in contact with different lots of the product and OD_{570b} is the average OD of all the wells of group b. All the values were final ODs after the subtraction of background absorbance.

3. Results and Discussion

3.1. Optimum Combination of Factors for the Application of Dressings

3.1.1. Taguchi Method to Optimize Dressings

Uniform fiber diameters and smaller diameters in the scaffold for the application of dressings can provide a higher surface area and interconnected holes to promote the exchange of nutrients and oxygen and enhance the proliferation ability of cells. In the formation of nanofibers, the ratio of silk fibroin to polycaprolactone, the chitosan content, the flow rate, and the voltage are crucial factors affecting the nanofiber diameter. In Taguchi designed experiments, the higher values of the signal-to-noise ratio (S/N) identify control factor settings that minimize the effects of the noise factors. Using the Equation (1) of the smaller the better method (i.e., the smallest diameter of the nanofibers was selected based on maximum S/N ratio), the S/N ratio of the fiber fineness (the diameter of the nanofibers) in the SEM micrograph of the nanofiber could be calculated, and the results are shown in Table 2. According to the results from the L_9 (3^4) sample, the average S/N ratio of the four factor levels was calculated to perform the next analysis, as listed in Table 3. The influence of the four factors on the fiber diameter followed the order of the ratio of silk fibroin and polycaprolactone ($\Delta = 1.80$) > flow rate ($\Delta = 1.46$) > applied voltage ($\Delta = 1.26$) > chitosan addition ($\Delta = 1.10$). This finding suggested that the ratio of silk fibroin and polycaprolactone was the most significant factor for achieving a small electrospun nanofiber diameter for the application of dressings. Table 3 also shows the contribution of the four parameters to the influence of the SF/PCL/CS composite nanofiber diameter. The ratio of the silk fibroin and polycaprolactone was an important factor affecting the diameter of the nanofibers due to the highest contribution percentage (32.0%). Furthermore, the results indicated that the ratio of silk fibroin and polycaprolactone affected the viscosity of the electrospinning solution to produce a stable Taylor cone. The results were in accordance with the Taguchi experimental S/N design.

Table 3. Smaller the better of the fiber fineness signal-to-noise ratio (S/N) analysis.

	Ratio of Silk Fibroin and Polycaprolactone	Chitosan Content	Flow Rate	Voltage
1	12.99	12.96	12.41	12.42
2	13.47	12.03	13.59	12.23
3	11.67	13.13	12.13	13.48
Δ	1.80	1.10	1.46	1.26
Factor influence order	1	4	2	3
Contribution (%)	32.0	19.1	26.2	22.7

The average value of the confirmation experiments was 170.00 ± 55.76 nm under the optimal parameters of a silk fibroin to polycaprolactone ratio of 1:2, a chitosan addition of 0.5%, a rate of advancement of 0.3 mL/h, and an operating voltage of 25 kV (Table 2), which provided the highest average value compared with the nine groups of quality data. As shown in Figures 1 and 2, the results indicated that the optimal parameters inferred by the Taguchi method had a smaller fiber diameter, were smoother, and had a low distribution. Conclusively, the comparison of the optimal parameters inferred by the Taguchi method with the data results of the orthogonal table proved that the inferred optimal parameters were appropriate.

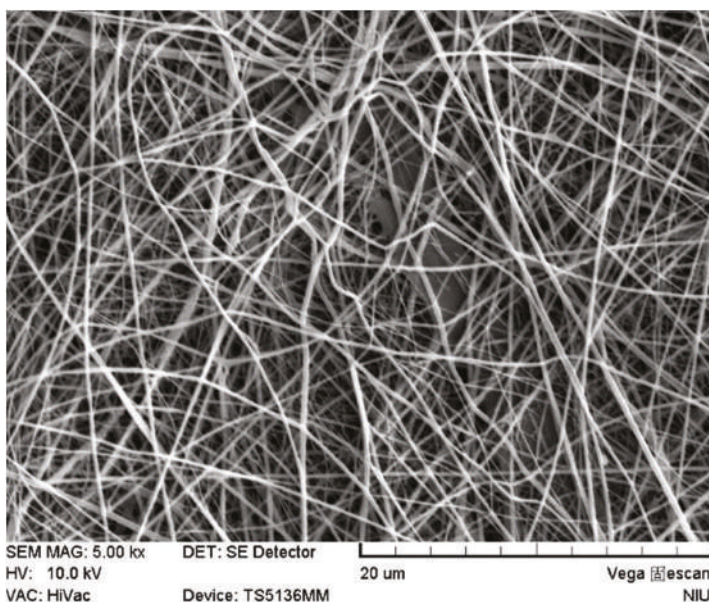


Figure 1. SEM photomicrograph of the silk fibroin (SF), polycaprolactone (PCL), and chitosan (CS) (SF/PCL/CS) nanofibers under optimal conditions.

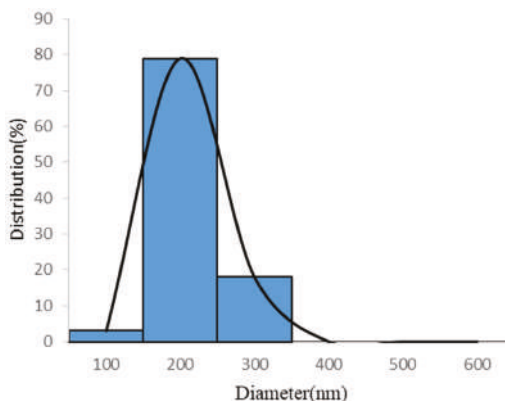


Figure 2. Fiber diameter distribution of the SF/PCL/CS nanofibers under optimal conditions.

3.1.2. Porosity and Water Uptake Abilities

The adequate pore size and interconnected pores of a scaffold provides a sufficient opportunity for cell migration and proliferation. The ability of a dressing to control water loss can be determined by the water vapor transmission rate (WVTR). The ability of a scaffold to preserve water is also important in order to evaluate its property for tissue engineering. Table 2 describes the WVTR of the SF/PCL/CS nanofibers. The porosity of the nine samples ($L_9 (3^4)$) of the SF/PCL/CS nanofibers in this study was more than 80% and was significantly higher than the pure PCL scaffolds, which had a 70% porosity, as reported by [29]. The highly porous SF/PCL/CS nanofibers could provide an appropriate environment for initial cell growth (by their structural stability), accelerated degradation (by their large surface area), and the sustained delivery of bioactive molecules (by their high porosity).

In this study, SF/PCL/CS nanofibers with graded WVTR were prepared by changing the porosity of the membrane (Table 2). The corresponding average WVTR of the samples was in the range of between 4330.71 and 4768.71 g m⁻²·24 h (extremely high permeability, L₉ (3⁴)). An extremely high WVTR may lead to the dehydration of a wound, whereas an unacceptably low WVTR may cause the accumulation of wound exudates. Hence, a dressing with a suitable WVTR is required to provide a moist environment that can establish the best environment for natural healing. Thus, a dressing prepared by optimal condition with a WVTR of approximately 4768.71 g/m²·24 h could also maintain the optimal moisture content for the proliferation and function of cells and fibroblasts. According to SEM and the appropriate porosity of the SF/PCL/CS nanofiber, it was considered to have great potential for skin tissue engineering due to its interconnected pore network and suitable WVTR.

3.1.3. Cytotoxicity Tests

Cytotoxicity assays are necessary for the assessment and characterization of the potentially toxic and harmful effects of a biomaterial's compounds [28]. They are a feasible and reliable in vitro technique used for the biocompatibility evaluation of materials. Table 4 shows phase contrast images of the cultures in the experiment after 24 h, including blank, negative control (polyethylene, PE), positive control (dimethylsulfoxide, DMSO), and SF/PCL/CS under optimal conditions. In cultures exposed to blank, negative control, positive control, and SF/PCL/CS, the viability was 100, 100, 13, and 57% at 24 h of continued growth in the culture, respectively. A tested product (SF/PCL/CS) has non-cytotoxic potential for application to tissue engineering when the cell culture viability increases to >50% in comparison to the positive control (dimethylsulfoxide, DMSO), which was set at a 13% viability. The study also proposed the similar results that the tested product could be considered non-toxic as the viability of these cultures exceeded 50% [30]. Furthermore, the viability of 57% for the tested product (SF/PCL/CS) in this study was higher than that of 50.2% for the CNTs-doped PLGA nanofibers [31]. The research [31] show that the PLGA and the HNTs- or CNTs-doped PLGA nanofibers display appreciable MTT formazan dye sorption, corresponding to a 35.6–50.2% deviation from the real cell viability assay data. From Figure 3, the DMSO treatment substantially altered the morphology and attachment of cells in concurrence with a significant reduction in the cell viability. The results showed that the electrospun scaffolds (SF/PCL/CS) could support the attachment and the proliferation of mouse fibroblast L929 cells. In addition, the cells cultured on the scaffolds exhibited normal cell shapes. The obtained results confirmed the potential for use of the electrospun fiber as scaffolds for skin tissue engineering.

Table 4. Viability of cell L 929 according to the MTT test method.

Test Item	Absorbance (%)	Viability (%)
Blank	0.504 ± 0.011	100
Negative control	0.502 ± 0.005	100
Positive control	0.064 ± 0.002	13
Sample (SF/PCL/CS)	0.288 ± 0.020	57

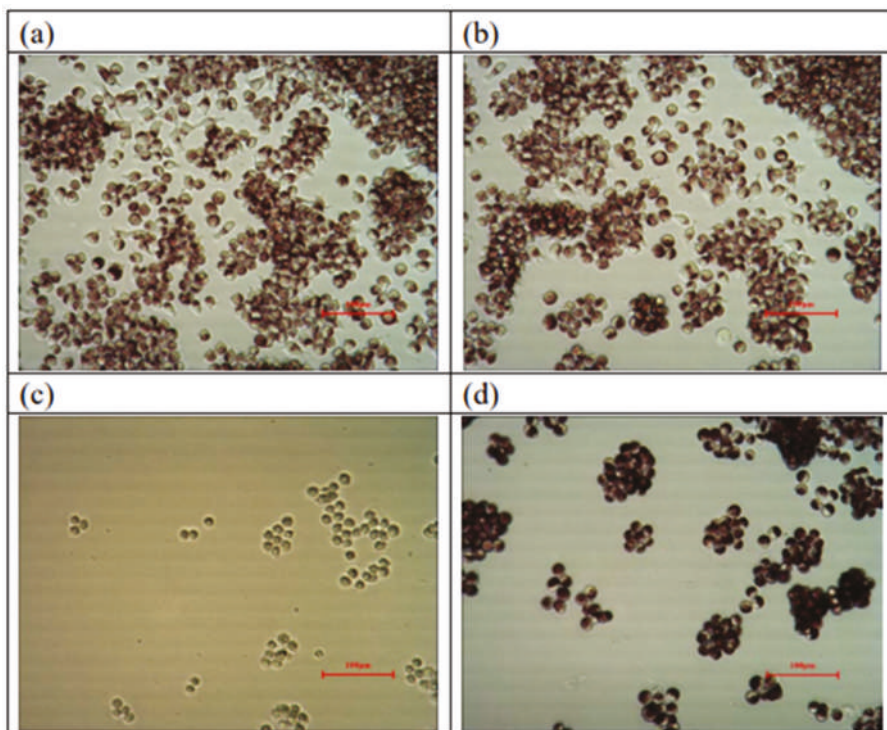


Figure 3. Photomicrograph of cell L 929 by direct contact method within 24 hours: (a) blank; (b) negative control (polyethylene, PE); (c) positive control (dimethylsulfoxide, DMSO); and (d) the sample (SF/PCL/CS under optimal conditions).

3.2. Effect of the Ratio of Silk Fibroin to Polycaprolactone on Fiber Diameter

In the electrospinning process, the solution concentration is considered to be the most important parameter affecting the fiber morphology [31,32]. Figure 4 shows the effect of the ratio of silk fibroin to polycaprolactone on the fiber diameter. At a silk fibroin to polycaprolactone ratio of 1.0, the entanglement between the polymer chains formed obvious beads because the low viscosity of the solution did not provide a stable jet. As the ratio of silk fibroin to polycaprolactone decreased from 0.5 to 0.25, the average fiber diameter increased from 208.27 ± 68.27 nm to 664.23 ± 131.54 nm in this study. The main reason was that the increase in viscosity hindered the bending stability of the jet to produce a coarser fiber [33,34].

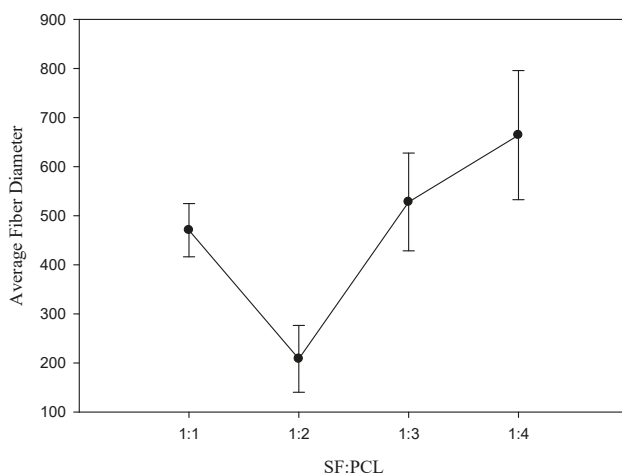


Figure 4. Effect of the ratio of silk fibroin to polycaprolactone on the fiber diameter.

3.3. Effect of Chitosan Addition on Fiber Diameter, Antimicrobial Activity, and Equilibrium Water Content

Figure 5 depicts the evaluation results of the fiber diameter of the electrospinning scaffold with different chitosan additions. The average fiber diameter decreased from 523.23±92.60 nm to 181.45±41.57 nm with the increased chitosan addition from 0.25% to 1.00% because of the charge density. The chitosan addition enhanced the higher charge density of the jet to produce the thinner fibers due to the increase in conductivity [21,35]. Compared to the chitosan addition of 1.00%, the average fiber diameter of the electrospinning scaffold was increased to 308.90±74.98 nm with a chitosan addition of 1.50%, because the increase in viscosity caused the bending instability of the jet and the accelerating solidification of the polymer jet [34,36].

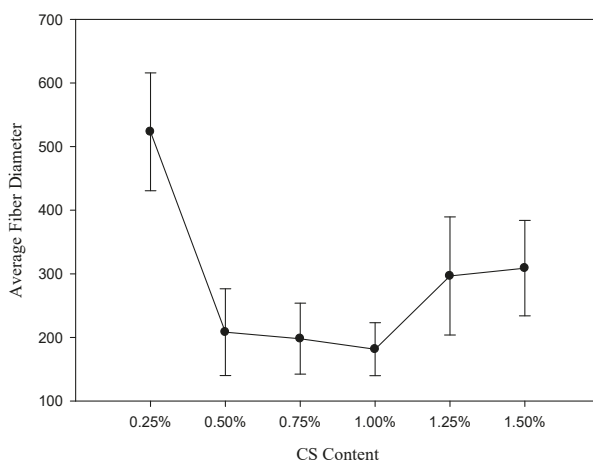


Figure 5. Effect of the chitosan addition on the fiber diameter.

The results from Table 5 revealed the mean diameter of inhibition zone for *E. coli* with the chitosan amounts of 0.25%, 0.5%, 0.75%, and 1.00% were 65, 63, 64, and 63 mm, respectively, proving the strong antibacterial property. Moreover, the samples with the chitosan amounts of 0.25%, 0.5%, 0.75%, and 1.00% exhibited the inhibition zone diameters for *S. aureus* of 58, 55, 51, and 55 mm, respectively. As

illustrated in Figures 6 and 7, the activity intensity could be visually determined by agar well diffusion assay testing via assessing the local inhibition. The results of the experiments conducted using different chitosan additions had an inhibitory effect on the mean diameter of the inhibition zone for two types of bacteria (*E. coli* and *S. aureus*). The results exhibited better inhibitory effects against gram-positive bacterium *S. aureus* compared to the gram-negative bacterium *E. coli*, which was in agreement with the results attained in previously published works [37,38]. The results in this study proposed that unmodified chitosan generally acts stronger on gram-negative strains than on gram-positive strains, owing to the electrostatic interaction between positively charged R-N(CH₃)₃⁺ sites and negatively charged microbial cell membranes.

Table 5. Effect of chitosan addition on the mean diameter of the inhibition zone of *E. coli* and *S. aureus* at different chitosan amounts.

Name of the Sample	Conc. (%)	Mean Diameter of Inhibition Zone (mm)	
		Staphylococcus Aureus	Escherichia Coli
Chitosan	0.25	58 ± 4	65 ± 0
	0.50	55 ± 1	63 ± 4
	0.75	51 ± 1	64 ± 0
	1.00	55 ± 1	63 ± 2

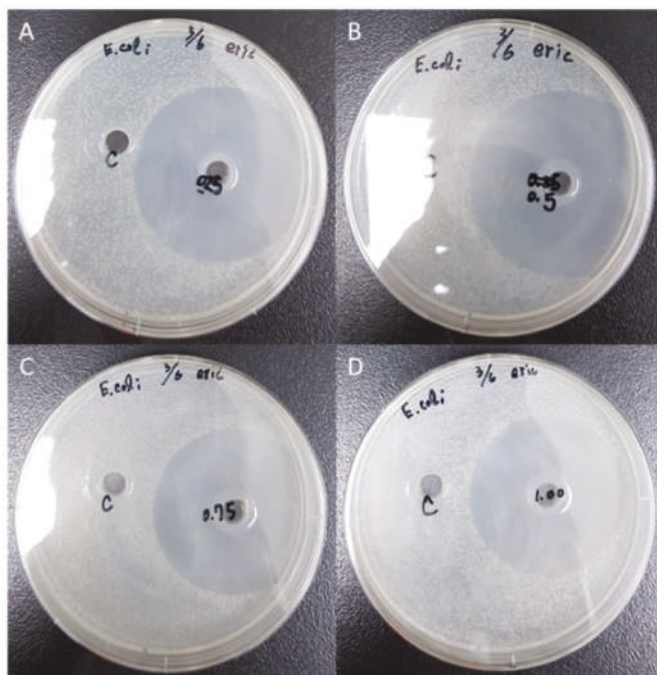


Figure 6. Effect of the chitosan addition on the antimicrobial activity of *E. coli* at different chitosan amounts: (A) 0.25; (B) 0.50; (C) 0.75; (D) 1.00 wt%.

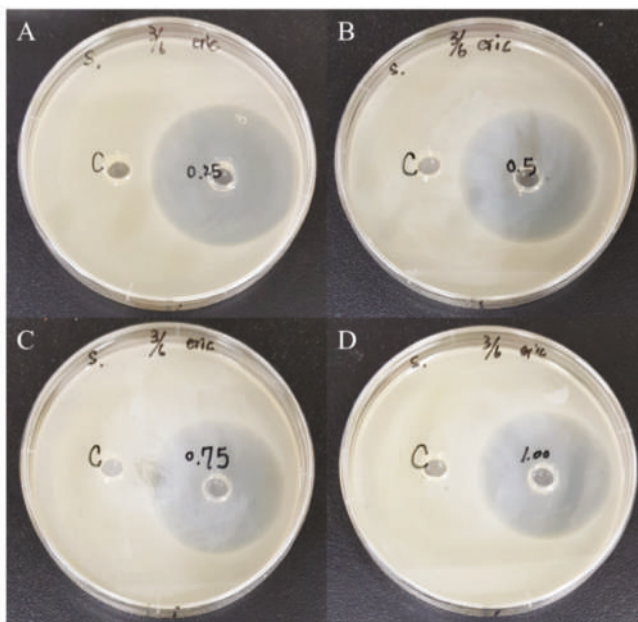


Figure 7. Effect of chitosan addition on the antimicrobial activity of *S. aureus* at different chitosan amounts: (A) 0.25; (B) 0.50; (C) 0.75; (D) 1.00 wt%.

The hydrophilicity of nanofibers (SF/PCL/CS) with different chitosan additions (0.25%, 0.50%, 0.75%, and 1.00%) was measured by gravimetric analysis and designated by the percentage equilibrium water content (EWC), as shown in Figure 8. The EWC was increased with the increasing chitosan addition due to the functional groups of $-OH$ and $-NH_2$. The equilibrium water content (EWC) of all the nanofibers (chitosan additions of 0.25%, 0.50%, 0.75%, and 1.00%) was in the range of 500% to 950% and was significantly higher than the YY0148-2006 standard for medical dressings [39] and the hydrogels for tissue engineering [40]. The copolymerization with the zwitterionic comonomer leads hydrogels with a high equilibrium water content (EWC) of up to 700% while maintaining mechanical robustness [40].

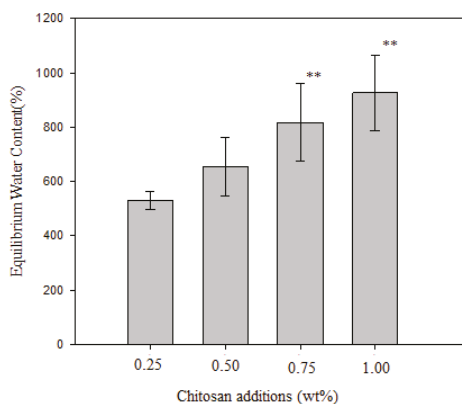


Figure 8. Effect of chitosan addition on the equilibrium water content.

3.4. Effect of Flow Rate on Fiber Diameter

In the electrospinning process, the flow rate is considered to be the most important parameter affecting the fiber uniformity [31,41]. The effect of the flow rate on the fiber diameter is shown in Figure 9a. As shown in Figure 9b, uniform beadless electrospun nanofibers were prepared via a critical flow rate of 0.3 mL/h for the polymeric solution. The shape of the Taylor cone at the tip of the capillary would not be maintained if the flow of the solution through the capillary was insufficient, and the insufficient intermolecular surface tension would be unable to resist the Coulomb force to maintain a stable jet [41]. However, at a higher flow rate, the solution would be wasted without differentiating adequately into the fibers. The short evaporation time of the solvent could result in the formation of beads and increase the average fiber diameter [32]. The morphology of the SF/PCL/CS nanofibers appeared to be inhomogeneous under a higher flow rate, as depicted in Figure 9c. The results could be explained by the inharmony between the fiber formation speed and the solution feed rate.

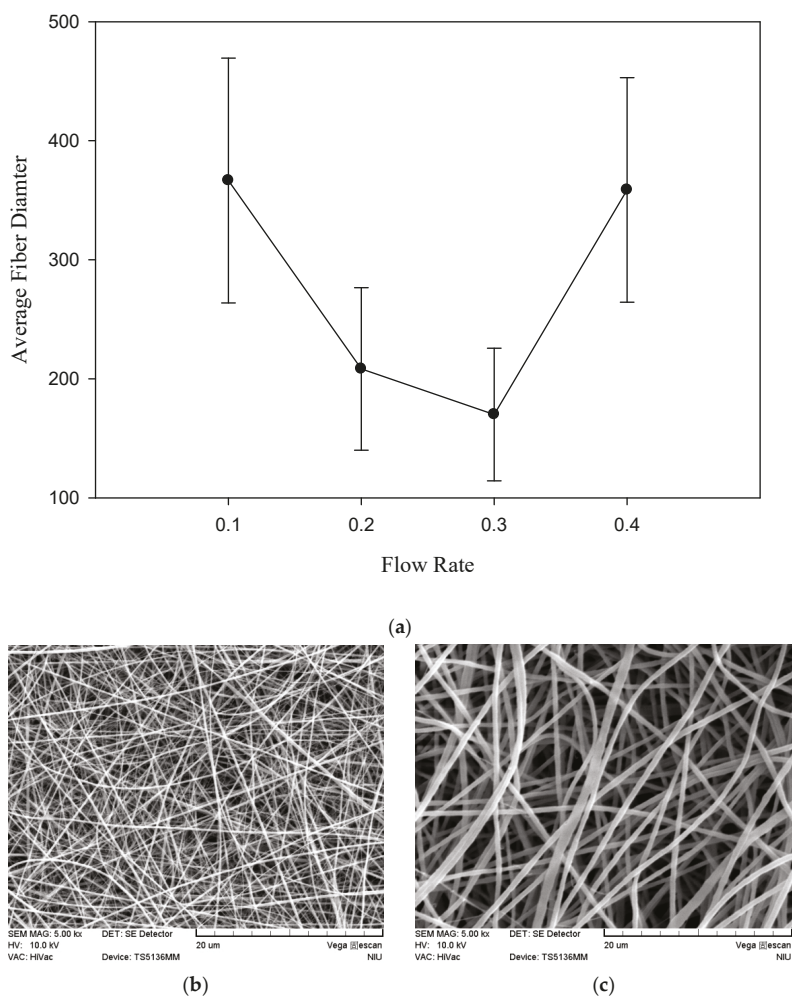


Figure 9. (a) Effect of flow rate on the fiber diameter of the SF/PCL/CS nanofibers, (b) SEM micrograph at 0.3 mL/h, (c) SEM micrograph at 0.4 mL/h.

3.5. Effect of Applied Voltage on Fiber Diameter

In general, the operating applied voltage must exceed the minimum threshold applied voltage before the Taylor cone appears to form ultrafine nanofibers [23]. As shown in Figure 10, the results revealed that the average fiber diameter significantly decreased from 440.69 ± 105.47 nm to 208.27 ± 55.76 nm as the applied voltage increased from 15 to 25 kV. This result could be explained by the force imbalance between the repulsive Coulombic force and the contracting viscoelastic force. With the increasing voltage, the intrinsic equilibrium became difficult to restore when the fibers were collected on the metal rod accompanied by the charge transfer.

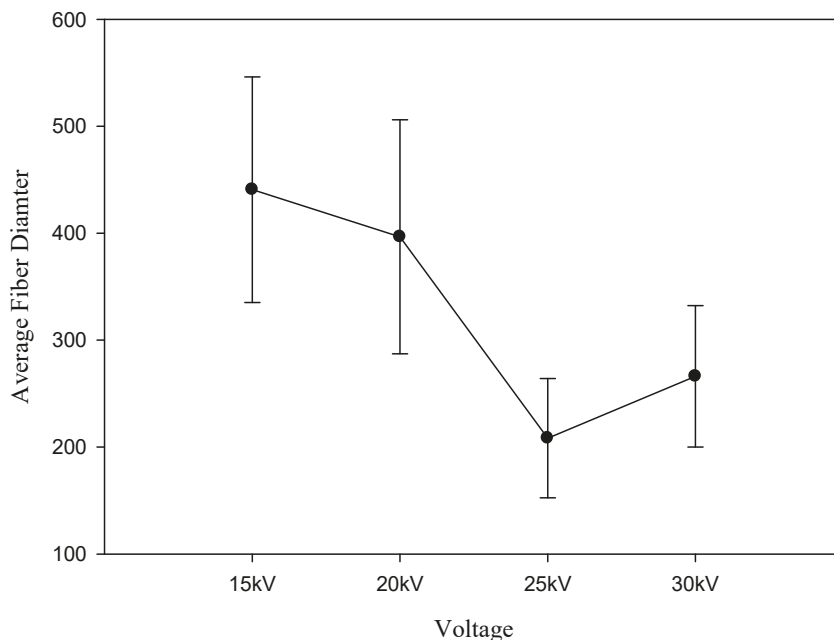


Figure 10. Effect of applied voltage on fiber diameter.

4. Conclusion

SF, PCL, and CS were blended in different concentrations and compositions and were evaluated for their fiber diameter to examine the optimum values for nanofibers. The S/N analysis via the Taguchi experimental design showed that the ratio of SF to PCL was the most influential parameter on the fiber diameter. A smooth and uniform distributed SF/PCL/CS nanofiber with a fiber diameter of 170.0 nm was synthesized at the optimal parameters of a 1:2 ratio of silk fibroin to polycaprolactone, a 0.5% chitosan addition, a 0.3 mL/h rate of advancement, and an operating voltage of 25 kV. The SF/PCL/CS (under optimal conditions) with a WVTR of approximately $4768.71 \text{ g/m}^2 \cdot 24 \text{ h}$ could maintain the optimal moisture content for the proliferation and function of cells and fibroblasts. The EWC of the SF/PCL/CS nanofiber was increased from 500% to 950% by increasing the chitosan additions from 0.25% to 1.00% and was significantly higher than the YY0148-2006 standard for medical dressings. The porosity of the nine samples ($L_9(3^4)$) of SF/PCL/CS in this study was more than 80% and was significantly higher than that of the pure PCL scaffolds. According to SEM and the appropriate porosity of the SF/PCL/CS nanofiber, it was considered to have great potential for skin tissue engineering due to its interconnected pore network and suitable WVTR.

Author Contributions: Project administration, M.-F.L.; Supervision, H.-W.C. All authors have read and agreed to the published version of the manuscript.

Funding: This research was supported in part by grant MOST 107-2221-E-197-001-MY2 from the Ministry of Science and Technology, Republic of China.

Conflicts of Interest: The authors declare no conflict of interest.

References

1. Ayutsede, J.; Gandhi, M.; Sukigara, S.; Micklus, M.; Chen, H.-E.; Ko, F. Regeneration of Bombyx mori silk by electrospinning. Part 3: Characterization of electrospun nonwoven mat. *Polymer* **2005**, *46*, 1625–1634. [[CrossRef](#)]
2. Yao, Y.; Wang, J.; Cui, Y.; Xu, R.; Wang, Z.; Zhang, J.; Wang, K.; Li, Y.; Zhao, Q.; Kong, D. Effect of sustained heparin release from PCL/chitosan hybrid small-diameter vascular grafts on anti-thrombogenic property and endothelialization. *Acta Biomater.* **2014**, *10*, 2739–2749. [[CrossRef](#)]
3. Dias, J.R.; Baptista-Silva, S.; Sousa, A.; Oliveira, A.L.; Bártolo, P.J.; Granja, P.L. Biomechanical performance of hybrid electrospun structures for skin regeneration. *Mater. Sci. Eng. C* **2018**, *93*, 816–827. [[CrossRef](#)]
4. Avsar, G.; Agirbasli, D.; Agirbasli, M.A.; Gunduz, O.; Oner, E.T. Levan based fibrous scaffolds electrospun via co-axial and single-needle techniques for tissue engineering applications. *Carbohydr. Polym.* **2018**, *193*, 316–325. [[CrossRef](#)] [[PubMed](#)]
5. Surucu, S.; Sasmazel, H.T. Development of core-shell coaxially electrospun composite PCL/chitosan scaffolds. *Int. J. Biol. Macromol.* **2016**, *92*, 321–328. [[CrossRef](#)] [[PubMed](#)]
6. Pakravan, M.; Heuzey, M.-C.; Aiji, A. A fundamental study of chitosan/PEO electrospinning. *Polymer* **2011**, *52*, 4813–4824. [[CrossRef](#)]
7. Narayanan, G.; Gupta, B.S.; Tonelli, A.E. Enhanced mechanical properties of poly(ϵ -caprolactone) nanofibers produced by the addition of non-stoichiometric inclusion complexes of poly(ϵ -caprolactone) and α -cyclodextrin. *Polymer* **2015**, *73*, 321–330. [[CrossRef](#)]
8. Yang, X.; Fan, L.; Ma, L.; Wang, Y.; Lin, S.; Yu, F.; Pan, X.; Luo, G.; Zhang, D.; Wang, H. Green electrospun Manuka honey/silk fibroin fibrous matrices as potential wound dressing. *Mater. Des.* **2017**, *119*, 76–84. [[CrossRef](#)]
9. Lin, L.; Zhu, Y.; Li, C.; Liu, L.; Surendhiran, D.; Cui, H. Antibacterial activity of PEO nanofibers incorporating polysaccharide from dandelion and its derivative. *Carbohydr. Polym.* **2018**, *198*, 225–232. [[CrossRef](#)] [[PubMed](#)]
10. Ahmed, R.; Tariq, M.; Ali, I.; Asghar, R.; Khanam, P.N.; Augustine, R.; Hasan, A. Novel electrospun chitosan/polyvinyl alcohol/zinc oxide nanofibrous mats with antibacterial and antioxidant properties for diabetic wound healing. *Int. J. Biol. Macromol.* **2018**, *120*, 385–393. [[CrossRef](#)]
11. Zhang, D.; Karki, A.B.; Rutman, D.; Young, D.P.; Wang, A.; Cocke, D.; Ho, T.H.; Guo, Z. Electrospun polyacrylonitrile nanocomposite fibers reinforced with Fe₃O₄ nanoparticles: Fabrication and property analysis. *Polymer* **2009**, *50*, 4189–4198. [[CrossRef](#)]
12. Zhu, J.; Wei, S.; Patil, R.; Rutman, D.; Kucknoor, A.S.; Wang, A.; Guo, Z. Ionic liquid assisted electrospinning of quantum dots/elastomer composite nanofibers. *Polymer* **2011**, *52*, 1954–1962. [[CrossRef](#)]
13. Aslan, T.; Arslan, S.; Eyvaz, M.; Güçlü, S.; Yüksel, E.; Koyuncu, İ. A novel nanofiber microfiltration membrane: Fabrication and characterization of tubular electrospun nanofiber (TuEN) membrane. *J. Membr. Sci.* **2016**, *520*, 616–629. [[CrossRef](#)]
14. Jiang, L.; Tu, H.; Lu, Y.; Wu, Y.; Tian, J.; Shi, X.; Wang, Q.; Zhan, Y.; Huang, Z.; Deng, H. Spherical and rodlike inorganic nanoparticle regulated the orientation of carbon nanotubes in polymer nanofibers. *Chem. Phys. Lett.* **2016**, *650*, 82–87. [[CrossRef](#)]
15. Yao, Y.; Wei, H.; Wang, J.; Lu, H.; Leng, J.; Hui, D. Fabrication of hybrid membrane of electrospun polycaprolactone and polyethylene oxide with shape memory property. *Compos. B. Eng.* **2015**, *83*, 264–269. [[CrossRef](#)]
16. Rao, M.; Geng, X.; Liao, Y.; Hu, S.; Li, W. Preparation and performance of gel polymer electrolyte based on electrospun polymer membrane and ionic liquid for lithium ion battery. *J. Membr. Sci.* **2012**, *399–400*, 37–42. [[CrossRef](#)]
17. Narayanan, G.; Tekbudak, M.Y.; Caydamli, Y.; Dong, J.; Krause, W.E. Accuracy of electrospun fiber diameters: The importance of sampling and person-to-person variation. *Polym. Test.* **2017**, *61*, 240–248. [[CrossRef](#)]

18. Yu, W.-J.; Xu, S.-M.; Zhang, L.; Fu, Q. Morphology and mechanical properties of immiscible polyethylene/polyamide12 blends prepared by high shear processing. *Chinese J. Polym. Sci.* **2017**, *35*, 1132–1142. [[CrossRef](#)]
19. Park, Y.R.; Ju, H.W.; Lee, J.M.; Kim, D.-K.; Lee, O.J.; Moon, B.M.; Park, H.J.; Jeong, J.Y.; Yeon, Y.K.; Park, C.H. Three-dimensional electrospun silk-fibroin nanofiber for skin tissue engineering. *Int. J. Biol. Macromol.* **2016**, *93*, 1567–1574. [[CrossRef](#)]
20. Aznar-Cervantes, S.D.; Daniel, V.C.; Luis, M.O.; Cenis, J.L.; Abel, L.P.A. Influence of the protocol used for fibroin extraction on the mechanical properties and fiber sizes of electrospun silk mats. *Mater. Sci. Eng. C* **2013**, *33*, 1945–1950. [[CrossRef](#)]
21. Calamak, S.; Aksoy, E.A.; Ertas, N.; Erdogdu, C.; Sagiroglu, M.; Ulubayram, K. Ag/silk fibroin nanofibers: Effect of fibroin morphology on Ag⁺ release and antibacterial activity. *Eur. Polym. J.* **2015**, *67*, 99–112. [[CrossRef](#)]
22. Vaz, J.M.; Taketa, T.B.; Hernandez-Montelongo, J.; Chevallier, P.; Cotta, M.A.; Mantovani, D.; Beppu, M.M. Antibacterial properties of chitosan-based coatings are affected by spacer-length and molecular weight. *Appl. Surf. Sci.* **2018**, *445*, 478–487. [[CrossRef](#)]
23. Albetran, H.; Dong, Y.; Low, I.M. Characterization and optimization of electrospun TiO₂/PVP nanofibers using Taguchi design of experiment method. *J. Asian Ceram. Soc.* **2015**, *3*, 292–300. [[CrossRef](#)]
24. Senthil, T.; Anandhan, S. Electrospinning of non-woven poly(styrene-co-acrylonitrile) nanofibrous webs for corrosive chemical filtration: Process evaluation and optimization by Taguchi and multiple regression analyses. *J. Electrostat.* **2015**, *73*, 43–55. [[CrossRef](#)]
25. Ryan, M.P.; Rea, M.C.; Hill, C.; Ross, R.P. An application in cheddar cheese manufacture for a strain of *Lactococcus lactis* producing a novel broad-spectrum bacteriocin, lacticin 3147. *Appl. Environ. Microbiol.* **1996**, *62*, 612–619. [[CrossRef](#)]
26. Duffy, G.; Whiting, R.C.; Sheridan, J.J. The effect of a competitive microflora, pH and temperature on the growth kinetics of *Escherichia coli* O157:H7. *Food Microbiol.* **1999**, *16*, 299–307. [[CrossRef](#)]
27. Rosengren, A.; Faxius, L.; Tanaka, N.; Watanabe, M.; Bjursten, L.M. Comparison of implantation and cytotoxicity testing for initially toxic biomaterials. *J. Biomed. Mater. Res. A* **2005**, *75*, 115–122. [[CrossRef](#)]
28. Izquierdo, R.; Garcia-Giralt, N.; Rodriguez, M.T.; Cáceres, E.; García, S.J.; Ribelles, J.L.G.; Joan, M.M.; Monllau, C.; Suay, J. Biodegradable PCL scaffolds with an interconnected spherical network for tissue engineering. *J. Biomed. Mater. Res. A* **2008**, *85*, 25–35. [[CrossRef](#)]
29. Mehrabani, M.G.; Karimian, R.; Rakhshaei, R.; Pakdel, F.; Eslami, H.; Fakhrazadeh, V.; Rahimi, M.; Salehi, R.; Kafil, H.S. Chitin/silk fibroin/TiO₂ bio-nanocomposite as a biocompatible wound dressing bandage with strong antimicrobial activity. *Int. J. Biol. Macromol.* **2018**, *116*, 966–976. [[CrossRef](#)]
30. Zhou, J.; Cao, C.; Ma, X. A novel three-dimensional tubular scaffold prepared from silk fibroin by electrospinning. *Int. J. Biol. Macromol.* **2009**, *45*, 504–510. [[CrossRef](#)]
31. Qi, R.; Shen, M.; Cao, X.; Guo, R.; Tian, X.; Yu, J.; Shi, X. Exploring the dark side of MTT viability assay of cells cultured onto electrospun PLGA-based composite nanofibrous scaffolding materials. *Analyst* **2011**, *14*, e1800403. [[CrossRef](#)] [[PubMed](#)]
32. Sutasinpromprae, J.; Jitjaicham, S.; Nithitanakul, M.; Meechaisue, C.; Supaphol, P. Preparation and characterization of ultrafine electrospun polyacrylonitrile fibers and their subsequent pyrolysis to carbon fibers. *Polym. Int.* **2006**, *55*, 825–833. [[CrossRef](#)]
33. Jacobs, V.; Anandjiwala, R.D.; Maaza, M. The influence of electrospinning parameters on the structural morphology and diameter of electrospun nanofibers. *J. Appl. Polym. Sci.* **2010**, *115*, 3130–3136. [[CrossRef](#)]
34. Jia, Y.-T.; Gong, J.; Gu, X.-H.; Kim, H.-Y.; Dong, J.; Shen, X.-Y. Fabrication and characterization of poly(vinyl alcohol)/chitosan blend nanofibers produced by electrospinning method. *Carbohydr. Polym.* **2007**, *67*, 403–409. [[CrossRef](#)]
35. Vrieze, S.D.; Westbroek, P.; Camp, T.V.; Clerck, K.D. Solvent system for steady state electrospinning of polyamide 6.6. *J. Appl. Polym. Sci.* **2010**, *115*, 837–842. [[CrossRef](#)]
36. Da Silva, L.P.; De Britto, D.; Selegim, M.H.R.; Assis, O.B.G. In vitro activity of water-soluble quaternary chitosan chloride salt against *E. coli*. *World J. Microbiol. Biotechnol.* **2010**, *26*, 2089–2092. [[CrossRef](#)]
37. No, H.K.; Park, N.Y.; Lee, S.H.; Meyers, S.P. Antibacterial activity of chitosans and chitosan oligomers with different molecular weights. *Int. J. Food Microbiol.* **2002**, *75*, 65–72. [[CrossRef](#)]

38. Li, S.; Li, L.; Guo, C.; Qin, H.; Yu, X. A promising wound dressing material with excellent cytocompatibility and proangiogenesis action for wound healing: Strontium loaded Silk fibroin/Sodium alginate (SF/SA) blend films. *Int. J. Biol. Macromol.* **2017**, *104*, 969–978. [[CrossRef](#)]
39. Someswararao, M.V.; Dubey, R.S.; Subbarao, P.S.V.; Singh, S. Electrospinning process parameters dependent investigation of TiO₂ nanofibers. *Results Phys.* **2018**, *11*, 223–231. [[CrossRef](#)]
40. Kostina, N.Y.; Blanquer, S.; Pop-Georgievski, O.; Rahimi, K.; Dittrich, B.; Höcherl, A.; Michálek, J.; Grijpma, D.W.; Rodriguez-Emmenegger, C. Zwitterionic functionalizable scaffolds with gyroid pore Architecture for tissue engineering. *Macromol. Biosci.* **2019**, *19*, e1800403. [[CrossRef](#)]
41. Jin, H.-J.; Fridrikh, S.V.; Rutledge, G.C.; Kaplan, D.L. Electrospinning Bombyx mori silk with poly(ethylene oxide). *Biomacromolecules* **2002**, *3*, 1233–1239. [[CrossRef](#)] [[PubMed](#)]



© 2020 by the authors. Licensee MDPI, Basel, Switzerland. This article is an open access article distributed under the terms and conditions of the Creative Commons Attribution (CC BY) license (<http://creativecommons.org/licenses/by/4.0/>).